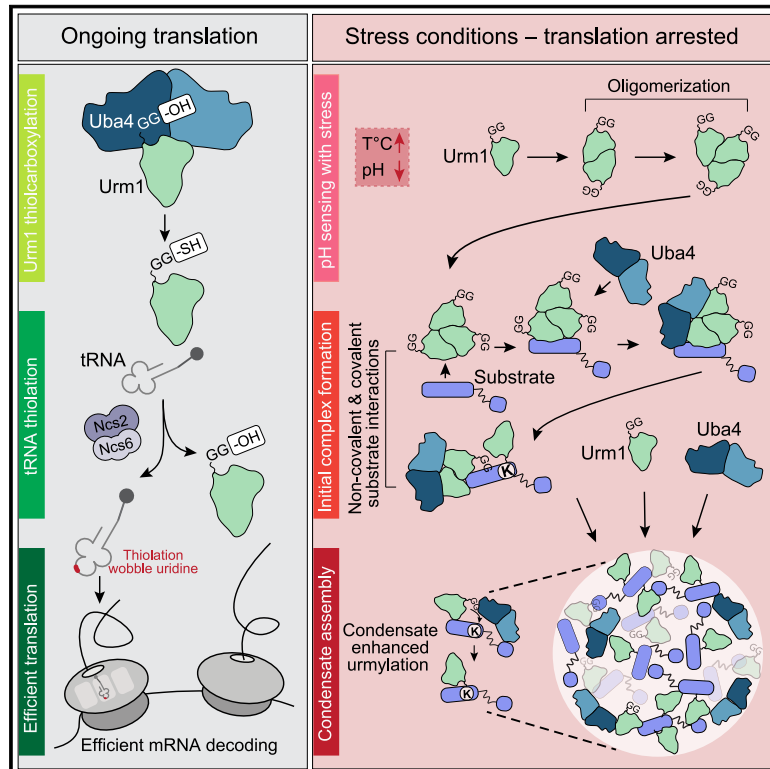# Stress-dependent condensate formation regulated by the ubiquitin-related modifier Urm1

Graphical abstract

Authors

Lucas V. Cairo, Xiaoyu Hong, Martin B.D. Müller, ..., Sae-Hun Park, Manajit Hayer-Hartl, F. Ulrich Hartl

Correspondence

rpark@biochem.mpg.de (S.-H.P.),
mhartl@biochem.mpg.de (M.H.-H.),
uhartl@biochem.mpg.de (F.U.H.)

In brief

Urmylation, a post translational modification mediated by the ubiquitin-like modifier Urm1, facilitates stress-dependent phase separation of target proteins to ensure stress resilience and cell survival.

Highlights

- Cell stress induces Urm1 upregulation and modification of target proteins

- Urm1 modification enhances phase separation of proteins under stress

- Co-condensation of Urm1 with its E1-like enzyme Uba4 drives target urmylation

- Urm1 function is required for cellular fitness and stress resilience

Article

Stress-dependent condensate formation regulated by the ubiquitin-related modifier Urm1

Lucas V. Cairo,[1] Xiaoyu Hong,[1,4] Martin B.D. Müller,[1,3,4] Patricia Yuste-Checa,[1] Chandhuru Jagadeesan,[1] Andreas Bracher,[1] Sae-Hun Park,[1,*] Manajit Hayer-Hartl,[1,*] and F. Ulrich Hartl[1,2,5,*]
[1]Department of Cellular Biochemistry, Max Planck Institute of Biochemistry, Martinsried, Germany
[2]Munich Cluster for Systems Neurology (SyNergy), Munich, Germany
[3]Present address: Gene Center, Ludwig-Maximilians-Universität, Munich, Germany
[4]These authors contributed equally
[5]Lead Contact
*Correspondence: rpark@biochem.mpg.de (S.-H.P.), mhartl@biochem.mpg.de (M.H.-H.), uhartl@biochem.mpg.de (F.U.H.)
https://doi.org/10.1016/j.cell.2024.06.009

SUMMARY

The ability of proteins and RNA to coalesce into phase-separated assemblies, such as the nucleolus and stress granules, is a basic principle in organizing membraneless cellular compartments. While the constituents of biomolecular condensates are generally well documented, the mechanisms underlying their formation under stress are only partially understood. Here, we show in yeast that covalent modification with the ubiquitin-like modifier Urm1 promotes the phase separation of a wide range of proteins. We find that the drop in cellular pH induced by stress triggers Urm1 self-association and its interaction with both target proteins and the Urm1-conjugating enzyme Uba4. Urmylation of stress-sensitive proteins promotes their deposition into stress granules and nuclear condensates. Yeast cells lacking Urm1 exhibit condensate defects that manifest in reduced stress resilience. We propose that Urm1 acts as a reversible molecular "adhesive" to drive protective phase separation of functionally critical proteins under cellular stress.

INTRODUCTION

Eukaryotic cells use elaborate mechanisms to cope with stress conditions that put the integrity of the proteome at risk.[1–3] A conserved strategy of maintaining protein homeostasis involves upregulation of molecular chaperones and other quality control machinery, known as the heat shock response (HSR).[4,5] The HSR is accompanied by arrest of protein synthesis combined with downregulated ribosome biogenesis.[6] This is achieved by sequestering ribosome biogenesis factors and unassembled ribosomal proteins into nuclear assemblies, while multiple translation factors and untranslated mRNAs are partitioned into cytosolic stress granules (SGs).[6–14] In this way, upon the cessation of stress, energetically expensive processes such as protein synthesis can resume.

Liquid-liquid phase separation has been recognized as the organizing principle underlying the formation of biomolecular condensates, including SGs, the nucleolus, and other membraneless organelles.[15–21] Phase separation involves the concentration of proteins (with or without RNA) into a dense phase, or condensate, through multivalent interactions often involving low-complexity amino acid sequences or prion-like domains (PrDs). Heat stress and starvation cause cellular acidification to induce condensate formation, with specific SG components phase separating in acidic conditions.[19,22–25] Reestablishing normal pH then results in condensate dissolution.

Ubiquitin and the ubiquitin-related modifier Sumo function in various aspects of the cellular stress response, such as targeting misfolded proteins to degradation, regulating transcription, and recovery from stress.[26–30] In contrast, the role of the less abundant ubiquitin-related modifier-1 (Urm1) has remained enigmatic.[31–33] Urm1 acts as a sulfur carrier for the thiolation of wobble uridines in tRNAs, enhancing codon-anti codon pairing during translation[34] and as a lysine- and serine-directed protein modifier under oxidative stress.[31,33,35–38] Both reactions require activation by transfer of sulfur onto the C terminus of Urm1 by the E1-like enzyme Uba4[39–41] and are independent of E2 and E3 enzymes.[42,43]

Here, we show that under conditions of heat stress or starvation, Urm1 modification of target proteins is utilized to enhance the formation of reversible protein condensates, including perinucleolar assemblies and SGs. This function is facilitated by an intrinsic ability of Urm1 to self-associate in response to the stress-induced drop in pH. Notably, Uba4 phase separates with Urm1, allowing localized urmylation without dedicated E2 and E3 enzymes. These findings identify Urm1 as a ubiquitin-like modifier with a critical function in regulating biomolecular condensate assembly during cell stress.
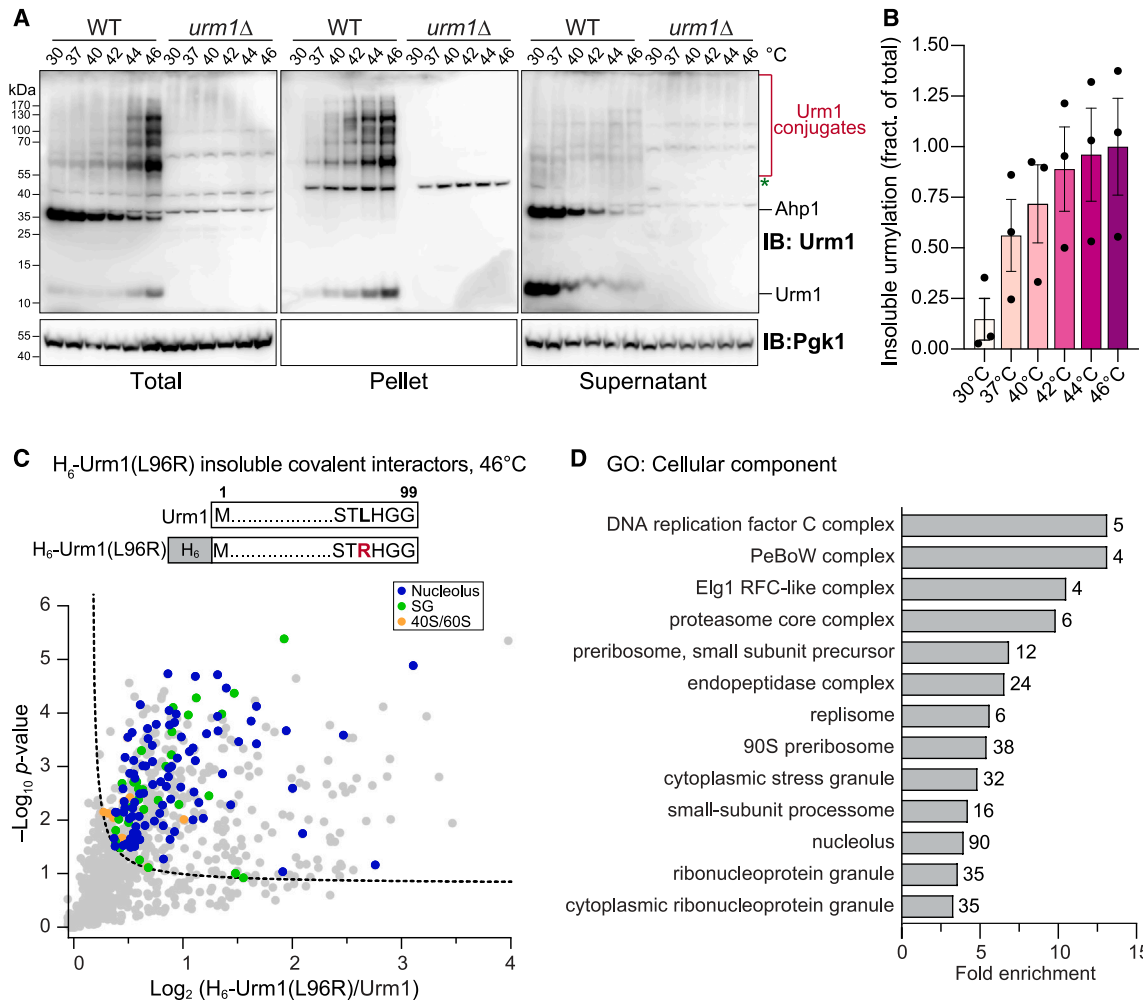
Figure 1. Stress-induced urmylation of insoluble proteins

(A) Urm1-modified proteins upon heat stress (HS). WT and *urm1Δ* cells were incubated at the indicated temperatures for 15 min, then lysed and fractionated (see STAR Methods). Immunoblotting with anti-Urm1 antibody was conducted using Pgk1 as loading control. Equivalent amounts of total, supernatant, and pellet fractions were analyzed. Asterisk indicates cross-reactivity. The position of Ahp1 is indicated (*n* = 3).

(B) Quantification of insoluble urmylation with densitometry normalized to total fraction urmylation (*n* = 3). Error bars: mean ± SEM.

(C and D) Identification of urmylated proteins upon HS (46°C, 15 min) using His₆-Urm1 (H₆-Urm1(L96R)) (C, top). Enriched insoluble H₆-Urm1(L96R) conjugates were analyzed with label free proteomics (STAR Methods).

(C) Enrichment of urmylated proteins in H₆-Urm1(L96R) cells relative to WT. Nucleolar, ribosomal, and SG proteins are highlighted. Line indicates FDR cutoff of 0.05 (*n* = 3). See also Table S1C.

(D) GO term analysis (cellular component) shows categories of urmylated proteins. Numbers indicate proteins per category.

See also Table S1D and Figures S1 and S2.

RESULTS

Accumulation of insoluble, urmylated proteins upon heat stress

To gain insight into the consequences of protein modification by Urm1, we investigated this process in *S. cerevisiae* under stress conditions including heat stress (HS). Urmylation was low in logarithmic phase cells at 30°C (Figure 1A). However, exposure to HS for 15 min (at 37°C–46°C) led to an accumulation of urmylated proteins above ~55 kDa in size (Figure 1A). Urmylation occurred within minutes upon HS (Figure S1A), similar to ubiquitylation and sumoylation.[27,44–48] Cell fractionation revealed that

Urm1-modified proteins were largely insoluble (Figures 1A and 1B), while the majority of ubiquitin-modified proteins remain soluble.[44] Urmylation peaked 15 min after HS and then decreased during a 1 h recovery (Figure S1B). Urmylated proteins also accumulated when cell growth reached stationary phase (S.P.) at 30°C (Figure S1C). Total Urm1 levels increased ~2- to 3-fold upon acute HS or in S.P. (Figures S1D and S1E; Tables S1A and S1B and STAR Methods), as confirmed by monitoring the levels of endogenously expressed non-conjugatable Urm1-HA (Figures S1F and S1G). A prominent urmylated protein of ~35 kDa, previously identified as the peroxiredoxin Ahp1,[49] was detected at normal temperature in wild-type (WT) cells but

not *ahp1Δ* or *urm1Δ* cells (Figures 1A, S1C, and S1H). The effect of urmylation on Ahp1 function remains unclear.[49] Urm1-modified Ahp1 decreased rapidly upon HS (Figures 1A and S1A), while total Ahp1 levels were maintained (Table S1A), suggesting active deurmylation.

Interestingly, not only urmylated proteins but also free Urm1 was recovered in the insoluble fraction upon HS (Figure 1A). We used *uba4Δ* cells to explore this effect in the absence of urmylation (Figure S1I). Free Urm1 shifted essentially quantitatively to the insoluble fraction in a temperature-dependent manner (Figures S1I and S1J).

In summary, stress conditions induce urmylation along with increased Urm1 levels. Urmylated proteins accumulate in the insoluble fraction, consistent with stress-induced insolubility of free Urm1.

Identification of Urm1 target proteins

To identify Urm1 target proteins, we isolated urmylated proteins from the insoluble fraction of cells expressing an N-terminally His$_6$-tagged variant of Urm1, H$_6$-Urm1(L96R), followed by label-free mass spectrometry (LC-MS/MS) (Figure 1C; Table S1C and STAR Methods). Isolation under denaturing conditions resulted in purification of covalent Urm1 interactors (Figure S2A). The use of Urm1(L96R) allowed for the generation, upon trypsin cleavage, of branched peptides containing the C-terminal di-glycine motif of Urm1 (Figure 1C).[50,51] In total, 488 proteins coprecipitated with H$_6$-Urm1(L96R), henceforth defined as Urm1-covalent interactors (Table S1C). Among these, Uba4 was enriched, consistent with Uba4 self-urmylation.[31,37] Notably, a large fraction (~26%; 129 proteins) of Urm1 targets are RNA-binding proteins (RBPs) (Figure S2B), with gene ontology analysis showing categories of nuclear and nucleolar structure and function as enriched (Figure 1D; Table S1D). Interestingly, all subunits of the DNA replication factor C complex (RFC) and the nucleolar PeBoW complex were identified (Figure 1D; Table S1D), suggesting that the respective complexes remain assembled during shift to the insoluble fraction. Proteasome subunits, as well as 40S/60S ribosomal components (including preribosome), known to localize to insoluble assemblies, were also enriched (Figures 1C and 1D; Table S1C).[8,52,53] Importantly, Urm1 covalent interactors included multiple SG constituents, suggesting that a subset of urmylated proteins are localized to SGs (Figures 1C and 1D; Table S1C).

Analysis of branched peptides from the H$_6$-Urm1(L96R) pulldown detected Urm1 modifications on both lysine and serine residues, but coverage was low. To improve identification of urmylation sites, we analyzed branched peptides from the insoluble fraction of heat-stressed *urm1(L96R)* cells (46°C, 15 min). Using this approach, we identified 33 proteins containing lysine and serine urmylations, as well as 115 and 94 proteins with only modified lysines or serines, respectively (Figure S2C; Tables S1E–S1H). Branched peptides corresponding to K18 of Urm1 were also detected (Table S1E), suggesting possible Urm1 chain assembly. Using the AlphaFold2 database,[54] we found most modifications (at 155 lysine and 126 serines) occurred within structured regions of target proteins as opposed to within disordered sequences (Figure S2D; Table S1G). Modified lysine and serine residues of the same protein were some-

times found in close spatial proximity, exemplified by Rps13 and Tma16 (Figure S2E; Table S1H).

We also analyzed urmylation in the soluble fraction upon HS, which contained only low amounts of modified proteins (Figure 1A). Nevertheless, 279 Urm1 interactors were identified, including the thiolation components Ncs2 and Ncs6, but not Uba4 (Figure S2F; Table S1I). Only few of these interactors belong to SGs and the nucleolus, consistent with a small degree of overlap between soluble and insoluble Urm1 interactomes (Figure S2G; Table S1I). GO analysis identified factors involved in DNA replication as enriched (Figure S2H; Table S1J).

Taken together, the majority of Urm1-modified proteins upon stress are detected in the insoluble fraction, including multiple factors that form cytoplasmic or nuclear condensates. Urm1 modifies lysine and serine residues, favoring structured regions within target proteins.

### Urm1 forms nuclear and cytoplasmic foci

To investigate the localization of Urm1 by microscopy, we expressed mNeonGreen-Urm1 (mNG-Urm1) from its endogenous promoter. The nucleus was visualized by expressing the nuclear pore complex protein Nup49 fused to mRFPmars (Nup49-Mars). Under basal growth conditions at 30°C, mNG-Urm1 was diffusely distributed (Figure 2A). Strikingly, following HS (15 min, 37°C–46°C), the majority of cells formed cytosolic and nuclear mNG-Urm1 foci within minutes, increasing in number and size with more severe HS (Figures 2A, 2B, and S3A). In contrast, mNG alone remained diffuse (Figure S3B). Notably, endogenously expressed mNG-Uba4 also formed foci following acute HS, independent of Urm1 (Figure S3C).

mNG-Urm1 recapitulated the function of Urm1 in covalently modifying insoluble target proteins upon HS. Using H$_6$-mNG-Urm1 (Figures S3D and S3E), we identified 239 modified proteins (Figures S3F and S3G; Table S2A) belonging to GO categories "cytoplasmic stress granule," "preribosome," and "nucleolus" (Figure S3G; Table S2B), analogous to the H$_6$-Urm1 interactome (Figure 1D). However, the number of H$_6$-mNG-Urm1 conjugates was reduced compared to H$_6$-Urm1 (488 proteins) (Tables S2A and S1C). A similar effect was also observed for GFP-Sumo, without significantly altering Sumo function.[55] As evident below, both covalent and non-covalent interactions of Urm1 with target proteins cooperate in enhancing the formation of condensates.

Under mild HS (37°C), nuclear mNG-Urm1 foci were predominant, while at higher temperatures both cytoplasmic and nuclear foci were equally abundant (Figure 2B). Foci in both locations were reversible upon recovery (Figure S3H). mNG-Urm1 foci also formed upon energy depletion with 2-deoxyglucose (2-DG), during S.P. growth, or following oxidative stress with tertiary butyl hydroperoxide (t-BuOOH) (Figure 2C). In contrast to 2-DG and t-BuOOH stress, exclusively cytoplasmic foci formed at S.P. (Figures 2C and 2D). Consistently, Urm1 was detected as enriched in the insoluble proteome of WT cells following 2-DG treatment and acute HS (Tables S2C and S2D).

Stress-triggered foci and other biomolecular condensates exhibit sensitivity to 6-hexanediol (1,6-HD).[52,56] Indeed, treatment of chemically starved cells with 1,6-HD led to the dispersal of mNG-Urm1 foci within minutes, followed by reformation upon washout into 2-DG-containing media (Figure S3I). Thus,
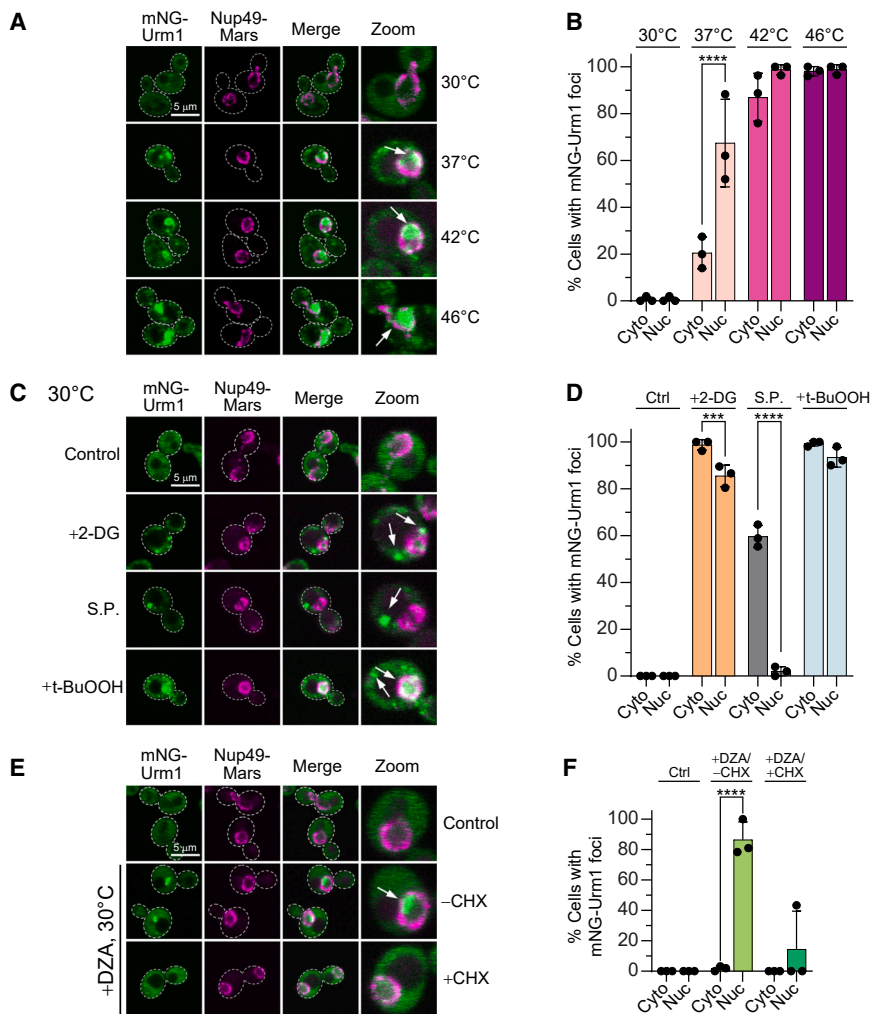
Figure 2. Urm1 assembles into condensates following stress

(A) Localization of mNG-Urm1 with stress. Cells expressing mNG-Urm1 and Nup49-Mars (from endogenous promoters) were grown at 30°C, followed by 15 min HS at the indicated temperatures. Live cell confocal microscopy was performed (n = 3). Arrows point to mNG-Urm1 peri-nucleolar foci. Brightness and contrast adjustments were made to enhance the Nup49-Mars signal.

(B) Quantification of mNG-Urm1 foci from (A). Bar graphs display percentage of foci-containing cells. Error bars: mean ± SEM (n = 3). p values by two-way ANOVA with Holm-Sidak correction. ****p < 0.0001.

(C) Localization of mNG-Urm1 upon 2-DG treatment, stationary phase (S.P.) growth, or oxidative stress. Cells starved with 60 μg/mL 2-DG for 2 h, grown to S.P. for 3 days, or treated with 10 mM tert-butyl hydroperoxide (t-BuOOH) for 1 h were imaged as in (A) (n = 3). Arrows indicate cytoplasmic foci. Brightness/contrast adjusted to enhance Nup49-Mars signal.

(D) Quantification of mNG-Urm1 foci from (C). Error bars: mean ± SEM (n = 3). p values by two-way ANOVA with Holm-Sidak correction. ***p < 0.001; ****p < 0.0001.

(E) Distribution of mNG-Urm1 relative to Nup49-Mars following inhibition of 60S ribosome assembly in cells at 30°C. Cells were treated with 10 μg/mL of diazaborine (DZA) for 30 min, either without (top) or with (bottom) 100 μg/mL cycloheximide (CHX) (STAR Methods). Imaging as in (A). Arrows indicate foci distribution (n = 3).

(F) Quantification of mNG-Urm1 foci from (E). Error bars: mean ± SEM (n = 3). p values by two-way ANOVA with Holm-Sidak correction. ****p < 0.0001.

See also Figure S3.

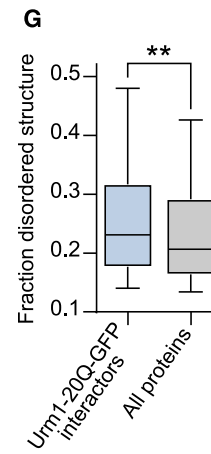mNG-Urm1 foci possess biophysical properties consistent with bio-condensates.
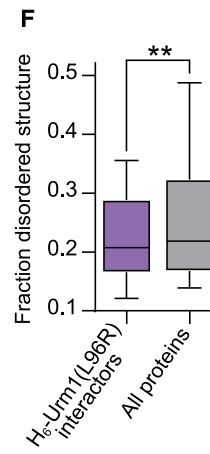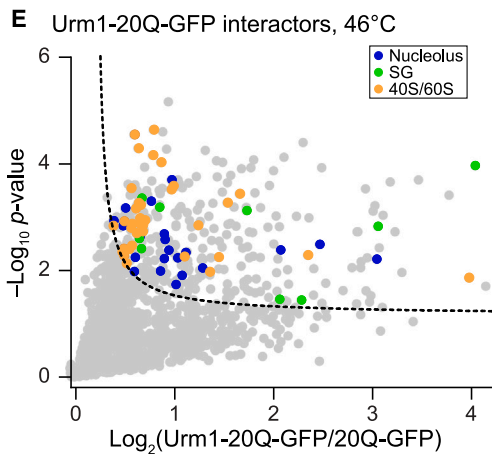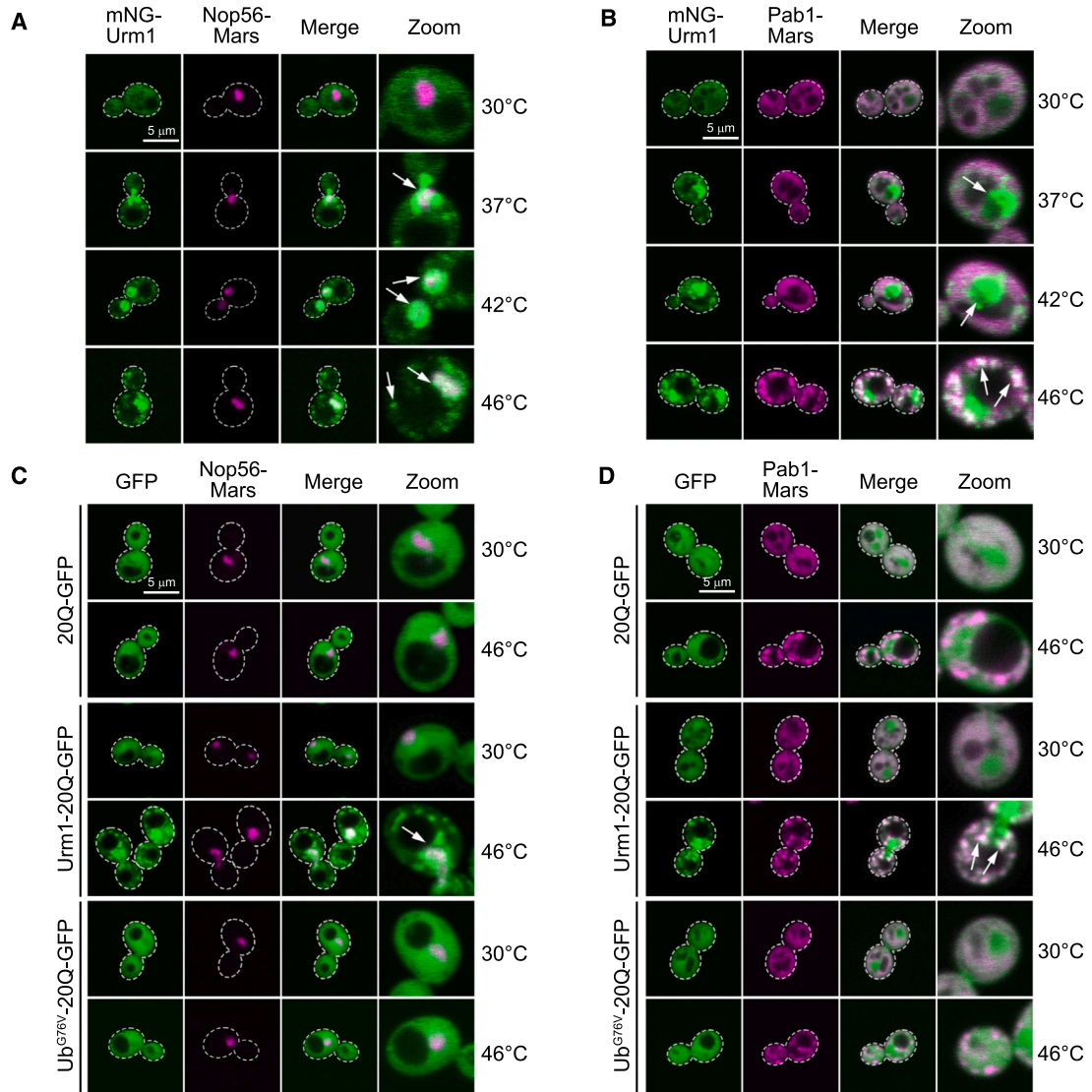
A conserved phenomenon among stress conditions is the inhibition of ribosome production.[57,58] In yeast, arrested ribosome assembly leads to accumulation of ribosome biogenesis factors and unassembled ribosomal proteins within perinucleolar condensates.[8] Since these proteins are prominent insoluble Urm1 targets (Figures 1C, 1D, S3F, and S3G), we tested whether arresting ribosome assembly is sufficient to cause Urm1 condensation. To this end, we inhibited 60S ribosome assembly with diazaborine (DZA), an inhibitor of the AAA-ATPase Drg1 required for 60S assembly, resulting in nuclear accumulation of ribosomal proteins.[8,59] Strikingly, DZA treatment induced nuclear mNG-Urm1 foci (Figures 2E and 2F). Foci formation was blocked by the translation inhibitor cycloheximide (CHX), suggesting that it was triggered, in part, by newly synthesized ribosomal proteins (Figures 2E and 2F). The Hsp40 chaperone Sis1 interacts with unassembled ribosomal proteins upon HS[53] and localizes to nuclear condensates following DZA treatment.[8] We found Sis1 (Sis1-Mars) to colocalize with mNG-Urm1 upon

DZA treatment and HS (Figures S3J and S3K). Remarkably, under all stress conditions analyzed, mNG-Urm1 foci formed without Uba4, indicating conjugation is dispensable for foci formation (Figures S3L and S3M).

In summary, both Urm1 and Uba4 assemble upon stress into cytoplasmic and nuclear foci. These foci share properties of stress-inducible condensates, consistent with the identification of condensate-forming proteins as Urm1 targets.

Urm1 targets to perinucleolar condensates and stress granules

The DZA-triggered formation of nuclear mNG-Urm1 foci suggested that Urm1 co-condenses with unassembled ribosomal proteins and ribosome assembly factors at the nucleolus. Using Nop56-Mars as nucleolar marker, we found mNG-Urm1 accumulated in ring-like structures around the nucleolus under conditions of mild HS (37°C and 42°C) (Figure 3A). The mNG-Urm1 signal became increasingly overlapping with Nop56-Mars at 46°C, coinciding with a change in nucleolar morphology under severe HS[60] (Figure 3A). These mNG-Urm1 assemblies also

A mNG-Urm1 | Nop56-Mars | Merge | Zoom

B mNG-Urm1 | Pab1-Mars | Merge | Zoom

C GFP | Nop56-Mars | Merge | Zoom

D GFP | Pab1-Mars | Merge | Zoom

E Urm1-20Q-GFP interactors, 46°C

F

G

(legend on next page)

colocalized with the nucleolar proteins Ytm1 and Ett1 (endogenously expressed with Mars-tags) (Figure S4A), both covalent Urm1 interactors (Table S1C). Note that while diffusely distributed in the nucleoplasm at 30°C,[9] Ett1 forms foci in the nucleolus under HS (see also Figure S7J). mNG-Uba4 did not significantly concentrate in the nucleolus (Figure S4B). The identification of Urm1 targets (Figures 1C, 1D, S3F, and S3G) suggested an association of Urm1 with SGs. To test this, we coexpressed mNG-Urm1 and the SG marker protein Pab1 (Pab1-Mars).[24] Under HS at 37°C and 42°C, Pab1 remained diffuse in the cytosol, while mNG-Urm1 formed nuclear foci (Figure 3B). However, under severe HS (15 min at 46°C), Pab1-Mars accumulated in SGs that co-localized with cytoplasmic foci of mNG-Urm1 (Figure 3B). Co-localization with Ola1 and Sup45 (endogenously expressed with Mars-tags) (Figure S4A), both covalent Urm1 interactors of SGs (Table S1C), confirmed that these mNG-Urm1 foci as SGs. mNG-Uba4 phenocopied Urm1 in SGs (Figure S4C), suggesting co-assembly of Urm1 and Uba4.

To test whether formation of Urm1 foci is evolutionarily conserved, we monitored the localization of GFP-Urm1 in HeLa cells using nucleophosmin (NPM1) and elongation factor 4G (eIF4G) as nucleolar and SG markers, respectively. In the absence of stress, GFP-Urm1 exhibited a homogeneous signal throughout the cell with some enrichment inside the nucleus (Figures S4D and S4E). Upon HS (2 h at 43°C), GFP-Urm1 formed cytoplasmic foci coinciding with eIF4G, as well as foci distributed throughout the nucleoplasm (Figures S4D and S4E). Some GFP-Urm1 accumulated inside the nucleolus (Figure S4D).

These results show that nuclear foci of Urm1 formed under HS localize around the nucleolus, while the cytoplasmic foci colocalize with SGs. Uba4, the E1-like enzyme of Urm1, also accumulates in SGs.

Urm1 fusion partitions proteins into condensates

The results above suggested that urmylation may facilitate partitioning of target proteins into phase-separated condensates. To explore this, we fused soluble proteins to the C terminus of Urm1, mimicking urmylated substrates. We chose 20Q-GFP, a model protein containing a 20-glutamine low-complexity sequence,[61,62] and the metabolic enzyme phosphoglycerate kinase (Pgk1).[9] In contrast to proteins containing expanded poly-glutamine tracts (>40 Q),[62,63] 20Q-GFP remained diffusely distributed following HS at 46°C and showed no colocalization with Nop56-Mars (nucleolus) or Pab1-Mars (SGs) (Figures 3C and 3D). Urm1-20Q-GFP was diffusely distributed at 30°C but targeted to perinucleolar condensates and SGs upon HS (Figures 3C and 3D), similar to mNG-Urm1 (Figures 3A and 3B). Likewise, a fraction of Urm1-Pgk1-GFP colocalized with Pab1-Mars in SGs under HS, while Pgk1-GFP remained diffusely distributed (Figure S4F). A (non-cleavable) ubiquitin fusion construct, Ub[G76V]-20Q-GFP, did not form visible foci upon HS (Figures 3C and 3D), underscoring that Urm1 exhibits a specific affinity for phase-separated condensates.

Consistently, fusion of Urm1 to an aggregation-prone mutant of firefly luciferase (Urm1-LucDM-GFP)[64] led to larger, more frequent foci under mild HS (37°C, 18 h) as compared to LucDM-GFP (Figure S4G). Notably, large Urm1-LucDM-GFP foci sequestered Pab1 generating "ring-like" assemblies of Pab1-Mars (Figure S4G). Thus, when attached to target proteins, Urm1 mediates non-covalent interactions with RBPs like Pab1, possibly "seeding" higher order assembly. In support of this notion, the interactome of Urm1-20Q-GFP and Urm1-Pgk1-GFP upon HS contained multiple RBPs known to undergo stress-induced phase separation, including SG, nucleolar, and 40S/60S ribosomal proteins that were identified as covalent Urm1 interactors (Figures 3E, S4H, and S4I; Tables S3A and S3B).

These observations suggested that urmylation lowers the threshold for protein condensation. Numerous proteins targeting to condensates contain low-complexity sequences or intrinsically disordered regions (IDRs).[65–67] However, proteins lacking disordered sequences are fundamental constituents of phase-separated assemblies as well.[20,68,69] We therefore analyzed the sequence features of Urm1 interactors using the AlphaFold database. Intriguingly, while the set of urmylated proteins (Table S1C) contains numerous RBPs, we found that covalent Urm1 interactors tend to be less unstructured than proteins on average (Figure 3F; Table S3C), consistent with urmylation occurring preferentially in structured regions (Figure S2D). Of note, several SG proteins identified as covalent Urm1 interactors are fully structured, including the most enriched Urm1 interactor of SGs, Ola1 (Table S1C), a cytoplasmic translation regulator.[69] Interestingly, the HS-dependent interactors of Urm1-20Q-GFP,

---

Figure 3. Urm1 condensates coalesce around the nucleolus and in stress granules

(A) Localization of mNG-Urm1 relative to the nucleolus. Cells co-expressing mNG-Urm1 and Nop56-Mars were grown at 30°C, then shifted to the indicated temperatures for 15 min. Imaging was performed as in Figure 2. Arrows indicate mNG-Urm1 peri-nucleolar foci ($n = 3$).

(B) Distribution of mNG-Urm1 relative to SGs. Cells expressing mNG-Urm1 and Pab1-Mars were cultured and imaged as in (A). Arrows indicate nuclear mNG-Urm1 foci at 37°C and 42°C and co-localization with cytoplasmic SGs at 46°C ($n = 3$).

(C and D) Localization of Urm1 and ubiquitin (Ub[G76V]) fused 20Q-GFP constructs.

(C) Localization of Urm1-20Q-GFP, Ub[G76V]-20Q-GFP, and 20Q-GFP relative to Nop56-Mars in cells at 30°C or following HS (46°C, 15 min) ($n = 3$).

(D) Localization of 20Q-GFP fusion constructs relative to Pab1-Mars. Arrows indicate positioning of Urm1-20Q-GFP ($n = 3$).

(E) Urm1-20Q-GFP interactome following HS (46°C, 15 min). Cell extracts were subjected to anti-GFP immunoprecipitation (STAR Methods), followed by label-free proteomics. 20Q-GFP served as background control. Proteins of interest are highlighted. Line indicates FDR cutoff of 0.05 ($n = 4$). See also Table S3A.

(F) Structural features of H$_6$-Urm1(L96R) covalent interactors. A boxplot compares disordered structure frequencies in insoluble proteins modified by H$_6$-Urm1(L96R) using AlphaFold2 (RRID: SCR_023662) (Table S3C). Boxes indicate the 25th to 75th percentile, whiskers show the 10th to 90th percentile, and the line indicates the median. p values by unpaired t test. **$p < 0.01$.

(G) Structural features of Urm1-20Q-GFP non-covalent interactors. A boxplot as in (F) compares disordered structure frequency in Urm1-20Q-GFP non-covalent interactors versus all detected proteins (Table S3C). p values by unpaired t test. **$p < 0.01$.

See also Figure S4.
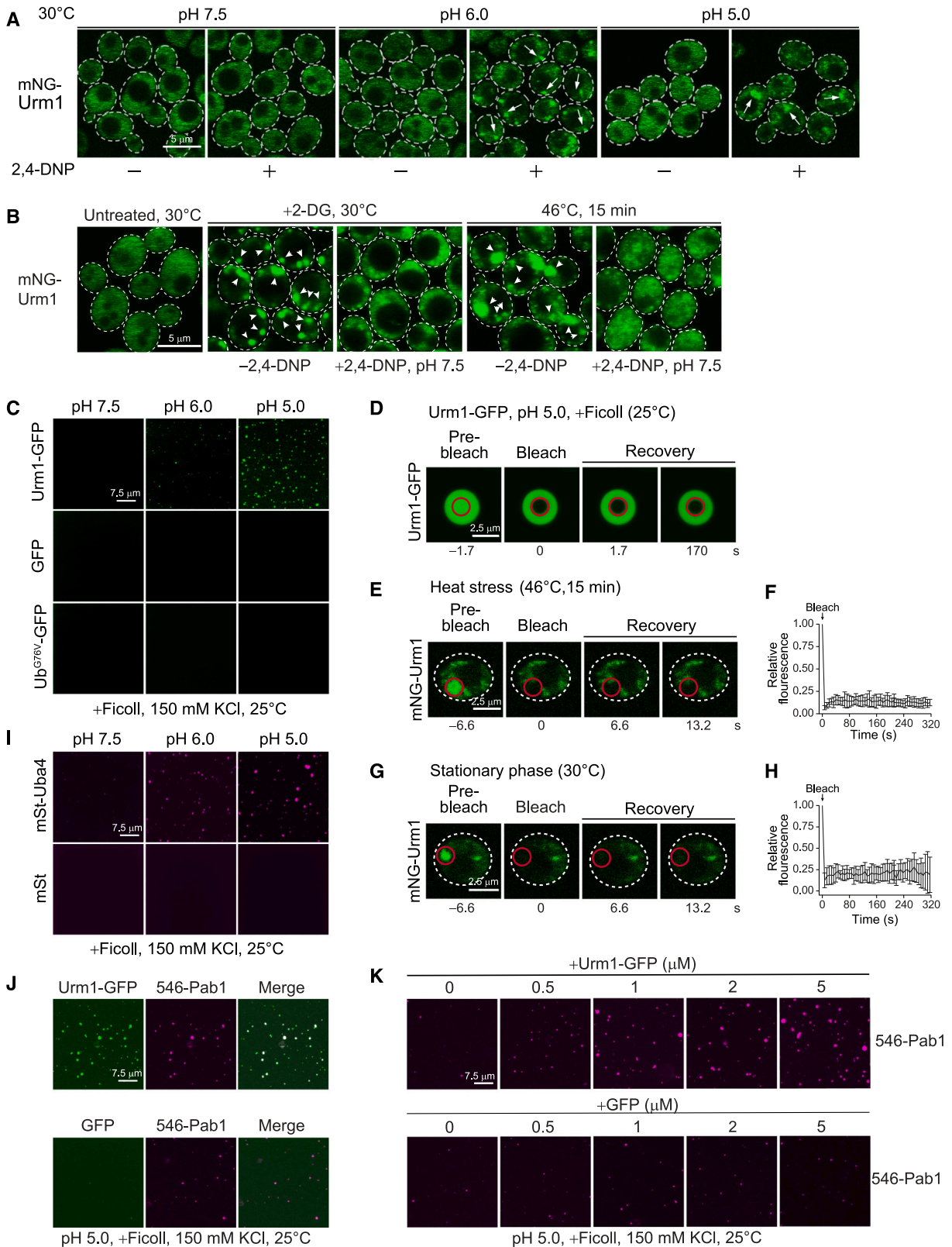
(legend on next page)

which comprise non-covalent Urm1 interactions, showed a trend toward more disorder (Figure 3G; Table S3D), suggesting that non-covalent interactions of Urm1 have a preference for unstructured sequences.

One proposed function of SGs is to protect sequestered proteins from degradation under stress.[70] To investigate whether Urm1 modification may protect against proteolysis, we fused Urm1 to the terminally misfolded, aggregation-prone model protein CG* (CPY*-GFP), which undergoes rapid ubiquitin-dependent proteasomal degradation.[71,72] Under both basal growth conditions and mild HS at 37°C, foci formation of Urm1-CG* (under the *GAL1* promoter) was enhanced compared to CG*. At 37°C, Urm1-CG*, but not CG*, colocalized in foci with Pab1-Mars (Figure S4J), confirming that Urm1 has affinity for SG proteins. Metabolic shut-off by shift to glucose medium revealed marked stabilization of Urm1-CG* compared to CG*, especially at 37°C (Figures S4K and S4L). Thus, Urm1-mediated partitioning of proteins can protect against degradation.

In summary, Urm1 modification is sufficient to mediate partitioning of soluble model proteins into condensates, affording protection against degradation. Covalent and non-covalent protein interactions of Urm1 cooperate in promoting condensate formation.

Urm1 and Uba4 phase separate in response to changes in pH

Stress conditions trigger acidification of the cellular milieu, functioning as a regulator of condensate formation.[19,23–25] To test whether Urm1 foci form upon acidification alone, we incubated cells expressing mNG-Urm1 at 30°C in buffer of various pH values in the presence of the proton carrier 2,4-dinitrophenol (2,4-DNP).[19] Urm1 foci readily formed in the presence of 2,4-DNP at or below pH 6.0, but not at pH 7.5 (Figure 4A). Acidification also induced the assembly of mNG-Uba4 foci (Figure S5A). On the other hand, maintaining pH 7.5 using 2,4-DNP during starvation and HS inhibited mNG-Urm1 foci formation (Figure 4B), and Pab1-Mars failed to co-assemble with mNG-Urm1 into SGs (Figure S5B). Consistently, HS-induced urmylation was reduced at pH 7.5 in both the total and insoluble cell fractions (Figures S5C and S5D). Thus, intracellular acidification is required for Urm1 condensation and efficient urmylation of target proteins.

Next, to understand whether condensate formation upon acidification is intrinsic to Urm1, we analyzed the behavior of recombinantly expressed and purified Urm1-GFP. At pH 7.5, Urm1-GFP (10 μM at 150 mM KCl with crowding agent Ficoll) did not form visible foci (Figure 4C). However, small foci were observed at pH 6 and round droplets of ~0.1–1.5 μm diameter formed at pH 5 (Figure 4C). In contrast, both GFP and Ub^{G76V}-GFP did not form foci. Increasing the sensitivity of fluorescence detection revealed small Urm1-GFP foci at submicromolar concentrations (Figure S5E). Ficoll generally shifted condensate assembly to lower concentrations (Figure S5F). Condensate formation was sensitive to high salt (Figure S5G), indicating involvement of electrostatic interactions. Combining mildly acidic conditions (pH 6.8) with elevated temperature (46°C) to simulate HS[24] slightly increased Urm1-GFP condensate number and size (Figure S5H). The condensates partially dissolved upon shift into neutral buffer (Figure S5I), suggesting pH-regulated reversibility.

Fluorescence recovery after photo bleaching (FRAP) experiments at pH 5 showed that Urm1-GFP condensates were not dynamic (Figure 4D). mNG-Urm1 condensates formed *in vivo* also lacked dynamicity (Figures 4E–4H), independent of Uba4 (Figures S5J–S5M). This lack of dynamicity is consistent with the behavior of other proteins in yeast undergoing phase separation into SGs.[65]

The finding that acidic pH is an important cue for Urm1 self-assembly led us to analyze the surface properties of the Urm1 structure. At pH 7, Urm1 has a negative electrostatic potential (isoelectric point of 4.08). Strikingly, upon shift to pH 5, one face of the molecule is predicted to become increasingly positive, while the opposite face retains net negative charge, possibly triggering higher order assembly (Figure S5N). By comparison, the electrostatic potential of ubiquitin is mostly positive (isoelectric point 7.85) and no major change is predicted upon shift to pH 5 (Figure S5N), consistent with Ub^{G76V}-GFP not undergoing phase separation (Figure 4C). Indeed, in the crystal

Figure 4. Urm1-GFP condensation with decreasing pH

(A) mNG-Urm1 localization at acidic pH. Cells expressing mNG-Urm1 grown at 30°C as in Figure 2A were shifted to phosphate buffer (100 mM) of the indicated pH with (+) or without (−) 2,4-dinitrophenol (2,4-DNP, 2 mM) for 1 h, followed by live cell confocal imaging. Arrows indicate large mNG-Urm1 foci (n = 3).

(B) Analysis of mNG-Urm1 following inhibition of intracellular acidification upon stress. Cells producing mNG-Urm1 as in (A) were treated with 2-DG (2 h) or HS (15 min, 46°C) in pH 7.5 media, in the absence or presence of 2,4-DNP (n = 2). Arrowheads indicate mNG-Urm1 foci.

(C) Condensate formation of purified Urm1-GFP with decreasing pH was analyzed by confocal microscopy to follow the behavior of 10 μM Urm1-GFP, Ub^{G76V}-GFP, or GFP (10 μM each) in buffer containing 150 mM KCl/20% Ficoll at the indicated pH values at 25°C (STAR Methods) (n = 3). Contrast adjustments were made to reduce diffuse background.

(D) Fluorescence recovery after photo bleaching (FRAP) of Urm1-GFP condensates formed as in (C) following incubation in buffer of the indicated salt concentration and pH (STAR Methods). Representative images display fluorescence recovery pre- and post-bleach (n = 3). Red circle marks the bleached area.

(E) FRAP analysis of mNG-Urm1 condensates *in vivo* following HS (n = 3). Red circle marks the bleached area.

(F) Normalized and corrected FRAP values with error bars of 10 independent experimental replicates from (E).

(G) FRAP analysis of mNG-Urm1 condensates *in vivo* following starvation induced by S.P. growth (n = 3). Red circle marks the bleached area.

(H) Normalized and corrected FRAP values with error bars of 10 independent experimental replicates from (G).

(I) Condensate formation of purified mSt-Uba4 across a pH gradient. Purified mSt-Uba4 and mSt alone (2 μM each) were incubated and imaged as in (C) (n = 4).

(J) Co-demixing of Urm1-GFP and Pab1. Purified Pab1 (2 μM), labeled with AlexaFluor 546 (STAR Methods), mixed 1:10 with unlabeled protein, was incubated with Urm1-GFP or GFP (2 μM each) in pH 5 buffer/150 mM KCl/20% Ficoll at 25°C (n = 3).

(K) Co-demixing of Urm1-GFP and Pab1 driving enhanced condensate formation. 546-labelled Pab1(2 μM) was mixed with either Urm1-GFP or GFP, at the indicated concentrations, as described in (J) (n = 3).

See also Figure S5.
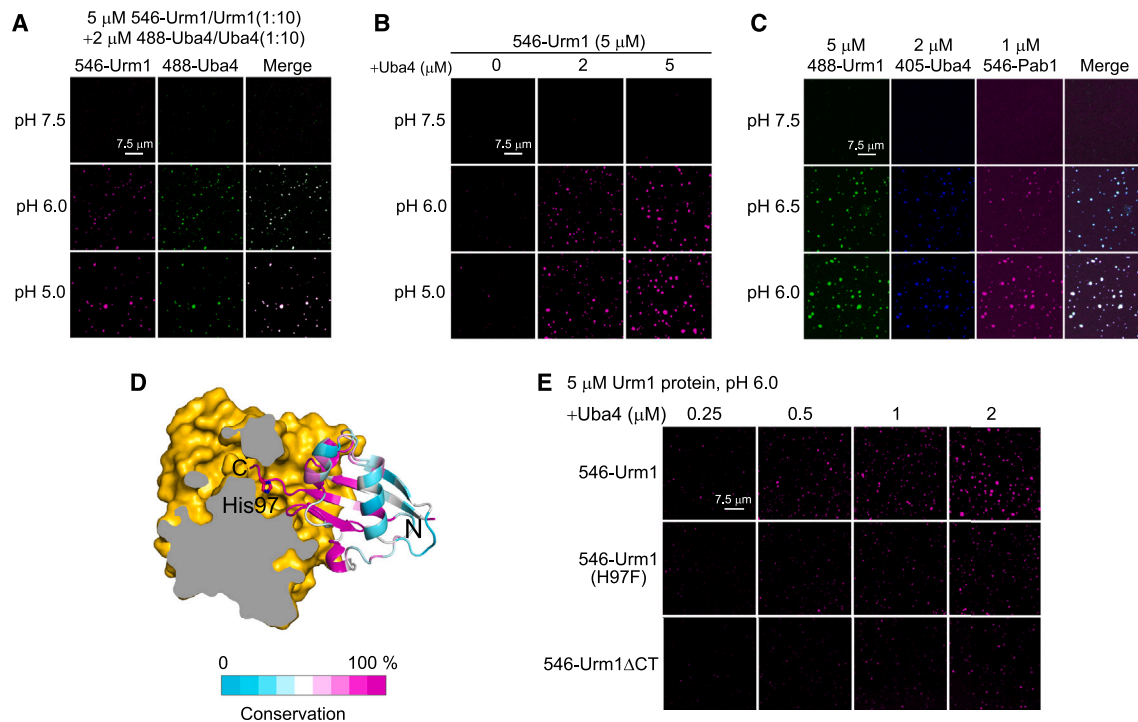
Figure 5. Urm1-Uba4 co-condensate formation

(A) Urm1-Uba4 co-condensate formation *in vitro*. Urm1 (5 μM) and Uba4 (2 μM) were combined in buffer containing 150 mM KCl/20% Ficoll at the indicated pH values at 25°C. Both proteins were labeled with either AlexaFluor 546 or 488 (STAR Methods) and mixed 1:10 with unlabeled protein (*n* = 3). Contrast adjustments were applied to reduce background.

(B) Urm1 condensate formation as a function of Uba4 concentration. Purified Urm1 (5 μM) was incubated alone (0 μM) or with 2 μM or 5 μM Uba4 as in (A). Urm1 was used at a 1:10 mixture of labeled and unlabeled protein, while Uba4 was unlabeled (*n* = 3).

(C) Urm1, Uba4, and Pab1 co-condensate formation *in vitro*. Urm1 (5 μM), Uba4 (2 μM), and Pab1 (1 μM), mixed 1:1:1, were incubated as in (A) at the indicated pH values. Urm1, Uba4, and Pab1 labeled with AlexaFluor 488, 405, and 546, respectively, were used at a 1:10 ratio of labeled:unlabeled protein (*n* = 3).

(D) Conservation of the Urm1-Uba4 interface in the AlphaFold model of *Sc*Urm1 bound to the adenylation domain of Uba4. One copy of the dimeric domain is shown. A cross section (gray) of Uba4 in surface mode is displayed (yellow). Urm1 is shown in ribbon representation. Color gradient indicates amino acid conservation in Urm1. The His97 side chain is shown in stick representation.

(E) Co-condensate formation of Urm1 C-terminal mutant proteins and Uba4. Purified WT Urm1, Urm1(H97F), and Urm1ΔCT (5 μM each) were incubated with Uba4 at increasing concentrations as in (C). Urm1 proteins labeled with AlexaFluor 546 were mixed at a 1:10 ratio with unlabeled protein. Uba4 was unlabeled (*n* = 3). See also Figure S6.

lattice of *S. cerevisiae* Urm1 at pH 6.5 (PDB: 2PKO),[73] the positively charged surface of one Urm1 molecule contacts the negatively charged surface of a neighboring molecule, suggesting an interaction surface for condensate formation.

Interestingly, mScarlet-Uba4 (mSt-Uba4) also showed an intrinsic ability to undergo phase separation like mNG-Urm1 in terms of dependence on pH (Figure 4I), temperature, concentration, and salt sensitivity (Figures S5O–S5Q). However, unlike Urm1-GFP, phase separation of mSt-Uba4 was observed only in the presence of Ficoll (Figure S5P).

Based on these results, Urm1, and to a lesser extent Uba4, has an intrinsic ability to demix into immobile condensates at acidic pH values prevailing in the cellular milieu under stress. Condensate formation appears to be mainly driven by electrostatic interactions.

Co-assembly of Urm1, Uba4, and target proteins *in vitro*

Our analysis had suggested that under stress, Urm1 targets proteins through both covalent and non-covalent interactions. This would imply that Urm1 has an affinity for proteins that accumulate in condensates. To explore this possibility, we used purified Urm1-GFP and Pab1. Incubation of Urm1-GFP (2 μM) with equimolar Pab1 (labeled with Alexa 546 and mixed 1:10 with unlabeled protein) in acidic buffer resulted in co-condensate formation, while pH-induced demixing of 546-Pab1 alone (or with GFP) was less efficient (Figure 4J). Enhanced Pab1 condensate formation was dependent on Urm1-GFP concentration (Figure 4K). Thus, Urm1 has affinity for condensate-forming RBPs, as suggested by the non-covalent interactome of Urm1 (Figures 3E, S4H, and S4I).

Non-covalent association of Urm1 with target proteins may facilitate subsequent urmylation by Uba4, consistent with both proteins accumulating in the same condensates *in vivo* and *in vitro*. We found that purified Urm1 and Uba4 (N-terminally labeled with Alexa Fluor 546 and 488, respectively, and mixed 1:10 with unlabeled protein) formed co-condensates in a pH-dependent manner (Figure 5A). Co-assembly was also reproduced with tagged proteins (Figure S6A). The efficiency of
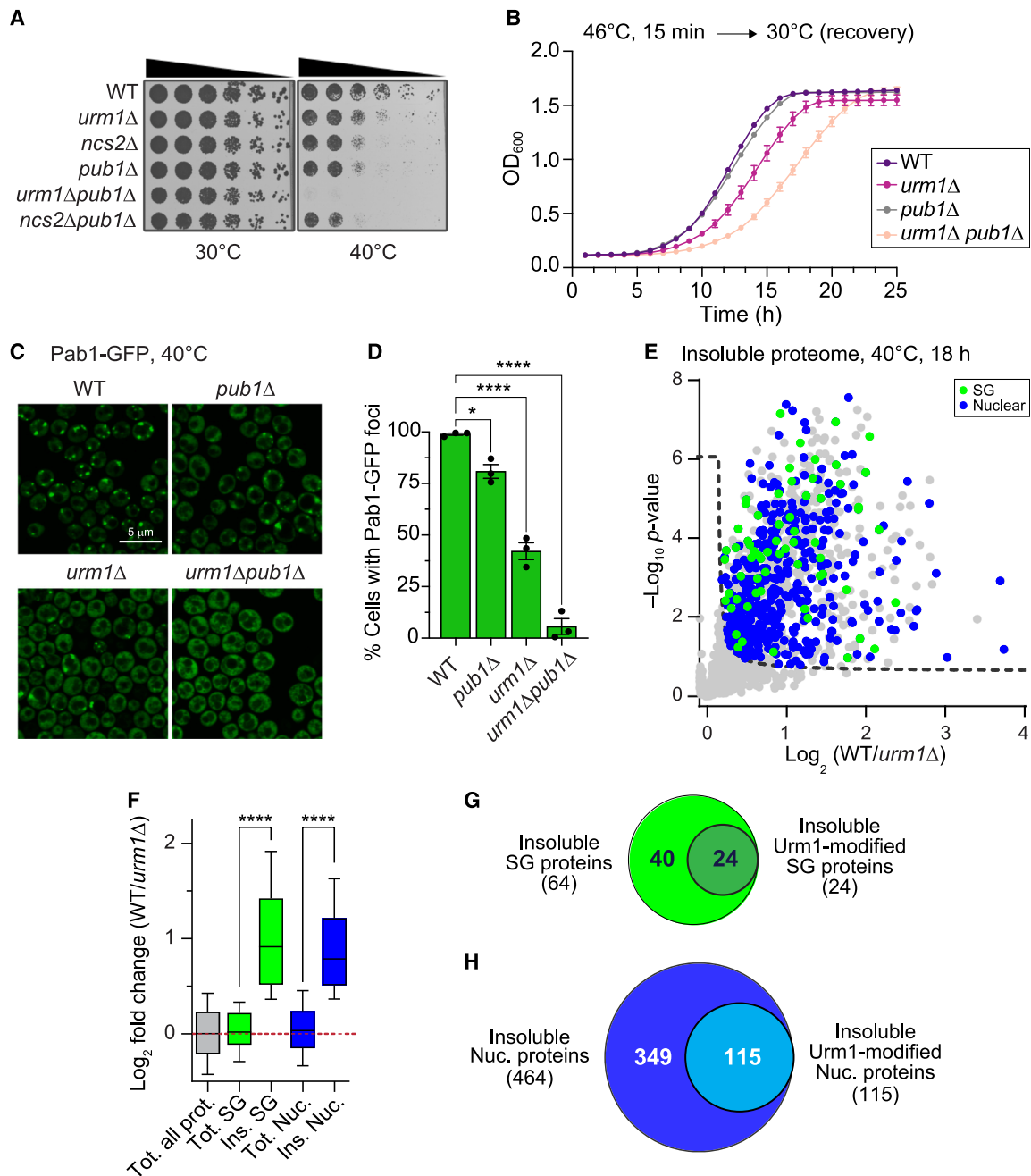
Figure 6. Physiological consequences of Urm1 deficiency

(A) Synthetic growth defect of *URM1* deletion with mutations conferring defective SG assembly. Growth rate analysis of *urm1Δ* cells combined with SG assembly or tRNA thiolation mutants. Cultures were grown in SC-media at 30°C and spotted onto SC media/2% glucose in 5-fold dilution steps. Plates were incubated at 30°C for 2–3 days and at 40°C for 3–4 days (*n* = 3).

(B) Growth defect of *URM1* deletion upon recovery from acute HS. Cells grown as in (A) were exposed to acute HS (15 min, 46°C). Recovery was monitored post-HS at 30°C using a plate reader. A dashed line indicates mid-log OD_{600}. Error bars: mean ± SEM (*n* = 3).

(C) Pab1-GFP assembly in the absence of Urm1 and Pub1. WT, *pub1Δ*, *urm1Δ*, and *urm1Δ pub1Δ* cells expressing Pab1-GFP were grown at 40°C for 18 h, then analyzed using live cell confocal microscopy (*n* = 3).

(D) Quantification of Pab1-GFP foci formation as in (C). Bar graph displays percentage of cells containing Pab1-GFP foci. Error bars: mean ± SEM (*n* = 3). *p* values by one-way ANOVA with Dunnetts's correction. *$p < 0.05$; ****$p < 0.0001$.

(E) Label-free proteomic analysis of WT and *urm1Δ* insoluble proteomes highlighting SG (green) and nuclear proteins (blue). Detergent-solubilized extracts, isolated from WT and *urm1Δ* cells, grown for 18 h at 40°C, were fractionated and insoluble protein subjected to LC-MS/MS (STAR Methods). Black dashed line indicates FDR cutoff of 0.05 (*n* = 4) (Table S4A).

(legend continued on next page)

Urm1 condensation was enhanced by increasing concentrations of Uba4 (Figure 5B). Phase separation was sensitive to increasing ionic strength (Figure S6B), suggesting a role for electrostatics in co-assembly. Notably, incubation of purified Urm1 with Uba4 and ATP resulted in urmylation of Uba4 at acidic pH, with modified Uba4 and free Urm1 sedimenting in the insoluble fraction (Figure S6C). Thus, Uba4 acted both as E1 enzyme and Urm1 target, consistent with its identification as covalent Urm1 interactor under stress (Table S1C). Using differentially labeled Urm1, Uba4, and Pab1, we observed robust co-condensation of all three proteins (Figure 5C). These results suggest that phase separation into co-condensates generates "reaction centers" for urmylation.

We next explored in more detail the interaction between Urm1 and Uba4. An AlphaFold2 model of the *S. cerevisiae* Urm1-Uba4 complex closely resembled the crystal structure of the complex of *Chaetomium thermophilum* (*Ct*) (PDB: 6YUC),[31] revealing a high degree of conservation of Urm1 at the interface with Uba4 (Figure 5D). This interface includes the conserved histidine residue His97 (His99 in *Ct*) in the flexible C-terminal peptide of Urm1.[74] This histidine may contribute to pH sensing during phase separation. It forms van der Waals contacts with Uba4 and is located at a distance (∼2.8 Å) conducive to hydrogen bond formation with Y209 in Uba4 (Y186 in *Ct*Uba4). Notably, protonation of His97 would lead to a charge pair interaction increasing complex stability, providing a critical contact between the two proteins. Indeed, mutation of His97 to Phe, Urm1(H97F), led to a significant reduction in Urm1 phase separation with Uba4, highlighting the importance of the Urm1 C terminus in complex formation and co-condensation (Figure 5E). In line with these findings, deletion of the flexible C-terminal peptide of Urm1 (*urm1ΔCT*) resulted in reduced Uba4-Urm1 co-condensate assembly (Figure 5E).

Taken together, the ability of both Urm1 and Uba4 to phase separate in response to acidification suggests that their stress-dependent functions are coordinated. Formation of co-condensates of Urm1 with Uba4 and Urm1 targets such as Pab1 provides a mechanism allowing specific urmylation of condensate-forming proteins.

Urm1 enhances condensate assembly and is required for stress resilience

What is the physiological significance of stress-dependent Urm1 accumulation in condensates and the modification of proteins within such assemblies? To address this question, we analyzed the effect of HS (3 days at 40°C on solid media) on the growth of *urm1Δ* cells (Figure 6A). Such conditions of prolonged HS, resulting in urmylation in WT cells (Figure S7A), have previously served to evaluate the cellular fitness of SG assembly mutants.[24] As control for the loss of tRNA thiolation by Urm1, we analyzed cells lacking Ncs2.[32,34] Both *urm1Δ* and

ncs2Δ cells displayed a mild growth defect at 40°C, while growing like WT at 30°C (Figure 6A). However, Urm1 deletion combined with deletion of Pub1 (polyadenylated RNA binding-protein 1), causing defective SG assembly,[75] resulted in a strong synthetic growth defect at elevated temperatures (Figure 6A). This growth defect was more pronounced than that of the *ncs2Δpub1Δ* double deletion (Figure 6A) and thus was not caused by defective tRNA thiolation. Consistently, we also observed a delayed growth recovery from acute HS (46°C, 15 min) in *urm1Δ* cells, an effect that was enhanced in the *urm1Δpub1Δ* mutant (Figure 6B).
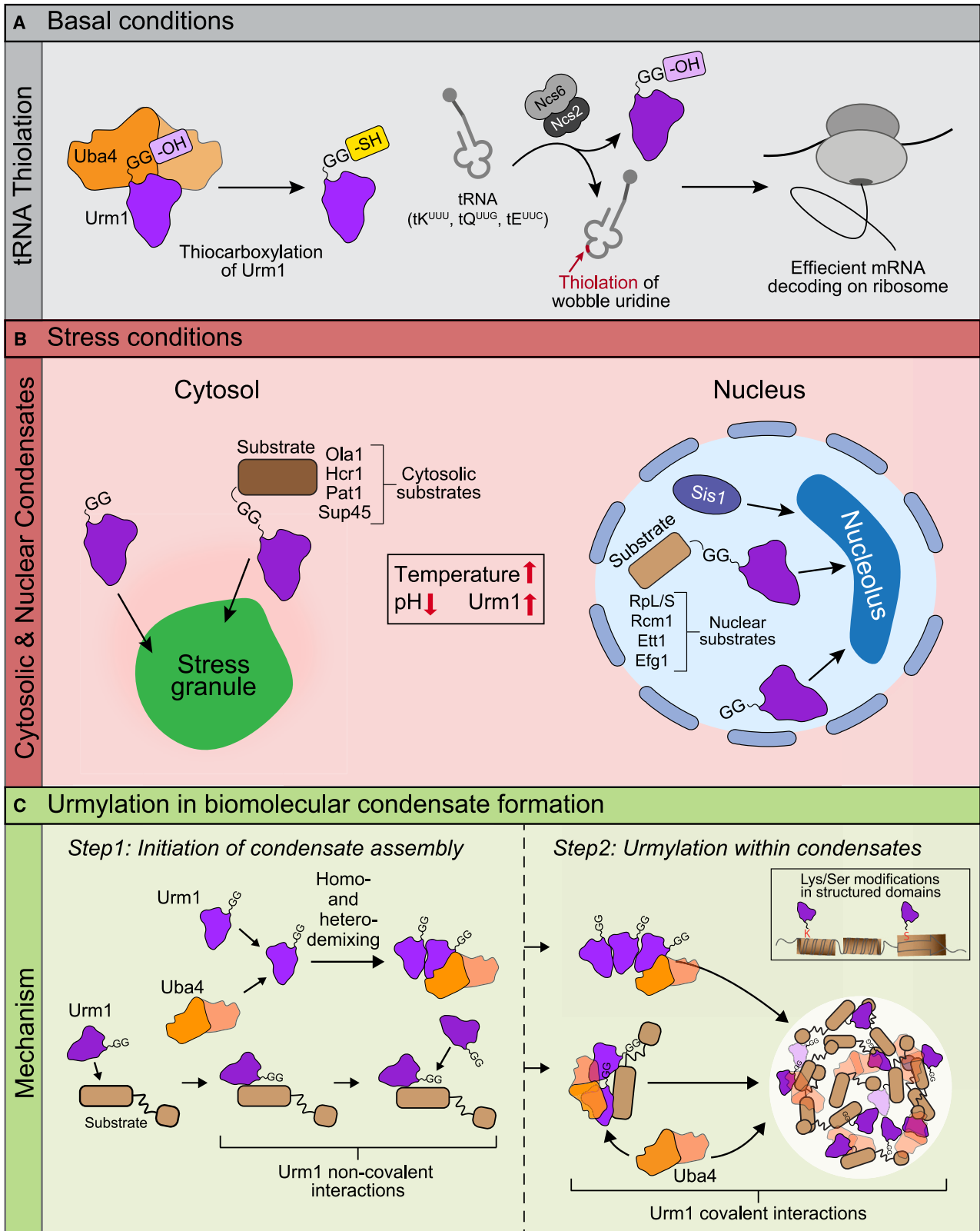
The observed genetic interaction between *URM1* and *PUB1* led us to evaluate SG formation in cells lacking Urm1 under HS conditions that allow for reliable SG quantification (40°C, 18 h). WT cells efficiently formed Pab1-GFP foci, with a modest reduction in *pub1Δ* cells (Figures 6C and 6D). Strikingly, *urm1Δ* cells displayed a pronounced reduction in Pab1-GFP foci, which was further enhanced in the *urm1Δpub1Δ* double mutant, likely explaining the genetic interaction (Figures 6C and 6D). Expression of *URM1* restored Pab1-GFP assembly in *urm1Δ* cells (Figure S7B), while overexpression of three tRNAs (tK^{UUU}, tQ^{UUG}, tE^{UUC}) undergoing thio-modification in WT did not rescue (Figure S7B), demonstrating that defective SG formation was not due to disruption of tRNA thiolation.[32] SG assembly was also defective in *urm1Δ* cells upon acute HS (46°C, 5 min) (Figure S7C) and Pab1 insolubility was reduced (Figures S7D and S7E). Induction of SGs by sodium arsenite[76] was also compromised in *urm1Δ* cells (Figures S7F and S7G).

To assess the SG defect of *urm1Δ* cells at the proteome level, we performed cell fractionation and mass spectrometry. Numerous proteins were significantly less insoluble in *urm1Δ* cells upon HS (40°C, 18 h) compared to WT (Figures 6E and 6F; Table S4A), while their total levels remained unchanged (Figure 6F; Table S4B). Among these were 64 SG proteins (Figures 6E and 6F), comprising 24 of the 32 identified Urm1-modified SG constituents (Figure 6G; Tables S1C and S4A). Indeed, the SG proteins Sup45 and Ola1, both urmylated in heat-stressed WT cells (Table S4A), failed to assemble into Pab1-GFP foci in *urm1Δ* cells (Figures S7H and S7I). Likewise, 464 nuclear proteins were less insoluble in *urm1Δ* cells than in WT upon stress (Figures 6E and 6F), including 115 identified Urm1 targets (Figure 6H; Tables S1C and S4A). As an example, Ett1-GFP, a covalent Urm1 substrate colocalizing within mNG-Urm1 foci (Figure S4A; Table S1C), was diffusely distributed in the nucleoplasm at 30°C and formed foci around the nucleolus under HS in WT cells (Figure S7J). In contrast, Ett1-GFP remained mainly diffuse in *urm1Δ* cells (Figure S7J). Similar to Ett1, many nuclear proteins, including ribosome biogenesis factors and unassembled ribosomal proteins, also form perinucleolar condensates upon HS[8,52] and are urmylation targets (Figure 1C). Many of these proteins were less insoluble upon acute

---

(F) Quantification of SG and nuclear proteins (Nuc.) after HS in WT total (Tot.) and insoluble (Ins.) proteomes compared to *urm1Δ* cells from (E). Boxplot displays total abundance of all proteins identified (3,435 proteins), 62 SG proteins, and 391 nuclear proteins (Nuc.) (Table S4B) as well as the abundance in the insoluble fraction of 64 SG and 464 nuclear proteins (Table S4A). *p* values by unpaired t test. ****$p < 0.0001$.

(G and H) Venn diagrams showing the overlap between insoluble SG and nuclear proteins from (F) with covalent Urm1 interactors identified (Figure 1C; Tables S1C and S4A).

See also Figure S7.

A Basal conditions

tRNA Thiolation

Uba4 / Urm1 / GG -OH → Thiocarboxylation of Urm1 → GG -SH

tRNA (tK^UUU, tQ^UUG, tE^UUC) → Ncs6 / Ncs2 → GG -OH

Thiolation of wobble uridine

Effiecient mRNA decoding on ribosome

B Stress conditions

Cytosolic & Nuclear Condensates

Cytosol

Substrate — Ola1 / Hcr1 / Pat1 / Sup45 — Cytosolic substrates

GG

GG → Stress granule

Temperature ↑
pH ↓   Urm1 ↑

Nucleus

Sis1 → Nucleolus

Substrate — GG

RpL/S / Rcm1 / Ett1 / Efg1 — Nuclear substrates

GG

C Urmylation in biomolecular condensate formation

Mechanism

Step1: Initiation of condensate assembly

Urm1 -GG
Uba4

Homo- and hetero-demixing

Urm1 -GG
Substrate

Urm1 non-covalent interactions

Step2: Urmylation within condensates

Lys/Ser modifications in structured domains

Uba4

Urm1 covalent interactions

HS in *urm1Δ* cells compared to WT (Figure S7K; Table S4C), consistent with our finding that disrupting ribosomal biogenesis induces nuclear Urm1 foci (Figure 2E).

Next, to evaluate how Urm1 contributes to condensate formation in the absence of covalent conjugation, we analyzed *uba4Δ* cells under HS. Uba4 deletants also exhibited a de-enrichment of condensate-forming proteins in the insoluble fraction, including many RBPs, SG, and nuclear proteins (Figure S7L; Table S4D). However, the defect in condensate formation was less severe than in *urm1Δ* cells, underscoring the relevance of non-covalent Urm1 interactions. In total, 830 proteins were significantly de-enriched in the pellet fraction in *urm1Δ* cells, compared to 586 proteins in *uba4Δ* cells (Figure S7M; Table S4D). Thus, while non-covalent associations of Urm1 with target proteins contribute to condensate formation, conjugation is required for full Urm1 function. Supporting this conclusion, interactome analysis of Urm1-20Q-GFP (non-conjugatable Urm1-fusion) in *uba4Δ* cells showed a ~40% reduction in the number of associated proteins in the Urm1-20Q-GFP pull-down compared to WT (Figures S7N–S7P; Tables S4E and S4F), including nuclear and cytoplasmic condensate-forming proteins (Figure S7Q; Table S4F). Thus, covalent Urm1 modifications, along with non-covalent associations, generate a network of interactions that underlies efficient condensate formation and stability.

In summary, the function of Urm1 in enhancing condensate formation is required for cellular fitness and stress resilience. Both covalent and non-covalent interactions of Urm1 with target proteins cooperate in condensate assembly.

DISCUSSION

The ubiquitin-like modifier Urm1 mediates tRNA thiolation under normal growth conditions[32] (Figure 7A). Here, we found that upon stress, Urm1 functions to enhance the formation of biomolecular condensates (Figure 7B). Stress-dependent acidification triggers Urm1 phase separation together with the E1-like enzyme Uba4, allowing Urm1 conjugation to target proteins. Both covalent and non-covalent interactions of Urm1 function to "anchor" substrates to stress induced condensates (Figure 7C). Cells lacking Urm1 exhibit condensate defects and compromised stress resilience.

Urm1 as enhancer of stress-dependent phase separation

Urm1 modification enhances the sequestration of ribosomal biogenesis factors, unassembled ribosomal proteins, and translation factors (including SG components), thereby assisting stress-dependent inhibition of protein synthesis. Urm1 condensation would further downregulate translation by switching off tRNA thiolation, known to subside under stress[77,78] (Figures 7A and 7B). This function of Urm1 contrasts with the stress-related functions of ubiquitin. While accumulation of ubiquitin-modified substrates in condensates has been reported,[26] HS-induced ubiquitylation occurs predominantly on soluble targets.[44] This is in line with ubiquitin mediating proteasomal degradation[30,79,80] and its involvement in SG disassembly.[26] Indeed, unlike free Urm1, free ubiquitin does not phase separate at acidic pH (Figure 4C). In contrast, urmylation occurs predominantly on insoluble substrates, likely because of the physicochemical property of Urm1 to phase separate upon stress (Figure 4C). Therefore, the ability of Urm1 to enhance condensate formation may serve to protect Urm1 targets from ubiquitin-mediated degradation, as demonstrated for the terminally misfolded protein CG* (Figures S4J–S4L).

Urmylation modulates the biophysical properties of proteins, lowering the concentration required for phase separation. Fusion of Urm1 to highly soluble 20Q or Pgk1 was sufficient to induce stress-dependent phase separation of these proteins (Figures 3 and S4). However, given the limited abundance of Urm1, only a fraction of insoluble protein would typically be urmylated. Nevertheless, it is remarkable that deletion of Urm1 has major effects on protein insolubility and condensate formation (Figure 6). Thus, Urm1 modification of multiple proteins, amounting to a fraction of total for each individual species, appears to be highly effective in enhancing condensate formation.

Urm1 targets include both proteins enriched in low complexity sequences (such as RBPs) and proteins with ordered structure (Figure 3). We envision that Urm1 promotes condensate formation in a two-step mechanism: Phase separation is initiated through non-covalent interactions of Urm1 with substrates, coupled with multivalent Urm1 homo-demixing and hetero-demixing with Uba4 (Figure 7C, step 1). This is based on the finding that purified Urm1 phase separates in vitro (Figure 4C), co-assembles with condensate-forming RBPs (Figures 3, 4, 5, S3, and S5), and targets to nuclear and cytoplasmic condensates in the absence of conjugation (Figures S3L and S3M). These non-covalent Urm1 associations may be directed toward unstructured regions of phase-separating target proteins and are followed by covalent Urm1 modification of preferentially structured regions (Figure 7C, step 2). As a result, Urm1 profoundly modulates the composition and stability of condensates.

Covalent modifications are likely initiated at stress onset through heterotypic non-covalent interactions between Urm1, Uba4, and target proteins in the dilute phase (Figure 7C). As SG assembly occurs in distinct steps, involving the formation

---

Figure 7. Hypothetical model for Urm1 function in condensate formation

(A) Under basal growth conditions, the Urm1 pathway enables 2-thiolation of tRNAs, crucial for efficient mRNA decoding on ribosomes.

(B) Repurposing of the Urm1 pathway on the cellular scale. Cell stress is associated with a drop in cellular pH. Urm1 is upregulated and targets to SGs and the nucleolus. Stress-induced Urm1 modification enhances condensate assembly. Urm1-modified SG proteins include Ola1, Hcr1, Pat1, and Sup45 (Figures S7H and S7I; Table S1C). Urm1-modified proteins of perinucleolar condensates include ribosomal proteins (RpL/S), Rcm1, Ett1, and Efg1 (Figure S7J; Table S1C). Perinucleolar condensates accumulate the Hsp40 chaperone Sis1.

(C) Molecular details of Urm1-driven condensate assembly. Step 1: Condensate assembly is initiated by Urm1 self-associations along with non-covalent binding to target proteins containing unstructured regions (prevalent in RBPs). Step 2: Urm1, Uba4, and target proteins form a co-condensate in which covalent Urm1 modification of target proteins (preferentially in structured regions) is enhanced (see Discussion for details).

of "seeds" that merge into larger assemblies,[70] urmylation may "congeal" early intramolecular interactions. Co-condensation of Uba4 (Figures 5 and S6C) offers a plausible explanation as to why no E2 or E3 enzymes may be required for urmylation (Figure 7C).

How are condensates containing urmylated protein dispersed with the cessation of stress? The low dynamicity of Urm1 assemblies mirror the material properties of other HS-induced condensates in yeast, including SGs,[24,81] suggesting overlapping mechanisms of dissociation involving the (Sis1)/Hsp70/Hsp104 disaggregation machinery.[82] This would be consistent with the accumulation of Sis1 in mNG-Urm1 condensates (Figure S3J).

Mechanism of Urm1 stress sensing and phase separation

Under various stress conditions, Urm1 shifts from a soluble state to assembling into condensates (Figures 2, 3, and 4). HS and starvation are stresses resulting in acidification of the cellular milieu, correlating with Urm1 upregulation (Figures S1D–S1G). Assembly in response to acidification has been documented for other condensate-forming proteins, including Pab1 and Ded1,[19,23,24,83] which contain low-complexity sequences and/or PrDs.[66,84–88] Notably, such sequence features are absent in the compact beta-grasp fold of Urm1 and other ubiquitin-like modifiers.[43]

How then is Urm1 phase separation regulated? For both Pab1 and Ded1, secondary and tertiary structure conformational changes underly phase separation.[24,83,89] pH-induced conformational changes may also occur in Urm1, but its structure must remain intact to preserve interaction with Uba4, required for target urmylation. Urm1 condensates are sensitive to increasing ionic strength, suggesting electrostatic interactions play a critical role (Figure S5G). Consistently, *in silico* analysis predicts that the negative surface potential of Urm1 at pH 7 changes at lower pH, with part of the surface gaining positive electrostatic potential (Figure S5N). Thus, attractive electrostatic forces between surfaces may govern Urm1 multivalency, as reflected in the arrangement of Urm1 molecules in the crystal lattice.[73] In support of this proposed mechanism, removing the conserved His97 at the Urm1 C terminus reduced pH-induced phase separation in the presence of Uba4, thereby impairing co-condensation (Figure 5).

Limitations of the study

Our study supports a model where Urm1 functions to promote condensate formation under stress. However, further work is required to understand the molecular details underlying Urm1 phase separation. We note that the use of mNG-Urm1 for cellular imaging represents a technical limitation, as untagged Urm1 could not be visualized, possibly due to epitope inaccessibility. As a result of the reduced conjugation efficiency of mNG-Urm1, our imaging experiments may underrepresent the role of covalent modification relative to phase separation in Urm1 physiology. Nevertheless, the intrinsic ability of Urm1 to recognize and associate non-covalently with condensate-forming proteins deserves further investigation. An important question concerns the possible existence of "Urm1 interaction do-

mains" in target proteins. Finally, future experiments need to address how urmylation is reversed, as a deurmylase has not yet been identified.

STAR★METHODS

Detailed methods are provided in the online version of this paper and include the following:

- KEY RESOURCES TABLE
- RESOURCE AVAILABILITY
  - Lead contact
  - Materials availability
  - Data and code availability
- EXPERIMENTAL MODEL AND PARTICIPANT DETAILS
- METHOD DETAILS
  - Yeast strains
  - Plasmid construction
  - Heat stress, starvation, oxidative stress, diazaborine, and sodium arsenite treatment
  - Manipulation of cellular pH with 2,4-dinitrophenol
  - 1,6-Hexanediol treatment
  - Serial dilution growth assay
  - Real-time growth assay monitoring recovery from acute HS
  - Mammalian cell growth
  - Mammalian cell transfection
  - Preparation of whole cell extracts for immunoblotting analysis
  - Analysis by SDS-PAGE
  - Analysis by immunoblotting
  - CG* turnover assay using metabolic shut-off
  - Affinity purification of H_6-Urm1(L96R) and H_6-mNG-Urm1(L96R) modified proteins
  - Immunoprecipitation of Urm1-20Q-GFP and Urm1-Pgk1-GFP
  - Cell fractionation analysis
  - Fluorescence microscopy
  - Protein expression and purification
  - Imaging of protein condensates
  - *In vitro* urmylation assay
  - FRAP of protein condensates
  - In-Gel digestion for IP interactomes and insoluble proteomes
  - In-solution digestion for total proteomics
  - LC-MS/MS analysis for in-gel digestion
  - LC-MS/MS analysis for in-solution digestion
  - MS data analysis
  - Analysis of urmylation site structuredness
  - Modeling of the Urm1-Uba4 core complex from *S. cerevisiae*
  - Sequence alignment using ConSurf
  - Analysis of *sc*Urm1 and *sc*Ub electrostatic surface potential
- QUANTIFICATION AND STATISTICAL ANALYSIS

SUPPLEMENTAL INFORMATION

Supplemental information can be found online at https://doi.org/10.1016/j.cell.2024.06.009.

REFERENCES

1. Jayaraj, G.G., Hipp, M.S., and Hartl, F.U. (2020). Functional Modules of the Proteostasis Network. Biol. *12*, a033951. https://doi.org/10.1101/cshperspect.a033951.

2. Chen, B., Retzlaff, M., Roos, T., and Frydman, J. (2011). Cellular strategies of protein quality control. Cold Spring Harb. Perspect. Biol. *3*, a004374. https://doi.org/10.1101/cshperspect.a004374.

3. Balch, W.E., Morimoto, R.I., Dillin, A., and Kelly, J.W. (2008). Adapting proteostasis for disease intervention. Science *319*, 916–919. https://doi.org/10.1126/science.1141448.

4. Lindquist, S., and Craig, E.A. (1988). The heat-shock proteins. Annu. Rev. Genet. *22*, 631–677. https://doi.org/10.1146/annurev.ge.22.120188.003215.

5. Morimoto, R.I. (1998). Regulation of the heat shock transcriptional response: cross talk between a family of heat shock factors, molecular chaperones, and negative regulators. Genes Dev. *12*, 3788–3796. https://doi.org/10.1101/gad.12.24.3788.

6. Protter, D.S.W., and Parker, R. (2016). Principles and properties of stress granules. Trends Cell Biol. *26*, 668–679. https://doi.org/10.1016/j.tcb.2016.05.004.

7. Nuske, E., Marini, G., Richter, D., Leng, W., Bogdanova, A., Franzmann, T.M., Pigino, G., and Alberti, S. (2020). Filament formation by the translation factor eIF2B regulates protein synthesis in starved cells. Biol. Open *9*, bio046391. https://doi.org/10.1242/bio.046391.

8. Tye, B.W., Commins, N., Ryazanova, L.V., Wühr, M., Springer, M., Pincus, D., and Churchman, L.S. (2019). Proteotoxicity from aberrant ribosome biogenesis compromises cell fitness. Elife *8*, e43002. https://doi.org/10.7554/eLife.43002.

9. Wallace, E.W.J., Kear-Scott, J.L., Pilipenko, E.V., Schwartz, M.H., Laskowski, P.R., Rojek, A.E., Katanski, C.D., Riback, J.A., Dion, M.F., Franks, A.M., et al. (2015). Reversible, specific, active aggregates of endogenous proteins assemble upon heat stress. Cell *162*, 1286–1298. https://doi.org/10.1016/j.cell.2015.08.041.

10. Cherkasov, V., Grousl, T., Theer, P., Vainshtein, Y., Glässer, C., Mongis, C., Kramer, G., Stoecklin, G., Knop, M., Mogk, A., and Bukau, B. (2015). Systemic control of protein synthesis through sequestration of translation and ribosome biogenesis factors during severe heat stress. FEBS Lett. *589*, 3654–3664. https://doi.org/10.1016/j.febslet.2015.10.010.

11. Grousl, T., Ivanov, P., Malcova, I., Pompach, P., Frydlova, I., Slaba, R., Senohrabkova, L., Novakova, L., and Hasek, J. (2013). Heat shock-induced accumulation of translation elongation and termination factors precedes

12. Buchan, J.R., and Parker, R. (2009). Eukaryotic stress granules: the ins and outs of translation. Mol. Cell *36*, 932–941. https://doi.org/10.1016/j.molcel.2009.11.020.

13. Grousl, T., Ivanov, P., Frýdlová, I., Vasicová, P., Janda, F., Vojtová, J., Malínská, K., Malcová, I., Nováková, L., Janosková, D., et al. (2009). Robust heat shock induces eIF2alpha-phosphorylation-independent assembly of stress granules containing eIF3 and 40S ribosomal subunits in budding yeast, *Saccharomyces cerevisiae*. J. Cell Sci. *122*, 2078–2088. https://doi.org/10.1242/jcs.045104.

14. Kedersha, N., and Anderson, P. (2007). Mammalian stress granules and processing bodies. Methods Enzymol. *431*, 61–81. https://doi.org/10.1016/S0076-6879(07)31005-7.

15. Lafontaine, D.L.J., Riback, J.A., Bascetin, R., and Brangwynne, C.P. (2021). The nucleolus as a multiphase liquid condensate. Nat. Rev. Mol. Cell Biol. *22*, 165–182. https://doi.org/10.1038/s41580-020-0272-6.

16. Lyon, A.S., Peeples, W.B., and Rosen, M.K. (2021). A framework for understanding the functions of biomolecular condensates across scales. Nat. Rev. Mol. Cell Biol. *22*, 215–235.

17. Gomes, E., and Shorter, J. (2019). The molecular language of membraneless organelles. J. Biol. Chem. *294*, 7115–7127. https://doi.org/10.1074/jbc.TM118.001192.

18. Yoo, H., Triandafillou, C., and Drummond, D.A. (2019). Cellular sensing by phase separation: Using the process, not just the products. J. Biol. Chem. *294*, 7151–7159. https://doi.org/10.1074/jbc.TM118.001191.

19. Franzmann, T.M., Jahnel, M., Pozniakovsky, A., Mahamid, J., Holehouse, A.S., Nüske, E., Richter, D., Baumeister, W., Grill, S.W., Pappu, R.V., et al. (2018). Phase separation of a yeast prion protein promotes cellular fitness. Science *359*, eaao5654. https://doi.org/10.1126/science.aao5654.

20. Banani, S.F., Lee, H.O., Hyman, A.A., and Rosen, M.K. (2017). Biomolecular condensates: organizers of cellular biochemistry. Nat. Rev. Mol. Cell Biol. *18*, 285–298. https://doi.org/10.1038/nrm.2017.7.

21. Shin, Y., and Brangwynne, C.P. (2017). Liquid phase condensation in cell physiology and disease. Science *357*, eaaf4382. https://doi.org/10.1126/science.aaf4382.

22. Triandafillou, C.G., Katanski, C.D., Dinner, A.R., and Drummond, D.A. (2020). Transient intracellular acidification regulates the core transcriptional heat shock response. Elife *9*, e54880. https://doi.org/10.7554/eLife.54880.

23. Kroschwald, S., Munder, M.C., Maharana, S., Franzmann, T.M., Richter, D., Ruer, M., Hyman, A.A., and Alberti, S. (2018). Different material states of Pub1 condensates define distinct modes of stress adaptation and recovery. Cell Rep. *23*, 3327–3339. https://doi.org/10.1016/j.celrep.2018.05.041.

24. Riback, J.A., Katanski, C.D., Kear-Scott, J.L., Pilipenko, E.V., Rojek, A.E., Sosnick, T.R., and Drummond, D.A. (2017). Stress-triggered phase separation is an adaptive, evolutionarily tuned response. Cell *168*, 1028–1040.e19. https://doi.org/10.1016/j.cell.2017.02.027.

25. Munder, M.C., Midtvedt, D., Franzmann, T., Nüske, E., Otto, O., Herbig, M., Ulbricht, E., Müller, P., Taubenberger, A., Maharana, S., et al. (2016). A pH-driven transition of the cytoplasm from a fluid- to a solid-like state promotes entry into dormancy. Elife *5*, e09347. https://doi.org/10.7554/eLife.09347.

26. Maxwell, B.A., Gwon, Y., Mishra, A., Peng, J., Nakamura, H., Zhang, K., Kim, H.J., and Taylor, J.P. (2021). Ubiquitination is essential for recovery of cellular activities after heat shock. Science *372*, eabc3593. https://doi.org/10.1126/science.abc3593.

27. Keiten-Schmitz, J., Wagner, K., Piller, T., Kaulich, M., Alberti, S., and Müller, S. (2020). The nuclear SUMO-targeted ubiquitin quality control network regulates the dynamics of cytoplasmic stress granules. Mol. Cell *79*, 54–67.e7. https://doi.org/10.1016/j.molcel.2020.05.017.

assembly of stress granules in *S. cerevisiae*. PLoS One *8*, e57083. https://doi.org/10.1371/journal.pone.0057083.

28. Enserink, J.M. (2015). SUMO and the cellular stress response. Cell Div. *10*, 4. https://doi.org/10.1186/s13008-015-0010-1.

29. Flick, K., and Kaiser, P. (2012). Protein degradation and the stress response. Semin. Cell Dev. Biol. *23*, 515–522. https://doi.org/10.1016/j.semcdb.2012.01.019.

30. Finley, D., Ulrich, H.D., Sommer, T., and Kaiser, P. (2012). The ubiquitin-proteasome system of *Saccharomyces cerevisiae*. Genetics *192*, 319–360. https://doi.org/10.1534/genetics.112.140467.

31. Pabis, M., Termathe, M., Ravichandran, K.E., Kienast, S.D., Krutyhołowa, R., Sokołowski, M., Jankowska, U., Grudnik, P., Leidel, S.A., and Glatt, S. (2020). Molecular basis for the bifunctional Uba4-Urm1 sulfur-relay system in tRNA thiolation and ubiquitin-like conjugation. EMBO J. *39*, e105087. https://doi.org/10.15252/embj.2020105087.

32. Leidel, S., Pedrioli, P.G.A., Bucher, T., Brost, R., Costanzo, M., Schmidt, A., Aebersold, R., Boone, C., Hofmann, K., and Peter, M. (2009). Ubiquitin-related modifier Urm1 acts as a sulphur carrier in thiolation of eukaryotic transfer RNA. Nature *458*, 228–232. https://doi.org/10.1038/nature07643.

33. Pedrioli, P.G.A., Leidel, S., and Hofmann, K. (2008). Urm1 at the crossroad of modifications. 'Protein modifications: Beyond the usual suspects' Review Series. EMBO Rep. *9*, 1196–1202. https://doi.org/10.1038/embor.2008.209.

34. Nedialkova, D.D., and Leidel, S.A. (2015). Optimization of codon translation rates via tRNA modifications maintains proteome integrity. Cell *161*, 1606–1618. https://doi.org/10.1016/j.cell.2015.05.022.

35. Ravichandran, K.E., Kaduhr, L., Skupien-Rabian, B., Shvetsova, E., Sokołowski, M., Krutyhołowa, R., Kwasna, D., Brachmann, C., Lin, S., Guzman Perez, S., et al. (2022). E2/E3-independent ubiquitin-like protein conjugation by Urm1 is directly coupled to cysteine persulfidation. EMBO J. *41*, e111318. https://doi.org/10.15252/embj.2022111318.

36. Laxman, S., Sutter, B.M., Wu, X., Kumar, S., Guo, X., Trudgian, D.C., Mirzaei, H., and Tu, B.P. (2013). Sulfur amino acids regulate translational capacity and metabolic homeostasis through modulation of tRNA thiolation. Cell *154*, 416–429. https://doi.org/10.1016/j.cell.2013.06.043.

37. Van der Veen, A.G., Schorpp, K., Schlieker, C., Buti, L., Damon, J.R., Spooner, E., Ploegh, H.L., and Jentsch, S. (2011). Role of the ubiquitin-like protein Urm1 as a noncanonical lysine-directed protein modifier. Proc. Natl. Acad. Sci. USA *108*, 1763–1770. https://doi.org/10.1073/pnas.1014402108.

38. Goehring, A.S., Rivers, D.M., and Sprague, G.F., Jr. (2003). Attachment of the ubiquitin-related protein Urm1p to the antioxidant protein Ahp1p. Eukaryot. Cell *2*, 930–936. https://doi.org/10.1128/ec.2.5.930-936.2003.

39. Furukawa, K., Mizushima, N., Noda, T., and Ohsumi, Y. (2000). A protein conjugation system in yeast with homology to biosynthetic enzyme reaction of prokaryotes. J. Biol. Chem. *275*, 7462–7465. https://doi.org/10.1074/jbc.275.11.7462.

40. Jüdes, A., Bruch, A., Klassen, R., Helm, M., and Schaffrath, R. (2016). Sulfur transfer and activation by ubiquitin-like modifier system Uba4·Urm1 link protein urmylation and tRNA thiolation in yeast. Microb. Cell *3*, 554–564. https://doi.org/10.15698/mic2016.11.539.

41. Jüdes, A., Ebert, F., Bär, C., Thüring, K.L., Harrer, A., Klassen, R., Helm, M., Stark, M.J.R., and Schaffrath, R. (2015). Urmylation and tRNA thiolation functions of ubiquitin-like Uba4·Urm1 systems are conserved from yeast to man. FEBS Lett. *589*, 904–909. https://doi.org/10.1016/j.febslet.2015.02.024.

42. Termathe, M., and Leidel, S.A. (2021). Urm1: A non-canonical UBL. Biomolecules *11*, 139. https://doi.org/10.3390/biom11020139.

43. Cappadocia, L., and Lima, C.D. (2018). Ubiquitin-like protein conjugation: Structures, chemistry, and mechanism. Chem. Rev. *118*, 889–918. https://doi.org/10.1021/acs.chemrev.6b00737.

44. Lu, K., den Brave, F., and Jentsch, S. (2017). Receptor oligomerization guides pathway choice between proteasomal and autophagic degradation. Nat. Cell Biol. *19*, 732–739. https://doi.org/10.1038/ncb3531.

45. Fang, N.N., Zhu, M., Rose, A., Wu, K.P., and Mayor, T. (2016). Deubiquitinase activity is required for the proteasomal degradation of misfolded cytosolic proteins upon heat-stress. Nat. Commun. *7*, 12907. https://doi.org/10.1038/ncomms12907.

46. Seifert, A., Schofield, P., Barton, G.J., and Hay, R.T. (2015). Proteotoxic stress reprograms the chromatin landscape of SUMO modification. Sci. Signal. *8*, rs7. https://doi.org/10.1126/scisignal.aaa2213.

47. Fang, N.N., Chan, G.T., Zhu, M., Comyn, S.A., Persaud, A., Deshaies, R.J., Rotin, D., Gsponer, J., and Mayor, T. (2014). Rsp5/Nedd4 is the main ubiquitin ligase that targets cytosolic misfolded proteins following heat stress. Nat. Cell Biol. *16*, 1227–1237. https://doi.org/10.1038/ncb3054.

48. Golebiowski, F., Matic, I., Tatham, M.H., Cole, C., Yin, Y., Nakamura, A., Cox, J., Barton, G.J., Mann, M., and Hay, R.T. (2009). System-wide changes to SUMO modifications in response to heat shock. Sci. Signal. *2*, ra24. https://doi.org/10.1126/scisignal.2000282.

49. Brachmann, C., Kaduhr, L., Jüdes, A., Ravichandran, K.E., West, J.D., Glatt, S., and Schaffrath, R. (2020). Redox requirements for ubiquitin-like urmylation of Ahp1, a 2-Cys peroxiredoxin from yeast. Redox Biol. *30*, 101438. https://doi.org/10.1016/j.redox.2020.101438.

50. Psakhye, I., and Jentsch, S. (2016). Identification of substrates of protein-group SUMOylation. Methods Mol. Biol. *1475*, 219–231. https://doi.org/10.1007/978-1-4939-6358-4_16.

51. Lu, K., Psakhye, I., and Jentsch, S. (2014). Autophagic clearance of polyQ proteins mediated by ubiquitin-Atg8 adaptors of the conserved CUET protein family. Cell *158*, 549–563. https://doi.org/10.1016/j.cell.2014.05.048.

52. Ali, A., Garde, R., Schaffer, O.C., Bard, J.A.M., Husain, K., Kik, S.K., Davis, K.A., Luengo-Woods, S., Igarashi, M.G., Drummond, D.A., et al. (2023). Adaptive preservation of orphan ribosomal proteins in chaperone-dispersed condensates. Nat. Cell Biol. *25*, 1691–1703. https://doi.org/10.1038/s41556-023-01253-2.

53. Feder, Z.A., Ali, A., Singh, A., Krakowiak, J., Zheng, X., Bindokas, V.P., Wolfgeher, D., Kron, S.J., and Pincus, D. (2021). Subcellular localization of the J-protein Sis1 regulates the heat shock response. J. Cell Biol. *220*, e202005165. https://doi.org/10.1083/jcb.202005165.

54. Varadi, M., Anyango, S., Deshpande, M., Nair, S., Natassia, C., Yordanova, G., Yuan, D., Stroe, O., Wood, G., Laydon, A., et al. (2022). AlphaFold protein structure database: Massively expanding the structural coverage of protein-sequence space with high-accuracy models. Nucleic Acids Res. *50*, D439-d444. https://doi.org/10.1093/nar/gkab1061.

55. Takahashi, Y., Dulev, S., Liu, X., Hiller, N.J., Zhao, X., and Strunnikov, A. (2008). Cooperation of sumoylated chromosomal proteins in rDNA maintenance. PLoS Genet. *4*, e1000215. https://doi.org/10.1371/journal.pgen.1000215.

56. Wheeler, J.R., Matheny, T., Jain, S., Abrisch, R., and Parker, R. (2016). Distinct stages in stress granule assembly and disassembly. Elife *5*, e18413. https://doi.org/10.7554/eLife.18413.

57. Kraft, C., Deplazes, A., Sohrmann, M., and Peter, M. (2008). Mature ribosomes are selectively degraded upon starvation by an autophagy pathway requiring the Ubp3p/Bre5p ubiquitin protease. Nat. Cell Biol. *10*, 602–610. https://doi.org/10.1038/ncb1723.

58. Kusama, K., Suzuki, Y., Kurita, E., Kawarasaki, T., Obara, K., Okumura, F., Kamura, T., and Nakatsukasa, K. (2022). Dot6/Tod6 degradation fine-tunes the repression of ribosome biogenesis under nutrient-limited conditions. iScience *25*, 103986. https://doi.org/10.1016/j.isci.2022.103986.

59. Loibl, M., Klein, I., Prattes, M., Schmidt, C., Kappel, L., Zisser, G., Gungl, A., Krieger, E., Pertschy, B., and Bergler, H. (2014). The drug diazaborine blocks ribosome biogenesis by inhibiting the AAA-ATPase Drg1. J. Biol. Chem. *289*, 3913–3922. https://doi.org/10.1074/jbc.M113.536110.

60. Boulon, S., Westman, B.J., Hutten, S., Boisvert, F.M., and Lamond, A.I. (2010). The nucleolus under stress. Mol. Cell *40*, 216–227. https://doi.org/10.1016/j.molcel.2010.09.024.

61. Krobitsch, S., and Lindquist, S. (2000). Aggregation of huntingtin in yeast varies with the length of the polyglutamine expansion and the expression

of chaperone proteins. Proc. Natl. Acad. Sci. USA *97*, 1589–1594. https://doi.org/10.1073/pnas.97.4.1589.

62. Muchowski, P.J., Schaffar, G., Sittler, A., Wanker, E.E., Hayer-Hartl, M.K., and Hartl, F.U. (2000). Hsp70 and hsp40 chaperones can inhibit self-assembly of polyglutamine proteins into amyloid-like fibrils. Proc. Natl. Acad. Sci. USA *97*, 7841–7846. https://doi.org/10.1073/pnas.140202897.

63. Morley, J.F., Brignull, H.R., Weyers, J.J., and Morimoto, R.I. (2002). The threshold for polyglutamine-expansion protein aggregation and cellular toxicity is dynamic and influenced by aging in Caenorhabditis elegans. Proc. Natl. Acad. Sci. USA *99*, 10417–10422. https://doi.org/10.1073/pnas.152161099.

64. Gupta, R., Kasturi, P., Bracher, A., Loew, C., Zheng, M., Villella, A., Garza, D., Hartl, F.U., and Raychaudhuri, S. (2011). Firefly luciferase mutants as sensors of proteome stress. Nat. Methods *8*, 879–884. https://doi.org/10.1038/nmeth.1697.

65. Zhu, M., Kuechler, E.R., Zhang, J., Matalon, O., Dubreuil, B., Hofmann, A., Loewen, C., Levy, E.D., Gsponer, J., and Mayor, T. (2020). Proteomic analysis reveals the direct recruitment of intrinsically disordered regions to stress granules in *S. cerevisiae*. J. Cell Sci. *133*, jcs244657. https://doi.org/10.1242/jcs.244657.

66. Nott, T.J., Petsalaki, E., Farber, P., Jervis, D., Fussner, E., Plochowietz, A., Craggs, T.D., Bazett-Jones, D.P., Pawson, T., Forman-Kay, J.D., and Baldwin, A.J. (2015). Phase transition of a disordered nuage protein generates environmentally responsive membraneless organelles. Mol. Cell *57*, 936–947. https://doi.org/10.1016/j.molcel.2015.01.013.

67. Elbaum-Garfinkle, S., Kim, Y., Szczepaniak, K., Chen, C.C.H., Eckmann, C.R., Myong, S., and Brangwynne, C.P. (2015). The disordered P granule protein LAF-1 drives phase separation into droplets with tunable viscosity and dynamics. Proc. Natl. Acad. Sci. USA *112*, 7189–7194. https://doi.org/10.1073/pnas.1504822112.

68. Putnam, A., Cassani, M., Smith, J., and Seydoux, G. (2019). A gel phase promotes condensation of liquid P granules in Caenorhabditis elegans embryos. Nat. Struct. Mol. Biol. *26*, 220–226. https://doi.org/10.1038/s41594-019-0193-2.

69. Dannenmaier, S., Desroches Altamirano, C., Schüler, L., Zhang, Y., Hummel, J., Milanov, M., Oeljeklaus, S., Koch, H.G., Rospert, S., Alberti, S., and Warscheid, B. (2021). Quantitative proteomics identifies the universally conserved ATPase Ola1p as a positive regulator of heat shock response in *Saccharomyces cerevisiae*. J. Biol. Chem. *297*, 101050. https://doi.org/10.1016/j.jbc.2021.101050.

70. Glauninger, H., Wong Hickernell, C.J., Bard, J.A.M., and Drummond, D.A. (2022). Stressful steps: Progress and challenges in understanding stress-induced mRNA condensation and accumulation in stress granules. Mol. Cell *82*, 2544–2556. https://doi.org/10.1016/j.molcel.2022.05.014.

71. Park, S.H., Kukushkin, Y., Gupta, R., Chen, T., Konagai, A., Hipp, M.S., Hayer-Hartl, M., and Hartl, F.U. (2013). PolyQ proteins interfere with nuclear degradation of cytosolic proteins by sequestering the Sis1p chaperone. Cell *154*, 134–145. https://doi.org/10.1016/j.cell.2013.06.003.

72. den Brave, F., Cairo, L.V., Jagadeesan, C., Ruger-Herreros, C., Mogk, A., Bukau, B., and Jentsch, S. (2020). Chaperone-mediated protein disaggregation triggers proteolytic clearance of intra-nuclear protein inclusions. Cell Rep. *31*, 107680. https://doi.org/10.1016/j.celrep.2020.107680.

73. Yu, J., and Zhou, C.Z. (2008). Crystal structure of the dimeric Urm1 from the yeast *Saccharomyces cerevisiae*. Proteins *71*, 1050–1055. https://doi.org/10.1002/prot.21975.

74. Xu, J., Zhang, J., Wang, L., Zhou, J., Huang, H., Wu, J., Zhong, Y., and Shi, Y. (2006). Solution structure of Urm1 and its implications for the origin of protein modifiers. Proc. Natl. Acad. Sci. USA *103*, 11625–11630. https://doi.org/10.1073/pnas.0604876103.

75. Buchan, J.R., Muhlrad, D., and Parker, R. (2008). P bodies promote stress granule assembly in *Saccharomyces cerevisiae*. J. Cell Biol. *183*, 441–455. https://doi.org/10.1083/jcb.200807043.

76. Frydrýšková, K., Mašek, T., and Pospíšek, M. (2020). Changing faces of stress: Impact of heat and arsenite treatment on the composition of stress granules. RNA *11*, e1596. https://doi.org/10.1002/wrna.1596.

77. Alings, F., Sarin, L.P., Fufezan, C., Drexler, H.C.A., and Leidel, S.A. (2015). An evolutionary approach uncovers a diverse response of tRNA 2-thiolation to elevated temperatures in yeast. RNA *21*, 202–212. https://doi.org/10.1261/rna.048199.114.

78. Nawrot, B., Sochacka, E., and Düchler, M. (2011). tRNA structural and functional changes induced by oxidative stress. Cell. Mol. Life Sci. *68*, 4023–4032. https://doi.org/10.1007/s00018-011-0773-8.

79. Varshavsky, A. (2012). The ubiquitin system, an immense realm. Annu. Rev. Biochem. *81*, 167–176. https://doi.org/10.1146/annurev-biochem-051910-094049.

80. Ravid, T., and Hochstrasser, M. (2008). Diversity of degradation signals in the ubiquitin-proteasome system. Nat. Rev. Mol. Cell Biol. *9*, 679–690. https://doi.org/10.1038/nrm2468.

81. Kroschwald, S., Maharana, S., Mateju, D., Malinovska, L., Nüske, E., Poser, I., Richter, D., and Alberti, S. (2015). Promiscuous interactions and protein disaggregases determine the material state of stress-inducible RNP granules. Elife *4*, e06807. https://doi.org/10.7554/eLife.06807.

82. Yoo, H., Bard, J.A.M., Pilipenko, E.V., and Drummond, D.A. (2022). Chaperones directly and efficiently disperse stress-triggered biomolecular condensates. Mol. Cell *82*, 741–755.e11. https://doi.org/10.1016/j.molcel.2022.01.005.

83. Iserman, C., Desroches Altamirano, C., Jegers, C., Friedrich, U., Zarin, T., Fritsch, A.W., Mittasch, M., Domingues, A., Hersemann, L., Jahnel, M., et al. (2020). Condensation of Ded1p promotes a translational switch from housekeeping to stress protein production. Cell *181*, 818–831.e19. https://doi.org/10.1016/j.cell.2020.04.009.

84. Alberti, S., Gladfelter, A., and Mittag, T. (2019). Considerations and challenges in studying liquid-liquid phase separation and biomolecular condensates. Cell *176*, 419–434. https://doi.org/10.1016/j.cell.2018.12.035.

85. Kuechler, E.R., Budzyńska, P.M., Bernardini, J.P., Gsponer, J., and Mayor, T. (2020). Distinct Features of Stress Granule Proteins Predict Localization in Membraneless Organelles. J. Mol. Biol. *432*, 2349–2368. https://doi.org/10.1016/j.jmb.2020.02.020.

86. Posey, A.E., Holehouse, A.S., and Pappu, R.V. (2018). Phase separation of intrinsically disordered proteins. Methods Enzymol. *611*, 1–30. https://doi.org/10.1016/bs.mie.2018.09.035.

87. Smith, J., Calidas, D., Schmidt, H., Lu, T., Rasoloson, D., and Seydoux, G. (2016). Spatial patterning of P granules by RNA-induced phase separation of the intrinsically-disordered protein MEG-3. Elife *5*, e21337. https://doi.org/10.7554/eLife.21337.

88. Wang, J., Choi, J.M., Holehouse, A.S., Lee, H.O., Zhang, X., Jahnel, M., Maharana, S., Lemaitre, R., Pozniakovsky, A., Drechsel, D., et al. (2018). A molecular grammar governing the driving forces for phase separation of prion-like RNA binding proteins. Cell *174*, 688–699.e16. https://doi.org/10.1016/j.cell.2018.06.006.

89. Chen, R., Glauninger, H., Kahan, D.N., Shangguan, J., Sachleben, J.R., Riback, J.A., Drummond, D.A., and Sosnick, T.R. (2024). HDX-MS finds that partial unfolding with sequential domain activation controls condensation of a cellular stress marker. Proc. Natl. Acad. Sci. USA *121*, e2321606121. https://doi.org/10.1073/pnas.2321606121.

90. Mumberg, D., Müller, R., and Funk, M. (1995). Yeast vectors for the controlled expression of heterologous proteins in different genetic backgrounds. Gene *156*, 119–122. https://doi.org/10.1016/0378-1119(95)00037-7.

91. Catanzariti, A.M., Soboleva, T.A., Jans, D.A., Board, P.G., and Baker, R.T. (2004). An efficient system for high-level expression and easy purification of authentic recombinant proteins. Protein Sci. *13*, 1331–1339. https://doi.org/10.1110/ps.04618904.

92. Knop, M., Siegers, K., Pereira, G., Zachariae, W., Winsor, B., Nasmyth, K., and Schiebel, E. (1999). Epitope tagging of yeast genes using a PCR-based strategy: more tags and improved practical routines. Yeast *15*, 963–972. https://doi.org/10.1002/(SICI)1097-0061(199907)15:10B<963::AID-YEA399>3.0.CO;2-W.

93. Storici, F., and Resnick, M.A. (2006). The delitto perfetto approach to in vivo site-directed mutagenesis and chromosome rearrangements with synthetic oligonucleotides in yeast. Methods Enzymol. *409*, 329–345. https://doi.org/10.1016/S0076-6879(05)09019-1.

94. Gibson, D.G., Young, L., Chuang, R.Y., Venter, J.C., Hutchison, C.A., 3rd, and Smith, H.O. (2009). Enzymatic assembly of DNA molecules up to several hundred kilobases. Nat. Methods *6*, 343–345. https://doi.org/10.1038/nmeth.1318.

95. Schindelin, J., Arganda-Carreras, I., Frise, E., Kaynig, V., Longair, M., Pietzsch, T., Preibisch, S., Rueden, C., Saalfeld, S., Schmid, B., et al. (2012). Fiji: an open-source platform for biological-image analysis. Nat. Methods *9*, 676–682. https://doi.org/10.1038/nmeth.2019.

96. Quast, J.-P., Schuster, D., and Picotti, P. (2022). protti: an R package for comprehensive data analysis of peptide- and protein-centric bottom-up proteomics data. Bioinform. Adv. *2*, vbab041. https://doi.org/10.1093/bioadv/vbab041.

97. Ashkenazy, H., Abadi, S., Martz, E., Chay, O., Mayrose, I., Pupko, T., and Ben-Tal, N. (2016). ConSurf 2016: an improved methodology to estimate and visualize evolutionary conservation in macromolecules. Nucleic Acids Res. *44*, W344–W350. https://doi.org/10.1093/nar/gkw408.

STAR★METHODS

KEY RESOURCES TABLE

REAGENT or RESOURCE	SOURCE	IDENTIFIER
Antibodies		
Rabbit polyclonal anti-mNeonGreen (1:1000)	Cell Signaling	Cat# 53061; RRID: AB_2799426
Rabbit polyclonal anti-Urm1 (1:10000)	This study	N/A
Rat monoclonal anti-HA (1:2000)	Roche	Cat# 11867423001; RRID: AB_390918
Mouse monoclonal anti-Pgk1 (1:10000)	Thermo Fisher Scientific	Cat# 459250; RRID: AB_2532235
Goat anti-mouse IgG HRP conjugated (1:1000)	Dako, Agilent	Cat# P044701-2; RRID: AB_2617137
Goat anti-rabbit IgG HRP conjugated (1:10000)	Dako, Agilent	Cat# P044801-2; RRID: AB_2617138
Goat anti-rat IgG HRP conjugated (1:2000)	Sigma-Aldrich	Cat# A9037; RRID: AB_258429
Mouse monoclonal anti-eIF4γ (1:50)	Santa Cruz	Cat# sc-133155; RRID: AB_2095748
Mouse monoclonal anti-NPM1 (1:100)	Thermo Fisher Scientific	Cat# 32-5200; RRID: AB_2533084
Mouse monoclonal anti-Pab1(1:25000)	EnCor Biotechnology	Cat# MCA-1G1; RRID: AB_2572370
Mouse monoclonal anti-GFP (1:5000)	Roche	Cat# 11814460001; RRID: AB_390913
F(ab')2-Goat anti-Mouse IgG (H + L) Cross-Adsorbed Secondary Antibody, Alexa Fluor™ 633 (1:500)	Thermo Fisher Scientific	Cat# A-21053; RRID: AB_2535720
Goat anti-Mouse IgG (H + L) Cross-Absorbed Secondary Antibody, Cyanine5 (1:500)	Thermo Fisher Scientific	Cat# A10524; RRID: AB_2534033
Bacterial and virus strains		
Escherichia coli BL21(DE3)	Thermo Fisher Scientific	EC0114
Chemicals, peptides, and recombinant proteins		
2-Deoxy-D-glucose	Sigma-Aldrich	Cat# D8375
Sodium (meta)arsenite	Sigma-Aldrich	Cat# S7400
Luperox® TBH70X, *tert*-Butyl hydroperoxide solution	Sigma-Aldrich	Cat# 458139
Diazaborine	Calbiochem	Cat# 5307290001
Cyclohexamide solution	Sigma-Aldrich	Cat# C4859
2,4-Dinitrophenol	Sigma-Aldrich	Cat# 198501
DMEM, high glucose, pyruvate	Thermo Fisher Scientific	Cat# 11995073
Fetal Bovine Serum	Thermo Fisher Scientific	Cat# 10270106
Penicillin-Streptomycin	Thermo Fisher Scientific	Cat# 15140122
Lipofectamine 3000	Thermo Fisher Scientific	Cat# L3000001
Opti-MEM	Thermo Fisher Scientific	Cat# 31985062
N-ethylmaleimide	Pierce	Cat# 23030
β-mercaptoethanol	Sigma-Aldrich	Cat# M6250
NuPAGE™ 4–12% Bis-Tris Protein Gels, 1.0 mm, 10-well	Thermo Fisher Scientific	Cat# NP0321BOX
NuPAGE™ 4–12% Bis-Tris Protein Gels, 1.0 mm, 15-well	Thermo Fisher Scientific	Cat# NP0323BOX
NuPAGE™ 4–12% Bis-Tris Protein Gels, 1.0 mm, 12-well	Thermo Fisher Scientific	Cat# NP0322BOX
NuPAGE™ 4–12% Bis-Tris Protein Gels, 1.5 mm, 15-well	Thermo Fisher Scientific	Cat# NP0336BOX
NuPage 20X MES running buffer	Thermo Fisher Scientific	Cat# NP0002
PVDF membrane	Roche	Cat# 03010040001

Continued

REAGENT or RESOURCE	SOURCE	IDENTIFIER
Amersham™ Protran® Western blotting membranes, nitrocellulose	Amersham, GE	Cat# GE10600002
Amersham ECL Western Blotting Detection Reagent	Amersham, GE	Cat# RPN2106
Immobilon Forte Western HRP substrate	Millipore	Cat# WBLUF0100
Phusion High-Fidelity DNA Polymerase	NEB	Cat# M0530L
Q5 High-Fidelity DNA Polymerase	NEB	Cat# M0491L
EDTA-free protease inhibitor	Sigma-Aldrich	Cat# 03708969001
TALON® Magnetic Beads	Takara Bio.	Cat# 635636
GFP-Trap®_MA	Chromotek	Cat# gtma-20
Der Blaue Jonas	German Research Products	Cat# GRP1
NucBlue Fixed Cell ReadyProbes Reagent	Thermo Fisher Scientific	Cat# R37606
Fluorescence mounting medium	Dako, Agilent	Cat# S3023
Concanavalin A	MP biomedicals	Cat# 02195283.6
Bovine Serum Albumin Fraction V	Roche	Cat# 10735078001
Alexa Fluor™ 488 NHS Ester (Succinimidyl Ester)	Thermo Fisher Scientific	Cat# A20000
Alexa Fluor™ 546 NHS Ester (Succinimidyl Ester)	Thermo Fisher Scientific	Cat# A20002
Alexa Fluor™ 405 NHS Ester (Succinimidyl Ester)	Thermo Fisher Scientific	Cat# A30000
PageBlueTM Protein Staining Solution	Thermo Fisher Scientific	Cat# 24620
Sequencing Grade Modified Trypsin	Promega	Cat# V5111
Lys-C, Mass Spec Grade	Promega	Cat# VA1170
Ampicillin	Sigma-Aldrich	Cat# a9518
1 mM isopropyl β-D-1-thiogalactopyranoside	Roth	Cat# CN08.3
Lysozyme	Sigma	Cat# L6876
Recombinant GFP	K. Zhang	N/A
Deposited Data		
reviewer_pxd044486@ebi.ac.uk ProteomeXchange	This study	PXD044486
Biological samples		
BY4741 (*MATa his3Δ1 leu2Δ0 met15Δ0 ura3Δ0*)	Euroscarf	www.euroscarf.de
BY4741 *urm1Δ::kanMX4*	This study	YLVC1
BY4741 *uba4Δ::natMX4*	This study	YLVC2
BY4741 *ahp1Δ::kanMX4*	This study	YLVC3
BY4741 *mNeonGreen-Urm1* (see Star Methods)	This study	YLVC4
BY4741 *mNeonGreen-Urm1 nup49Δ::Nup49-Mars-hphMX4*	This study	YLVC5
BY4741 *mNeonGreen-Urm1 sis1Δ::Sis1-Mars-hphMX4*	This study	YLVC6
BY4741 *urm1ΔUrm1-HA₆-HIS3MX6*	This study	YLVC7
BY4741 *mNeonGreen-Uba4* (see Star Methods)	This study	YLVC8
BY4741 *mNeonGreen-Uba4 urm1Δ::hphMX4*	This study	YLVC9
BY4741 *mNeonGreen-Urm1 nup49Δ:: Nup49-Mars-hphMX4 uba4Δ::kanMX4*	This study	YLVC10
BY4741 *mNeonGreen-Urm1 nop56Δ::Nop56-Mars-hphMX4*	This study	YLVC11
BY4741 *mNeonGreen-Urm1 pab1Δ::Pab1-Mars-hphMX4*	This study	YLVC12
BY4741 *mNeonGreen-Uba4 nop56Δ::Nop56-Mars-hphMX4*	This study	YLVC13
BY4741 *mNeonGreen-Uba4 pab1Δ::Pab1-Mars-hphMX4*	This study	YLVC14
BY4741 *ncs2Δ::natMX4*	This study	YLVC15
BY4741 *pub1Δ::hph1MX4*	This study	YLVC16
BY4741 *urm1Δ::kanMX4 pub1Δ::hphMX4*	This study	YLVC17
BY4741 *ncs2Δ::natMX4 pub1Δ::hphMX4*	This study	YLVC18
BY4741 *pab1Δ::Pab1-GFP-HIS3MX6*	This study	YLVC19

(Continued on next page)

Continued

REAGENT or RESOURCE	SOURCE	IDENTIFIER
BY4741 *pab1Δ::Pab1-GFP-HIS3MX6 urm1Δ::kanMX4*	This study	YLVC20
BY4741 *pab1Δ::Pab1-GFP-HIS3MX6 pub1Δ::hph1MX4*	This study	YLVC21
BY4741 *pab1Δ::Pab1-GFP-HIS3MX6 urm1Δ:: kanMX4 pub1Δ::hphMX4*	This study	YLVC22
BY4741 *pab1Δ::Pab1-GFP-HIS3MX6 ola1Δ:: Ola1-Mars-natMX4*	This study	YLVC23
BY4741 *pab1Δ::Pab1-GFP-HIS3MX6 urm1Δ:: kanMX4 ola1Δ::Ola1-Mars-natMX4*	This study	YLVC24
BY4741 *pab1Δ::Pab1-GFP-HIS3MX6 pub1Δ:: hphMX4 ola1Δ::Ola1-Mars-natMX4*	This study	YLVC25
BY4741 *pab1Δ::Pab1-GFP-HIS3MX6 urm1Δ:: kanMX4 pub1Δ::hphMX4 ola1Δ:: Ola1-Mars-natMX4*	This study	YLVC26
BY4741 *pab1Δ::Pab1-GFP-HIS3MX6 Sup45Δ::Sup45-Mars-natMX4*	This study	YLVC27
BY4741 *pab1Δ::Pab1-GFP-HIS3MX6 urm1Δ:: kanMX4 Sup45Δ::Sup45-Mars-natMX4*	This study	YLVC28
BY4741 *pab1Δ::Pab1-GFP-HIS3MX6 pub1Δ:: hphMX4 Sup45Δ::Sup45-Mars-natMX4*	This study	YLVC39
BY4741 *pab1Δ::Pab1-GFP-HIS3MX6 urm1Δ:: kanMX4 pub1Δ::hphMX4 Sup45Δ:: Sup45-Mars-natMX4*	This study	YLVC30
BY4741 *ett1Δ::Ett1-GFP-HIS3MX6 nop56Δ:: Nop56-Mars-hphMX4*	This study	YLVC31
BY4741 *ett1Δ::Ett1-GFP-HIS3MX6 nop56Δ:: Nop56-Mars-hphMX4 urm1Δ::kanMX4*	This study	YLVC32
BY4741 *mNeonGreen*	This study	YLVC33
BY4741 *mNeonGreen-Urm1 ytm1Δ::Ytm1-Mars-natMX4*	This study	YLVC34
BY4741 *mNeonGreen-Urm1 rpa190Δ::Rpa190-Mars-natMX4*	This study	YLVC35
BY4741 *mNeonGreen-Urm1 ett1Δ::Ett1-Mars-natMX4*	This study	YLVC36
BY4741 *mNeonGreen-Urm1 ola1Δ::Ola1-Mars-natMX4*	This study	YLVC37
BY4741 *mNeonGreen-Urm1 ola1Δ::Sup45-Mars-natMX4*	This study	YLVC38
Experimental models: Cell lines		
HeLa cells	ATCC	Cat# CCL-2; RRID: CVCL_0030
Oligonucleotides		
CCCGGATCTAGAATGGTAAACGTGAAAGTGGA	This study	LCO1
CCCGGAGGATCCACCACCATGTAATGTTGAAG	This study	LCO2
CCCGGATCTAGAATGGTAAACGTGAAAGTGGA	This study	LCO3
CCCGGATCTAGAACCACCATGTAATGTTGAAG	This study	LCO4
CCCGGACATATGGTAAACGTGAAAGTGGA	This study	LCO5
CCCGGACATATGTTACTTGTACAGCTCGTCCA	This study	LCO6
CCCGGACATATGATGCAGATCTTCGTCAAGAC	This study	LCO7
CCCGGACATATGTTACTTGTACAGCTCGTCCA	This study	LCO8
AACAACAAACTGAGCAAGCTCGTACGCTGCAGGTCGAC	This study	LCO9
TTGTTAGCAGCCGGATCTTACTTGTACAGCTCGTCCATGC	This study	LCO10
TTGCGCCTCCGCGGTGGAATGGTAAACGTGAAAGTG	This study	LCO11
TGTAATGTACCACCAATTTTCGAATCTAGGCCGACG	This study	LCO12
ACATTATTTGGTGGTTAAAAGCTTAGATCCGGCTGC	This study	LCO13
GCAGCCGGATCTAAGCTTTTAACCACCAAATAATGT	This study	LCO14
TTGCGCCTCCGCGGTGGAATGAATGACTACCATCTC	This study	LCO15
GCAGCCGGATCTAAGCTTCTAATATTTAGGAATGGT	This study	LCO16

Continued

REAGENT or RESOURCE	SOURCE	IDENTIFIER
TTGCGCCTCCGCGGTGGAATGGTGAGCAAGGGCGAG	This study	LCO17
GCAGCCGGATCTAAGCTTCTACTTGTACAGCTCGTC	This study	LCO18
TGCGCCTCCGCGGTGGAATGGTAAACGTGAAAGTG	This study	LCO19
GCAGCCGGATCTAAGCTTTTATGTTGAAGTAAAAGA	This study	LCO20
CCCGGAACTAGTATGGTAAACGTGAAAGTGGA	This study	LCO21
CCCGGAACTAGTACCACCATGTAATGTTGAAG	This study	LCO22
CCCGGACTCGAGATGGCTGATATTACTGATAA	This study	LCO23
CCCGGAGGATCCTTAAGCTTGCTCAGTTTGTT	This study	LCO23
Recombinant DNA		
p416ADH1	Mumberg et al.[90]	N/A
p416ADH1HIS6-URM1L96R	This study	pYLVC1
pEF-HIS6-URM1L96R	This study	EUROFINS
pCU426GAL1-GFP	F. den Brave	Universität Bonn
pCU426GAL1-20Q-GFP	F. den Brave	Universität Bonn
pCU426GAL1-URM1-20Q-GFP	This study	pYLVC3
pGAL1-UBG76V-20Q-GFP	This study	pYLVC4
pEF-UBG76V	This study	EUROFINS
P415GAL	Mumberg et al.[90]	N/A
p415GAL1-PGK1-GFP	This study	pYLVC5
p415GAL1-URM1PGK1-GFP	This study	pYLVC6
pEF-PGK1-GFP	This study	EUROFINS
pEF-URM1PGK1-GFP	This study	EUROFINS
p415GAL1-LUCDM-GFP	This study	pYLVC7
p415GAL1-URM1LUCDM-GFP	This study	pYLVC8
pET11A-T7-URM1-GFP	This study	pYLVC9
pET11A-T7-UBG76V-GFP	This study	pYLVC10
pET11A-T7-mSCARLET-UBA4	This study	pYLVC11
pHUE	Catanzariti et al.[91]	N/A
pHUE-URM1	This study	pYLVC12
pHUE-urm1H97F	This study	pYLVC13
pHUE-UBA4	This study	pYLVC14
pHUE-mScarlet	This study	pYLVC15
pHUE-urm1ΔCT	This study	pYLVC16
p416ADH1HIS6-MNG-URM1	This study	pYLVC17
pEF-HIS6-MNG-URM1	This study	EUROFINS
p413GAL1-CG*	Park et al.[71]	N/A
p413GAL1-URM1-CG*	This study	pYLVC18
pET11A-T7-HIS6-PAB1	This study	pYLVC19
pGFP-*Hs*URM1	S. Jentsch	N/A
p tK^{UUU}, tE^{UUC},tQ^{UUG}	Leidel et al.[32]	N/A
Software and algorithms		
AIDA software (version 4.27)	Raytest	RRID: SCR_014440
MaxQuant computational platform (version 1.6.5.0)	MaxQuant	RRID: SCR_014485
Prism 9 (version 9.3.1)	GraphPad	RRID: SCR_002798
PyMol (version 2.5.3)	Schrodinger, LLC	RRID: SCR_000305
Perseus (version 1.6.15)	Perseus	RRID: SCR_015753
Fiji (version 2.0.0-rc-69/1.52)	ImageJ	RRID: SCR_002285
Adaptive Poisson-Boltzmann Solver (version 3.4.1)	APBS	RRID: SCR_008387

(Continued on next page)

RESOURCE AVAILABILITY

Lead contact
Further information and requests for resources and reagents should be directed to and will be fulfilled by the lead contact, F. Ulrich Hartl (uhartl@biochem.mpg.de).

Materials availability
Plasmids and strains generated in this study are available upon request to the lead contact.

Data and code availability
- All mass spectrometry raw data have been deposited to the ProteomeXchange Consortium via PRIDE partner repository (https://www.ebi.ac.uk/pride/archive/) with the identifier PXD044486 and is publicly accessible.
- This paper does not report original code.
- Any additional information required to reanalyze the data reported in this study is available from the lead contact upon request.

EXPERIMENTAL MODEL AND PARTICIPANT DETAILS

S. *cerevisiae* strains utilized for this study were of the BY4741 genetic background (EUROSCARF). Genotypes of strains utilized, and genetically manipulated derivatives thereof, are listed in KEY RESOURCES TABLE. Cells were propagated in yeast peptone (YP) media (1% yeast extract, 2% bactopeptone) or synthetic complete (SC) media (0.17% yeast nitrogen base, 0.5% ammonium sulfate) at 30°C containing 2% glucose (YPD, SCD), unless otherwise indicated. For *GAL1* over expression experiments, cells were grown ~16–18 h in SC media containing 3% Raffinose (SC-R), then were shifted into SC media containing 3% galactose (SC-G) for ~16–18 h. OD_{600} units were used to define the total concentration of yeast cells utilized in the various experiments (1 mL of a culture with an OD_{600} of 1 equals 1 OD_{600} of cells).

METHOD DETAILS

Yeast strains
Genetic manipulations required for strain construction (deletions, C-terminal 3xHA, C-terminal GFP and C-terminal Mars tagging) were carried out using homologous recombination of PCR amplified cassettes.[92] N-terminal tagging with mNeonGreen (mNG) and 3xHA at the *URM1* and *UBA4* endogenous gene loci were conducted using the two-step Delitto Perfetto approach.[93] Synthesis of PCR products was carried out using either Phusion High-Fidelity DNA Polymerase (NEB) or Q5 High-Fidelity DNA Polymerase (NEB). DNA cassettes, synthesized for the purpose of generating gene deletions, encoding for specific selection markers (*kanMX4*, *hphMX4*, *natMX4*, *LEU2MX4*, *HIS6MX4*, *URA3MX4*) were flanked by 60 bp sequences complementary to sequences directly up and downstream of the start and stop codon of the target ORF. To produce DNA cassettes for C-terminal 3xHA, GFP and Mars tagging, DNA sequences encoding *GFP, HA,* and *MARS* with the *ADH1* terminator and, containing either *HIS3MX4, kanMX4, hphNT1,* or *natMX4* selection markers, were flanked at the 5′ and 3′ ends by 60 bp sequence complementary to 60 bp upstream and downstream of the stop codon of the target gene. For Delitto Perfetto 2-step genomic integration, a cassette encoding for both *kanMX4/URA3MX4* markers was flanked by a 60 bp sequence at both 5′ and 3′ ends homologous to 60 bp directly up and downstream of the start codon of the gene of interest. A second DNA cassette, encoding for *MNEON*, was flanked with the identical 5′ and 3′ 60 bp sequences, as used in the previous step, for replacing the *kanMX4/URA3MX4* cassettes from the genome to achieve the final integration of the *MNEON* tag directly upstream of the target ORF (*URM1* or *UBA4*).

Plasmid construction
Plasmids, and primers used for their construction, are listed in the KEY RESOURCES TABLE. Molecular cloning of DNA fragments into target vectors was performed by DNA ligation using T4 DNA ligase (NEB) or, alternatively, with Gibson assembly.[94] In all cases, PCR products encoding genes of interest were generated using Phusion High-Fidelity DNA Polymerase (NEB) or Q5 High-Fidelity

CellPress
OPEN ACCESS

DNA Polymerase (NEB). Alternatively, gene synthesis products (EUROFINS) encoding for the appropriate ORFs were subcloned into target vectors of interest. A DNA fragment encoding H_6-urm1(L96R), generated by gene synthesis (EUROFINS), flanked by 5′XbaI and 3′XhoI restriction endonuclease sites, was subcloned into p416*ADH1*[90] to generate pYLVC1. For expression of Urm1-20Q-GFP from the *GAL1* promoter, a DNA fragment encoding for *URM1* was amplified from WT genomic DNA isolated from a BY4741 strain (KEY RESOURCES TABLE) with flanking 5′XbaI and 3′BamHI restriction endonuclease sites for cloning into a pGAL-20Q-GFP (pYLVC2) vector using the oligos LCO1 and LCO2 to generate pYLVC3. For expression of Ub^{G76V}-20Q-GFP from the *GAL1* promoter, a DNA fragment encoding *UBG76V* was subcloned from a gene synthesis product (EUROFINS) corresponding to *UBG76V* flanked by 5′XbaI and 3′BamHI sequences used for subcloning into pGAL-20Q-GFP to create pYLVC4. For expression of Pgk1-GFP and Urm1-Pgk1-GFP linear fusions from the *GAL1* promoter, gene synthesis products (EUROFINS) encoding *PGK1-GFP* and *URM1-PGK1-GFP* were subcloned into p415*GAL*[90] using 5′ BamHI and 3′ XhoI restriction endonuclease sites to generate pYLVC5 and pYLVC6, respectively. For expression of Urm1-LucDM-GFP, a DNA fragment encoding *URM1* amplified from WT genomic DNA, flanked by 5′ and 3′ XbaI restriction endonuclease sites were cloned into a p415*LUCDM* vector (pYLVC7) for expression from the *GAL1* promoter using the oligos LCO3 and LCO4 to create pYLVC8. For expression of Urm1-GFP in *E. coli*, a DNA fragment encoding *URM1-GFP*, with 5′ and 3′ NdeI restriction endonuclease sites, was amplified using oligos LCO5 and LCO6 for cloning into pET11a to create pYLVC9. For synthesis of UbG76V in *E. coli*, the DNA sequence corresponding to *UBG76V-GFP*, with 5′ and 3′ NdeI restriction endonuclease sites, was amplified using oligos LCO7 and LCO8 for cloning into pET11a to create pYLVC10. For expression of mSt-Uba4 in *E. coli*, the *MSCARLET-UBA4* ORF was cloned, using Gibson assembly with oligos LCO9 and LCO10, into pET11A to create pYLVC11. For expression of WT Urm1 in *E. coli*, DNA encoding *URM1* was generated using oligos LCO11 and LCO12 and the corresponding fragment was cloned into the pHUE vector backbone[91] using the Gibson assembly method to create pYLVC12. For synthesis of urm1H97F in *E. Coli* from the pHUE vector backbone, Gibson assembly was utilized with the oligo pair LCO13 and LCO14 for construction of pYLVC13. For expression of WT Uba4 in *E. coli*, a DNA fragment containing the sequence encoding for *UBA4* was amplified using oligos LCO15 and LCO16 and cloned into pHUE vector system using Gibson assembly for construction of pYLVC14. For expression of mScarlet (mSt) alone, the *MSCARLET* ORF was cloned, using Gibson assembly with oligos LCO17 and LCO18, into pHUE to create pYLVC15. For expression of urm1ΔCT, the *URM1ΔCT* ORF was cloned, using Gibson assembly using oligos LCO19 and LCO20, into pHUE to create pYLVC16. A DNA fragment encoding H_6-mNG-urm1(L96R), generated by gene synthesis (EUROFINS), flanked by 5′XbaI and 3′XhoI restriction endonuclease sites, was subcloned into p416*ADH1*[90] to generate pYLVC17. For expression of Urm1-CG*, a DNA fragment encoding *URM1* amplified from WT genomic DNA, flanked by 5′ and 3′ SpeI restriction endonuclease sites, was cloned into a p413*CG** vector[71] for expression from the *GAL1* promoter using the oligos LCO21 and LCO22 to create pYLVC18. For expression of Pab1 in *E.coli*, a DNA fragment encoding *PAB1*, amplified from WT genomic DNA, was cloned into pET11a using 5′XhoI and 3′BamHI with the oligos LCO23 and LCO24 for construction of pYLVC19.

Heat stress, starvation, oxidative stress, diazaborine, and sodium arsenite treatment

For acute HS experiments, yeast cells were propagated for ~16–18 h (30°C/140 r.p.m. shaking) to mid-logarithmic (log) phase (defined as OD_{600} = 0.4–0.8) in the appropriate media (SC-D, SC-G, or YPD). Cells were concentrated to a 500 μL volume then transferred to a 1.5 mL microcentrifuge tube (Eppendorf) for temperature-controlled incubations in a ThermoMixer C incubator (Eppendorf). For acute HS experiments, cells were allowed to incubate at 37°C, 40°C, 42°C, 44°C, or 46°C for 15 min, or at 46°C for 5 min, as described in the corresponding figure legends. For prolonged HS experiments, cultures were grown for ~16–18 h (30°C/140 r.p.m. shaking) to early log phase (OD_{600} = 0.3–0.4) then shifted to incubators set to 37°C, 40°C, and 42°C for 18 h (140 r.p.m. shaking). For recovery from acute HS (46°C, 15 min), cells were thermally challenged as described above, then resuspended in the appropriate media. Following resuspension, cultures were transferred to an incubator (30°C/140 r.p.m. shaking) with aliquots collected at various time intervals, as indicated in figure legends. For chemically induced starvation using 2-deoxyglucose, mid-log phase cells were harvested with centrifugation (4,000 x *g*/5 min), washed three times with 50 mL volumes of room temperature water followed by resuspension in SC media containing 60 μg/mL of 2-deoxyglucose (Sigma-Aldrich). Cells were incubated in the presence of 2-deoxyglucose (2-DG) for 2 h (30°C/140 r.p.m. shaking) to induce carbon starvation. For stationary phase experiments, mid-log phase cultures were allowed to continuously propagate (30°C/140 r.p.m. shaking) for 1-4 days to drive stationary phase induced starvation. Day 0 is defined as cultures having a mid-log phase OD_{600}. For oxidative stress experiments, mid-log phase cultures were treated with 10 mM *tert*-butyl hydroperoxide (Sigma-Aldrich) for a period 1 h (30°C/140 r.p.m. shaking). For diazaborine (Calbiochem) experiments, mid-log phase cells were treated with 10 μg/mL of diazaborine for 30 min (30°C/140 r.p.m. shaking). To block the production of newly synthesized proteins, cycloheximide (Sigma-Aldrich), was added to cultures at a final concentration of 100 μg/mL for 30 min (30°C/140 r.p.m. shaking). For treatment of cells with sodium arsenite experiments, mid-log phase cultures were treated with 1.0 mM NaArsenite (Sigma-Aldrich) for a period 1 h (30°C/140 r.p.m. shaking).

Manipulation of cellular pH with 2,4-dinitrophenol

Yeast cultures grown ~16–18 h (30°C/140 r.p.m. shaking) to mid-log phase in SC-D were harvested by centrifugation (4,000 x *g*/5 min), washed once in a 50 mL volume of water, then resuspended in 100 mM phosphate buffer of pH 7.5, 6.0 and 5.0 containing 2% glucose. Incubations were done either in the presence or absence of 2 mM 2,4-dinitrophenol (Sigma-Aldrich) for 1 h at 30°C with shaking at 140 r.p.m. For inhibition of intracellular acidification occurring with HS, cells were preincubated in

SC-D media pH 7.5 for 1 h, in the presence or absence of 2 mM 2,4-dinitrophenol, then exposed to HS (46°C, 15 min). For starvation experiments, cells were starved with 2-DG as described above in 'Heat Stress, Starvation, Oxidative Stress, Diazaborine, and Sodium Arsenite Treatment' in media pH 7.5, either in the presence or absence of 2 mM 2,4-dinitrophenol.

1,6-Hexanediol treatment

Yeast cells grown ∼16–18 h (30°C/140 r.p.m. shaking) to mid-log phase in SC-D media were harvested by centrifugation (4,000 x g/5 min) then subjected to 2-DG induced starvation as described above in 'Heat Stress, Starvation, Oxidative Stress, Diazaborine, and Sodium Arsenite Treatment'. Following starvation driven mNG-Urm1 condensate formation, cells were treated with 5% 1,6-hexanediol (Sigma-Aldrich) in the presence of 10 μg/mL digitonin for a total of 5 min. For washout experiments, cells were washed 2 x in 1 mL volumes of SC media lacking glucose followed by resuspension in media contain 60 μg/mL of 2-DG.

Serial dilution growth assay

Yeast cultures were grown ∼16–18 h (30°C/140 r.p.m. shaking) in YPD to late log phase (OD$_{600}$ = ∼3) and were diluted to equivalent densities (OD$_{600}$ = 1 per culture) in a 96 well microtiter plate (Greiner). 5-fold serial dilution steps were then carried out in fresh YPD for a total of 6 times. Cells were subsequently transferred onto YPD plates using an in-house manufactured 96-well metal stamp. Plates were incubated for 2–3 days at 30°C and 3–4 days at 40°C before being imaged.

Real-time growth assay monitoring recovery from acute HS

Yeast cultures were grown as described above in 'Serial Dilution Growth Assay' and were diluted to equivalent densities (OD$_{600}$ = 0.1 per culture) in a 96 well microtiter plate (Greiner). Cells were either exposed to HS at 46°C for 15 min or were directly transferred to the microtiter plate. Recovery was then monitored by measuring OD$_{600}$ at 1 h intervals using a Tecan Spark Multimode Microplate reader set at 30°C for up to 25 h post recovery.

Mammalian cell growth

HeLa cells used in this study (ATCC, CCL-2, RRID:CVCL_0030) were cultured at 37°C, 5% CO$_2$ in Dulbecco's modified Eagle's medium (DMEM high glucose, pyruvate, 4 mM L-glutamine) supplemented with 10% fetal bovine serum, and Penicillin-Streptomycin (10.000 U/mL) (Thermo Fisher Scientific).

Mammalian cell transfection

Approximately 70,000 HeLa cells per well were dispensed into a 24-well plate containing a poly-L-lysine coated coverslip (Neuvitro Corporation). 16–24 h later, the EGFP-Urm1 plasmid (KEY RESOURCES TABLE) was transfected using Lipofectamine 3000 (Thermo Fisher Scientific) as per the manufacturer's instructions. 0.75 μL of Lipofectamine 3000 was mixed with 25 μL of Opti-MEM (Thermo Fisher Scientific) and 0.5 μg DNA was mixed with 1μL of Lipofectamine P3000 reagent in 25 μL Opti-MEM. The mixtures from the previous step were combined and incubated for 20 min at room temperature. The combined reagents were then added directly to the cells with 1 mL of fresh medium.

Preparation of whole cell extracts for immunoblotting analysis

10 OD$_{600}$ of yeast cell pellets were resuspended in 1 mL of ice-cold water containing 20 mM N-ethylmaleimide (Pierce), 0.25 mM sodium hydroxide, and 0.1% β-mercaptoethanol (Sigma-Aldrich). Following resuspension, cells were repeatedly vortexed (5 × 10 s) with intermittent ice incubations. Next, trichloroacetic acid (TCA) was added to a final concentration of 5.5%, followed by additional rounds of vortexing (5 × 10 s) for complete lysis and efficient precipitation of protein. Protein pellets were harvested by high-speed centrifugation (20,000 x g/15 min/4°C) followed by aspiration of the supernatant. Protein pellets were subsequently dried and resuspended in 200 μL of HU buffer (8 M urea, 5% SDS, 200 mM Tris-HCl pH 6.8, 0.01% bromophenol blue, 2% β-mercaptoethanol) and, if necessary, pH was adjusted using 10 μL–20 μL of 1M Tris-HCl, pH 8.8. Samples were incubated at 65°C in a ThermoMixer C (Eppendorf) with shaking at 2000 r.p.m. until pellets were completely resolubilized (∼30–60 min).

Analysis by SDS-PAGE

Protein samples resuspended in HU buffer were separated by electrophoresis on 4–12% Bis-Tris acrylamide NuPAGE gels (Thermo Fisher Scientific) using MES NuPAGE SDS running buffer (Thermo Fisher Scientific) at 150V for ∼1 h.

Analysis by immunoblotting

Proteins separated on polyacrylamide gels were transferred to nitrocellulose (GE healthcare) or PVDF (Roche) membranes in blotting buffer (192 mM glycine, 25 mM Tris, 20% methanol) at a constant voltage of 55 V for 2.5 h using the Trans-Blot Turbo (Bio-Rad) apparatus. After transfer membranes were washed for 10 min in TBS-T buffer (10 mM Tris-HCl pH 7.5, 150 mM NaCl, 0.05% Tween 20) and subsequently blocked with 5% skim milk (resuspended TBS-T buffer) for a at least 1 h at room temperature. Blocked membranes were incubated with anti-Urm1, anti-Pgk (Invitrogen, Cat# 459250, RRID: AB_2532235), anti-HA (Roche, Cat# 11867423001, RRID: AB_390918), anti-GFP (Roche, Cat# 11814460001, RRID: AB_390913), anti-mNeonGreen (Cell Signaling Technology, Cat# 53061, RRID: AB_2799426) or anti-Pab1 (EnCor Biotechnology, Cat# MCA-1G1, RRID: AB_2572370) primary antibodies suspended in 5%

Milk/TBS-T buffer for ~20–24 h at 4°C. Membranes were washed 3 times with TBS-T (10 min wash steps) followed by 16 h incubation in the presence of goat anti-mouse (Dako, Agilent, Cat# P044701-2, RRID: AB_2617137), anti-rabbit (Dako, Agilent, Cat# P044801-2, RRID: AB_2617138), or anti-rat (Sigma-Aldrich, Cat# A9037, RRID: AB_258429) HRP-conjugated secondary antibody at room temperature or 4°C, respectively. Membranes were washed 3 times in TBS-T buffer (10 min wash steps), then submerged in ECL Western Blotting Detection Reagent (Amersham) or Immobilon Forte Western HRP substrate (Millipore). The ImageQuant IQ800 (GE Healthcare) was used for signal detection. Images of blots were analyzed using either Fiji (Fiji, RRID: SCR_002285) or AIDA software (Raytest, RRID: SCR_014440).

The immunoblots in Figures 1A, S1A, S1B, S1C, S1F, S1H, S1I, S2A, S3E, S4K, S5C, S6C, S7A, and S7D were conducted 2–4 times as specified in figure legends.

CG* turnover assay using metabolic shut-off

Yeast cultures were grown ~18 h (30°C or 37°C/140 r.p.m. shaking) in SC media to log phase (OD$_{600}$ = ~1) in the presence of galactose to maintain expression of CG* and Urm1-CG*. Cells were shifted into glucose containing media to silence expression of CG* and Urm1-CG* from the *GAL1* promoter. Post-shift, aliquots of cells were collected every 30 min then processed for SDS-PAGE and immunoblotting analysis as described above in 'Preparation of Whole Cell Extracts for Immunoblotting Analysis', 'Analysis by SDS-PAGE' and 'Analysis by Immunoblotting'.

Affinity purification of H$_6$-Urm1(L96R) and H$_6$-mNG-Urm1(L96R) modified proteins

Yeast cultures propagated ~16–18 h (30°C/140 r.p.m. shaking) to mid-log phase in SC-D media, expressing H$_6$-Urm1(L96R), or H$_6$-mNG-Urm1(L96R), from the *ADH1* promoter, were subjected to HS at 46°C as described in 'Heat Stress, Starvation, Oxidative Stress, Diazaborine, and Sodium Arsenite Treatment'. Cells, at a concentration of 200 OD$_{600}$, were harvested by centrifugation and resuspended in 600 μL of IP buffer (20 mM NEM, 1% Triton X-100, 50 mM Tris-HCl pH 7.5, 20 mM KCl, 10 mM MgCl$_2$, and Protease Inhibitor Cocktail [Sigma-Aldrich]). Lysates were generated by 3 bead beating cycles with zirconia/silica beads in an MP Beadbeater 24 (60 s at 6.0 m/s) with intermittent cooling on ice. In between each cycle, lysate/bead mixtures were briefly centrifuged (~2 s/4,000 x *g*) and partially clarified lysates were transferred to a fresh 2 mL microcentrifuge tube (Eppendorf). An additional centrifugation step was included to clear excess cell debris at 1000 x *g* for 10 min at 4°C. Clarified lysates were subjected to high-speed centrifugation at 20,000 x *g* for 30 min at 4°C to remove insoluble material. Pelleted protein was washed with 1 mL of IP buffer followed by an additional centrifugation step at 20,000 x *g* for 5 min at 4°C. Excess buffer was removed, and insoluble protein was resolubilized in 120 μL of denaturing solubilization buffer (8 M urea, 5% SDS, 200 mM Tris-HCl pH 6.8) with incubation at 65°C for 1 h in a ThermoMixer C at 2000 r.p.m. (Eppendorf). After resolubilzation, 1.3 mL of denaturing IP binding buffer (6 M urea, 20 mM NEM, 1% Triton X-100, 50 mM Tris-HCl pH 7.5, 20 mM KCl, 10 mM MgCl$_2$) was added, followed by centrifugation (20,000 x g/5 min/room temperature). Cleared resolubilzed protein was transferred to fresh 1.5 mL low-binding tubes (Eppendorf). Next, 200 μL of Talon Magnetic Beads (Takara) was added for a ~18–20 h incubation at 4°C with gentle end-on-end rotation. The following day, metal affinity beads were separated from the flowthrough fraction using a magnetic stand and bead-bound immunoprecipitated material was subjected to 10× 1 mL washing steps with IP wash buffer (1.0% Triton X-100, 50 mM Tris-HCl pH 7.5, 20 mM KCl, 10 mM MgCl$_2$). For immunoblotting analysis of H$_6$-Urm1(L96R) modified proteins presented in Figure S1G, precipitated material was eluted by addition of HU buffer (8 M urea, 250 mM imidazole, 5% SDS, 200 mM Tris-HCl pH 6.8, 0.01% bromophenol blue, 2% β-mercaptoethanol) followed by incubation at 95°C for 3 min. For label free proteomic analysis of H$_6$-Urm1(L96R) modified proteins, bead bound material was subjected to in-solution digestion as described below in LC-MS/MS 'Analysis for In-Solution Digestion'.

Immunoprecipitation of Urm1-20Q-GFP and Urm1-Pgk1-GFP

Cultures of yeast cells, propagated ~16-18 h to mid-log phase (30°C/140 r.p.m. shaking), producing Urm1-20Q-GFP (or 20Q-GFP) and Urm1-Pgk1-GFP (or Pgk1-GFP), from the *GAL1* promoter, were grown in SC-G media, then shifted to 46°C as described in 'Heat Stress, Starvation, Oxidative Stress, Diazaborine, and Sodium Arsenite Treatment'. 200 OD$_{600}$ of cells were harvested by centrifugation followed by resuspension in 600 μL of IP buffer (20 mM NEM, 1% Triton X-100, 50 mM Tris-HCl pH 7.5, 20 mM KCl, 10 mM MgCl$_2$, and Protease Inhibitor Cocktail [Roche]). Total cell extracts were prepared by bead beating using an MP Beadbeater 24 (3 × 60 s at 6.0 m/s) with zirconia/silica beads as described in 'Affinity Purification of H$_6$-Urm1(L96R) Modified Proteins'. Cell debris was separated from the supernatant by centrifugation at 1000 x *g* for 10 min at 4°C. Clarified lysates were transferred to a fresh 2 mL microcentrifuge tube (Eppendorf) and immunoprecipitation of GFP tagged proteins was initiated by the addition of 100 μL of GFP-Trap_MA (ChromoTek GmbH) magnetic beads. Binding was carried out for 1 h at 4°C with gentle end-on-end rotation. Magnetic beads were collected on a magnetic stand and bead-bound immunoprecipitated material was washed successively with 1 mL volumes of IP buffer a total of 10 times. For label free proteomic analysis of Urm1-20Q-GFP interacting proteins, bead bound material was eluted by addition of HU buffer (8 M urea, 5% SDS, 200 mM Tris-HCl pH 6.8, 0.01% bromophenol blue, 2% β-mercaptoethanol) followed by incubation at 65°C for 30 min. Samples were run on an SDS-PAGE gel then subjected to in gel digestion as described in 'In-Gel Digestion for IP Interactomes and Insoluble Proteomes'.

Cell fractionation analysis

For analysis of protein solubility using fractionation, cells were handled and lysed as described in 'Affinity Purification of H_6-Urm1(L96R) Modified Proteins'. Briefly, mid-log cultures grown ~16–18 h in YPD media (30°C/140 r.p.m. shaking) were exposed to HS as described in 'Heat Stress, Starvation, Oxidative Stress and Diazaborine Treatment'. 200 OD_{600} of cells were harvested by centrifugation and resuspended in 600 μL of IP buffer. Lysates were generated by 3 x bead beating cycles with zirconia/silica beads in an MP Beadbeater 24 (60 s at 6.0 m/s) with intermittent cooling on ice. Lysates were clarified by centrifugation at 1000 x g for 10 min at 4°C. Next, total cell extracts (T) were separated into supernatant (S) and pellet (P) fractions by centrifugation at 20,000 x g for 30 min at 4°C. T and S fractions were transferred to fresh 1.5 mL microcentrifuge tubes and TCA at a final concentration of 5.5% was added to precipitate protein. To maximize protein precipitation, T and S fractions were allowed to incubate on ice with intermittent vortexing for ~30 min. Meanwhile, insoluble protein was washed in a 1 mL volume of IP buffer followed by an additional centrifugation step at 20,000 x g for 5 min at 4°C. In the case that insoluble material was analyzed using immunoblotting, insoluble protein was resuspended in 200 μL of HU buffer. For label free proteomic analysis of insoluble pellet fractions, protein pellets were washed once in 1x PBS followed by in-solution digestion as described below in LC-MS/MS 'Analysis for in-solution digestion'. For T and S fractions, following incubation on ice, TCA precipitated protein was harvested by centrifugation at 20,000 x g for 15 min at 4°C. TCA was aspirated and pellets were washed once with 750 μL of ice-cold acetone. Acetone washed pellets were subsequently air-dried and resuspended in 500 μL of HU buffer. Following resuspension in HU buffer, T, S, and P samples were incubated at 65°C for ~1 h in a ThermoMixer C (Eppendorf) with shaking at 2000 r.p.m.

Fluorescence microscopy
Yeast live cell imaging

Cultures of yeast cells were grown ~16-18 h to mid-log phase (30°C/140 r.p.m. shaking) in the appropriate SC-D or SC-G media. For acute HS, 2-DG induced starvation, stationary phase growth, DZA treatment, oxidative stress, and pH manipulation with 2,4-DNP, these experiments were conducted as described in sections 'Heat Stress, Starvation, Oxidative Stress and Diazaborine Treatment' and 'Manipulation of Cellular pH with 2,4-dinitrophenol'. Cells were harvested by centrifugation (4,000 x g/5 min) in 1.5 mL micro-centrifuge tubes, concentrated and spotted onto a microscope slide (Thermo Fisher Scientific) and covered with a coverslip (Thermo Fisher Scientific). Imaging was performed using an Olympus (Tokyo, Japan) FV1000 confocal microscope equipped with an Olympus PLAPON 60×/NA1.42 oil immersion objective. Proteins tagged with mNG or GFP fluorophores were detected using an excitation wavelength of 488 nm and emission of 505–540 nm. Detection of proteins tagged with Mars and mScarlet fluorophores was achieved using an excitation wavelength of 559 nm and emission of 575–675 nm. Image analysis was carried out in Fiji software (Fiji, RRID: SCR_002285).[95] In instances where the fluorescence intensity was deemed relatively weak, brightness and contrast adjustments were made to enhance the signal-to-noise ratio and have been indicated in the corresponding figure legends. All adjustments were done within the linear range using Fiji software (Fiji, RRID: SCR_002285).

Mammalian cell immunofluorescence

HeLa cells, cultured as described above in 'Mammalian Cell Growth', were fixed with 4% paraformaldehyde/PBS for 10 min, washed with PBS, and permeabilized with 0.1% Triton X-100/PBS for 5 min, 48 h following the initial transfection step and after HS for 2 h at 43°C. Blocking solution (8% BSA/PBS) was added for a 30 min incubation. Coverslips were transferred to a humid chamber and incubated for ~20 h at 4°C with the primary antibody diluted in 1% BSA/PBS (anti-eIF4G, Cat# sc-133155, RRID: AB_2095748), Santa Cruz Biotechnology, 1:50 dilution; anti-NPM1(Thermo Fisher Scientific, Cat# 32–5200, RRID: AB_2533084), 1:100 dilution). Cells were then washed with PBS, incubated with the corresponding secondary antibody (F(ab')2-Goat anti-Mouse IgG Alexa Fluor 633 (Thermo Fisher Scientific, Cat# A-21053, RRID: AB_2535720); Goat anti-Mouse IgG (H + L) Cross-Adsorbed Secondary Antibody, Cyanine5 (Thermo Fisher Scientific, Cat# A10524, RRID: AB_2534033) diluted in 1% BSA/PBS (1:500) for 1 h, washed with PBS and stained with NucBlue Fixed Cell ReadyProbes Reagent (Thermo Fisher Scientific). Coverslips were mounted with fluorescence mounting medium (Dako, Agilent). Confocal imaging was performed at the MPIB Imaging Facility (Martinsried, Germany) on a LEICA TCS SP8 AOBS confocal laser scanning microscope (Wetzlar, Germany) equipped with a LEICA HCX PL APO 63×/NA1.4 oil immersion objective. Images were analyzed using Fiji software (Fiji, RRID: SCR_002285).[95]

Yeast live cell FRAP

Cultures of mid-log phase yeast cells, grown ~16–18 h (30°C/140 r.p.m shaking), were exposed to HS (46°C, 15 min) or, alternatively, were propagated to stationary phase as described above in section 'Heat Stress, Starvation, Oxidative Stress and Diazaborine Treatment'. Following HS or starvation, cells were collected by centrifugation and adhered to the well of a μ-Slide (Ibidi, 80626) coated with concanavalin A (MP biomedicals), then imaged. *In vivo* fluorescence recovery after photo bleaching (FRAP) experiments were carried out on an Olympus (Tokyo, Japan) FV1000 confocal microscope equipped with an Olympus PLAPON 60×/NA1.42 oil immersion objective lens. Defined circular regions of interest (ROIs), corresponding to mNG-Urm1 condensates, were bleached using 25 iterations of 100% 488 nm light from a 488 nm diode laser following 2 pre-bleach scans. Pre- and post-bleach scanning was performed in 6.6 s intervals for a total of 100 frames. FRAP timeseries were analyzed using Fiji (Fiji, RRID: SCR_002285)[95] and data plotted using Prism (Graph Pad, RRID: SCR_002798).

Protein expression and purification

WT Urm1 and, urm1 mutant variants (urm1H97F, urm1ΔCT), were expressed and purified using *E. coli* BL21 (DE3) cells harboring a plasmid encoding for *URM1*, *urm1H97F*, or *urm1ΔCT* encoded on the pHUE vector backbone. Cells were propagated ~16–18 h (37°C/140 r.p.m. shaking) in Luria-Bertani (LB) ampicillin (Sigma-Aldrich) media to an OD_{600} of 0.3–0.5. Cultures were allowed to equilibrate for 1 h in an incubator pre-set to 20°C. Induction of target protein expression was initiated with 0.5 mM isopropyl β-D-1-thiogalactopyranoside (IPTG; Roth) for a total of 20 h. Cells were harvested by centrifugation (4,000 x *g*/1h/4°C) and pellets resuspended in Urm1 buffer A (20 mM Tris-HCl pH 7.5, 100 mM NaCl, 10% glycerol) containing 1g L^{-1} lysozyme (Sigma-Aldrich)/ 2.5 U mL^{-1}/*Sm*DNAse/complete protease inhibitor cocktail (Roche). Lysis was then carried out using an EmulsiFlex C5 (Avestin, Inc.) for 3x cycles at 15,000 kPa. Lysate were subject to centrifugation for using a Beckman 45 Ti rotor (40,000 x *g*/4°C/45 min). Clarified lysates were loaded on to gravity Ni-NTA metal affinity columns (Qiagen), equilibrated and washed with 3 column volumes of Urm1 buffer A, followed by 3 column volumes of 5% Urm1 buffer B (20 mM Tris-HCl pH 7.5, 100 mM NaCl, 15 mM imidazole, 10% glycerol) and 3 column volumes of 10% Urm1 buffer B. Protein bound to the column was eluted with 100% Urm1 buffer B (20 mM Tris-HCl pH 7.5, 100 mM NaCl, 300 mM imidazole, 10% glycerol). Proteolytic cleavage of His_6Ub was carried out using the ubiquitin-specific protease His_6Usp2 for ~16–18 h at 4°C. Next, buffer exchange was carried out on a HiPrep 26/10 desalting column (GE) to Urm1 buffer A (20 mM Tris-HCl pH 7.5, 100 mM NaCl, 10% glycerol). For subsequent removal of His_6Usp2, and any remaining His_6Ub-Urm1 fusion protein, eluates were applied to a Ni-NTA column. Flowthrough collected was then concentrated to a 7 mL volume, then applied to a size-exclusion column (HiLoad 16/600 Superdex 75 pg GE) equilibrated in Urm1 buffer C (20 mM Tris-HCl pH 7.5, 100 mM NaCl, 10% glycerol). Concentration of pooled fractions was performed using ultrafiltration and protein stocks were aliquoted, then flash-frozen in liquid N_2 for storage at −80°C.

Expression and purification of WT Uba4, encoded on the pHUE vector backbone, was conducted as described above with a few exceptions. Briefly, E. *coli* BL21 (DE3) carrying a plasmid encoding for *UBA4* were grown ~16–18 h (37°C/140 r.p.m. shaking), then shifted to a 20°C incubator following addition of 1 mM IPTG for 18 h. Centrifugation harvested cells (4,000 x *g*/1 h/4°C) were incubated in the presence of Uba4 buffer A (20 mM Tris-HCl pH 7.5, 250 mM NaCl, 20 mM imidazole, 10% glycerol) containing 1g L^{-1} lysozyme/ 2.5 U mL^{-1}/*Sm*DNAse/complete protease inhibitor cocktail (Roche) prior to lysis as described above. Lysates were centrifuged (40,000 x *g*/40 min/4°C) and the resulting supernatant was loaded onto a gravity Ni-NTA metal affinity columns (Qiagen), equilibrated, and washed with 3 column volumes of Uba4 buffer A followed by 3 column volumes of Uba4 buffer B (20 mM Tris-HCl pH 7.5, 250 mM NaCl, 40 mM imidazole, 10% glycerol). Bound protein was eluted with 1 column volume of Uba4 buffer C (20 mM Tris-HCl pH 7.5, 250 mM NaCl, 300 mM imidazole, 10% glycerol). Cleavage of the His_6Ub tag was conducted as described above using His_6Usp2 followed by buffer exchange using a HiPrep 26/10 desalting column (GE) to Uba4 buffer D (20 mM Tris-HCl pH 7.5, 250 mM NaCl, 10% glycerol). Removal of His_6 tagged fusion proteins was conducted as described above and concentrated flowthrough, in a 3 mL volume, was applied to a size-exclusion column (Superdex 200 pg; GE Healthcare) equilibrated in Uba4 buffer D (20 mM Tris-HCl pH 7.5, 250 mM NaCl, 10% glycerol). Protein fractions were pooled and concentrated using ultrafiltration, and aliquots were stored at −80°C.

Expression and purification of mScarlet, encoded on the pHUE vector backbone, was performed as described above for Urm1 with a few exceptions. Clarified lysates were loaded on to gravity Ni-NTA metal affinity columns (Qiagen), equilibrated and washed in mSt buffer A (20 mM Tris-HCl pH 7.0, 100 mM NaCl, 10% glycerol) followed by 5 column volumes of 2% mSt buffer B (20 mM Tris-HCl pH 7.0, 100 mM NaCl, 500 mM imidazole, 10% glycerol) to wash away unbound protein. Protein was then eluted in 4 column volumes of 8% mSt buffer B followed by 4 column volumes of 100% mSt buffer B. Proteolytic cleavage of the His_6Ub tag and removal of residual His_6-tagged proteins was performed as describe above. Finally, size exclusion chromatography was performed on a Sephacryl S-100 (GE Healthcare) pre-equilibrated in mSt buffer C (SEC and Storage buffer: 20 mM Tris-HCl pH 7.0, 100 mM NaCl, 10% glycerol) and subsequently washed with 1.5 column volumes of buffer C. Protein fractions were pooled and aliquots were stored at −80°C.

For expression and purification of Urm1-GFP in *E.coli*, BL21 (DE3) cells carrying a plasmid encoding for *URM1-GFP* were grown ~16–18 h (37°C/140 r.p.m. shaking) in LB ampicillin media to an OD_{600} 0.3–0.5. Cultures were equilibrated in an incubator pre-set to 18°C and expression of *URM1-GFP* was induced by the addition IPTG to a final concentration of 0.4 mM for a total of 16 h. Cells were harvested using centrifugation (4,000 x *g*/1 h/4°C) and pellets were resuspended with Urm1-GFP buffer A (20 mM Tris-HCl pH 7.0) containing 1g l^{-1} lysozyme/2.5 U mL^{-1}/*Sm*DNAse/complete protease inhibitor cocktail (Roche) prior to lysis using EmulsiFlex C5 (Avestin, Inc.) with 3 x cycles at 15,000 kPa. Following centrifugation (40,000 x *g*/45 min/4°C) clarified lysates were loaded onto a 70 mL self-made diethylaminoethanol (DEAE)-Sepharose column pre-equilibrated in 2% Urm1-GFP buffer B (20 mM Tris-HCl pH 7.0, 1000 mM NaCl). Unbound protein was washed away with 3 column volumes of 2% Urm1-GFP buffer B. A gradient was run with 10 column volumes of 2–50% Urm1-GFP buffer B and a second gradient with 2 column volumes of 50–100% buffer B. Next, buffer exchange was carried out on a HiPrep 26/10 desalting column (GE). Following desalting, protein was loaded onto a 20 mL Mono Q column (Cytiva) equilibrated and washed in 2 column volumes of 2% Urm1-GFP buffer B (20 mM Tris-HCl pH 7.0, 1 M NaCl). A gradient was run with 10 column volumes of 2–100% Urm1-GFP buffer B. Pooled fractions were then loaded onto a Sephacryl S-100 column (Merck) pre-equilibrated in Urm1-GFP buffer C (20 mM Tris-HCl, pH 7.5, 100 mM NaCl) and protein was eluted with 1.5 column volumes of Urm1-GFP buffer C. Pooled protein fractions were concentrated using ultrafiltration and aliquots of protein were flash-frozen in liquid N_2 for storage at −80°C.

Expression and purification of Ub^{G76V}-GFP in *E.coli* BL21 cells was conducted as described above for Urm1-GFP with a few exceptions. Post-centrifugation lysates were loaded onto a 160 mL DEAE Sepharose FastFlow (GE Healthcare) pre-equilibrated in 2%

Urm1-GFP buffer B (see above). Unbound proteins were washed away with 2 column volumes of 2% Urm1-GFP buffer B. A gradient was run with one column volume of 2–50% Urm1-GFP buffer B. Fractions collected were pooled and subsequently loaded onto an 8 mL ENrich High-Resolution Ion Exchange Column (BioRad) pre-equilibrated with 2% Urm1-GFP buffer B. Unbound protein was washed away with 5 column volumes of 2% buffer B. A gradient from 2 to 50% buffer B over 10 column volumes was run. Pooled fractions collected were collected and loaded onto a Sephacryl S-100 column (Merck) pre-equilibrated in Urm1-GFP buffer C. Bound protein was eluted with 1.5 column volumes of Urm1-GFP buffer C. Pooled fractions were concentrated using ultrafiltration and subsequently flash frozen and stored at $-80°C$.

Expression and purification of mScarlet-Uba4 (mSt-Uba4) was conducted as described above for Urm1-GFP with a few exceptions. Following induction of expression for ~16–18 h, cell pellets harvested by centrifugation were incubated in the presence of 10% mSt-Uba4 buffer B (20 mM $NaPO_4$ pH 7.5, 1 M NaCl) containing 1g L^{-1} lysozyme (Sigma-Aldrich)/2.5 U mL^{-1}/SmDNAse/complete protease inhibitor cocktail (Roche) prior to lysis using EmulsiFlex C5 (Avestin, Inc.) as described above. Clarified lysates were loaded onto a Mono Q 16/10 (Cytiva) column equilibrated with 10% mSt-Uba4 buffer B and unbound protein was washed away with 2 column volumes of mSt-Uba4 buffer A (20 mM $NaPO_4$ pH 7.5). A gradient was run with 10 column volumes of 1–100% of mSt-Uba4 buffer B. Pooled fractions were then loaded onto a Sephacryl S-200 column (GE Healthcare) pre-equilibrated with mSt-Uba4 buffer C (20 mM Tris-HCl/pH 7.0, 250 mM NaCl, 10% glycerol). The column was washed with 1 column volume of mSt-Uba4 buffer C and pooled fractions were finally loaded onto an 8 mL Mono Q column (Cytiva) equilibrated with 15% mSt-Uba4 buffer D (20 mM Tris-HCl pH 7.5, 1 M NaCl). A wash step with 3 column volumes of 15% mSt-Uba4 buffer D was carried out, followed by a gradient with 10 column volumes of 15–50% mSt-Uba4 buffer D followed by a second gradient of 50–100% buffer D. Finally, protein was concentrated as described above and aliquots were flash frozen in liquid N_2 and stored at $-80°C$.

Expression and purification of Pab1 was conducted using *E. coli* BL21 (DE3) cells harboring a plasmid encoding for *HIS₆PAB1* encoded on the pET11a vector backbone. Cells were propagated overnight in Luria-Bertani (LB) ampicillin (Sigma-Aldrich) media at 37°C to an OD_{600} 0.3–0.5. Cultures were transferred to an incubator pre-set to 18°C. Induction of protein expression was initiated by addition of 0.5 mM isopropyl β-D-1-thiogalactopyranoside (IPTG; Roth) for a total of 18 h with shaking at 130 r.p.m. Cells were harvested by centrifugation (4200 rpm for 1h at 4°C) and pellets incubated in the presence of Pab1-buffer A (20 mM HEPES/KOH, pH 7.3, 150 mM KCl, 2.5 mM $MgCl_2$, 10% glycerol) containing 1g L^{-1} lysozyme (Sigma-Aldrich)/2.5 U mL^{-1}/SmDNAse/complete protease inhibitor cocktail (Roche) prior to lysis using ultrasonication (1 min:15s gap on ice for 20 cycles). Lysates generated were subjected to centrifugation for 1 h using a Beckman 45 Ti rotor (40,000 x g/4°C). The supernatant yielded following high-speed centrifugation was loaded on to a 10 mL Ni-NTA affinity column (Qiagen), equilibrated and washed 1 x with 10 mL Pab1-buffer A. Protein bound to the column was washed 5 x with 10 mL volumes of Pab1 buffer A, followed by 5 x 10 mL volume washes with 2% Pab1-buffer B (20 mM HEPES/KOH, pH 7.3, 50 mM KCL, 2.5 mM $MgCl_2$, 10% glycerol, 1 mM DTT) and eluted with 100% Pab1-buffer B. Next, buffer exchange was carried out on a PD-10 desalting column (Merck) to Pab1-buffer A. Proteolytic cleavage of the His-tag was carried out using 2 mg/mL of TEV protease overnight at 4°C. For removal of the His₆ tag, eluates were applied to a Ni-NTA column equilibrated in Pab1-buffer A. Unbound proteins were washed away with Pab1-buffer A and the remaining protein eluted with 100% Pab1-buffer B, followed by buffer exchange into Pab1-buffer C (20 mM HEPES/KOH, pH 7.3, 50 mM KCL, 2.5 mM $MgCl_2$, 10% glycerol, 1 mM DTT). Protein was then loaded onto a heparin column pre-equilibrated with buffer C and pooled fractions where subjected to size exclusion on a Sephacryl S200 (GE Healthcare) column pre-equilibrated in SEC buffer (20 mM HEPES/KOH, pH 7.3, 150 mM KCL, 2.5 mM $MgCl_2$, 1 mM DTT). Flowthrough collected was then pooled and concentrated to 200 μL using ultrafiltration and protein stocks were aliquoted then flash-frozen in liquid N_2 for storage at $-80°C$.

Imaging of protein condensates

For imaging of condensates formed by proteins with a fluorescent tag (Urm1-GFP, Ub^{G76V}-GFP, GFP, mSt-Uba4, and mSt), proteins were diluted from their concentrated stock into buffer containing physiological salt (150 mM KCl) and 20% Ficoll, unless indicated otherwise. For incubations carried out at pH 7.5, protein was buffered in 20 mM 4-(2-hydroxyethyl)-1-piperazineethanesulfonic acid (HEPES). Incubations conducted at pH 6.5 and 6.0 were carried out in 50 mM 2-(N-morpholino) ethanesulfonic acid (MES). For incubation at pH 5.0, protein was incubated in 50 mM sodium acetate buffer. Protein and buffer were gently mixed with repeated pipetting in a 1.5 mL low bind microcentrifuge tube (Eppendorf) in a 200 μL volume. Protein-buffer mixtures were allowed to incubate for 5 min at 25°C in a tabletop ThemoMixer C (Eppendorf). Samples were subsequently transferred to a 15-well microscope slide (μ-Slide angiogenesis, Ibidi), in 60 μL aliquots, pre-coated with 2% bovine serum albumin (BSA).[83] An additional 15 min incubation step was included to allow for condensates to settle on the slide bottom. For heat treatment of purified protein presented in Figure S4C, Urm1-GFP, GFP, mSt-Uba4 and mSt were prepared exactly as described above including a 46°C incubation in a tabletop ThermoMixer C (Eppendorf) for 15 min. Following heat treatment, samples (60 μL aliquots) were transferred to a BSA coated microscope slide (μ-Slide angiogenesis, Ibidi), followed by an additional 15 min incubation. For microscopy-based analysis of proteins lacking a fluorescent tag, purified protein (Urm1, Urm1(H97F), urm1ΔCT, Uba4, and Pab1) was N-terminally labeled with AlexaFluor NHS ester (Thermo Fisher Scientific) according to the manufacturer's instructions. Briefly, WT Urm1, corresponding mutants, Uba4, and Pab1 were labeled with either Alexa Fluor 488, 504, and 546 NHS ester (ThermoFisher) fluorophores. Labeled and unlabeled protein were mixed at a 1:10 ratio in low bind tubes (Eppendorf) containing buffer of varying pH as described above. Following a 5 min incubation at 25°C in a ThermoMixer C (Eppendorf), samples (60 μL aliquots) were transferred to a BSA coated microscope slide (μ-Slide angiogenesis, Ibidi) and allowed to incubate for 15 min to allow condensates to settle on the bottom of

the slide. Images of purified recombinant proteins were acquired using an Olympus (Tokyo, Japan) FV1000 confocal microscope equipped with an Olympus PLAPON 60×/NA1.42 oil immersion objective as described above. In general, proteins purified from at least two separate batches were analyzed. With assembly imaging experiments using fluorescent proteins (Urm1-GFP, Ub^{G76V}-GFP, and GFP - corresponding to Figure 4C), contrast adjustments were made to significantly reduce background signal in the instances where a diffuse signal was observed. Additionally, in cases where condensates formed, brightness/contrast adjustment were performed to reduce background and enhance signal-to-noise. With respect to assembly imaging using fluorescently labeled protein, contrast adjustments were made to reduce background when indicated directly in the corresponding figure legends. Brightness/contrast adjustments were done within the linear range using Fiji software (Fiji, RRID: SCR_002285).[95]

In vitro urmylation assay

For *in vitro* reconstitution of protein urmylation, purified Urm1 and Uba4 at a concentration of 5 μM and 2 μM, respectively, were gently mixed in buffer containing 150 mM KCl, 20% Ficoll, and 2.5 mM ATP (200 μL final volume) in 1.5 mL low bind microcentrifuge tubes (Eppendorf). Incubations at pH 7.5 were carried out in 20 mM 4-(2-hydroxyethyl)-1-piperazineethanesulfonic acid (HEPES). At pH 6.5, 6.0, and 5.5 proteins were buffered in 50 mM 2-(N-morpholino) ethanesulfonic acid (MES). Incubations were carried out for 15 min at 25°C or 46°C in a tabletop ThermoMixer C (Eppendorf). Total protein mixtures were then separated into soluble and pellet fractions by centrifugation (20,000 x *g*/15 min/room temperature). Next, total and soluble fractions were transferred to fresh 1.5 mL microcentrifuge tubes containing HU buffer, while the pellet fraction was washed once with 500 μL of buffer of the appropriate pH (identical pH as incubation step) followed by resuspension in HU buffer. Samples were incubated at 65°C for 30 min in a tabletop Thermal Mixer C (Eppendorf) with mixing at 2000 r.p.m. Samples were loaded on 4–12% NuPAGE Bis-Tris SDS-PAGE gels (Invitrogen) and analyzed using SDS-PAGE and immunoblotting with an anti-Urm1 antibody (1:10,000).

FRAP of protein condensates

Purified Urm1-GFP was prepared exactly as described above in 'Imaging of Protein Condensates'. Briefly, Urm1-GFP suspended in buffer of the indicated pH (200 μL final volume) was incubated in 1.5 mL low bind microcentrifuge tubes (Eppendorf) for 5 min at 25°C to allow for efficient condensate formation. Protein suspended in buffer was then transferred in 60 μL aliquots to a 15-well microscope slide (μ-Slide angiogenesis, Ibidi) pre-coated with 2% bovine serum albumin (BSA). An additional 15 min incubation time was allowed for condensates to settle on the slide bottom. An FRAP based evaluation of condensate dynamicity was performed with an Olympus (Tokyo, Japan) FV1000 confocal microscope equipped with an Olympus PLAPON 60×/NA1.42 oil immersion objective. Defined, circular regions of interest (ROIs), within the center of an Urm1-GFP condensate, were bleached with 100 iterations of 100% intensity 488 nm light from a 488 nm diode laser, following 5 pre-bleach scans. Pre- and post-bleach monitoring of condensate behavior was done in 1.7 s intervals over a total of 100 frames. FRAP timeseries were analyzed using Fiji (Fiji, RRID: SCR_002285) and data plotted using Prism (Graph Pad, RRID: SCR_002798). Purified Urm1-GFP from two separate batches were subject to FRAP analysis.

In-Gel digestion for IP interactomes and insoluble proteomes

Samples, in HU buffer, were run on 10-well 4–12% NuPAGE SDS polyacrylamide gels (Thermo Fisher Scientific) for 15 min at 130V. Resolved protein was stained for ~16 h using PageBlue (Thermo Fisher Scientific) followed by ~5–6 wash steps with distilled water to remove excess stain. Individual gel lanes were then cut out in 1 mm³ pieces and were destained twice with 150 μL of destaining buffer (25 mM ammonium bicarbonate, 50% ethanol). Gel pieces were dehydrated two times in ~150 μL of 100% ethanol and dried using vacuum centrifugation. Then, 50 μL of digestion buffer (25 mM ammonium bicarbonate, 10 ng/μL of sequencing grade trypsin [Promega]) was added. After incubation for 20 min on ice, 50 μL of ammonium bicarbonate buffer (25 mM) was added and the gel pieces were incubated at 37°C–16 h. Next, extraction of trypsin digested peptides from gel pieces were carried out with 2 x 100 μL incubations with extraction buffer (30% acetonitrile, 3% trifluoroacetic acid (TFA) at 25°C with centrifugation to collect extracted peptides in solution. Finally, the gel pieces were dehydrated by incubation at 25°C in 100 μL of 100% acetonitrile and combined with peptides extracted in the previous step. Acetonitrile was removed by a vacuum-centrifugation step, followed by the addition of 2 M Tris-HCl, 10 mM tris(2-carboxyethyl) phosphine (TCEP) and 40 mM 2-cloroacetamide (CAA). After incubation for 30 min at 37°C, peptides were acidified to 1% TFA and desalted using silica and cation exchange (SCX) Stage Tips.

In-solution digestion for total proteomics

For total proteomic analysis, cell pellets (10 OD$_{600}$) were incubated at 95°C for 2 min in 700 μL of pre-heated lysis buffer (1% sodium deoxycholate, 40 mM CAA, 10 mM TCEP in 100 mM Tris, pH 8.0) and subsequently sonicated in a Bioruptor Plus sonication system (Diogenode) for 10 × 30 s at high intensity. Then, one-tenth of the samples were incubated once more at 95°C for 2 min, then sonicated. Before digestion, the samples were diluted 1:2 with water. Samples were digested for 4 h at 37°C with 1 μg of mass spec grade Lys-C (Promega) followed by an 16 h incubation at 37°C in the presence of 2 μg of trypsin (Promega). The solution of peptides was then acidified with TFA to a final concentration of 1%, followed by desalting via SCX Stage Tips. Eluted peptides were vacuum dried and re-suspended in 6 μL of 0.1% formic acid in MS grade water.

LC-MS/MS analysis for in-gel digestion

Purified and desalted peptides were loaded onto a 30-cm column (inner diameter: 75 microns; packed in-house with ReproSil-Pur C18-AQ 1.9-micron beads, Dr. Maisch GmbH) via the autosampler of the Thermo Easy-nLC 1200 (Thermo Fisher Scientific) at 60°C. Using the nanoelectrospray interface, eluting peptides were directly sprayed onto the benchtop Orbitrap mass spectrometer Q Exactive HF (Thermo Fisher Scientific). Peptides were loaded in buffer A (0.1% formic acid) at 250 nL/min and percentage of buffer B (80% acetonitrile, 0.1% formic acid) increased from 2 to 30% over 120 min, followed by an increase to 60% over 10 min, then 95% over the next 5 min. Percentage of buffer B was maintained at 95% for another 5 min. The mass spectrometer was operated in a data-dependent mode with survey scans from 300 to 1650 m/z (resolution of 60000 at m/z = 200), and up to 10 of the top precursors were selected and fragmented using higher energy collisional dissociation (HCD with a normalized collision energy of value of 28). The MS2 spectra were recorded at a resolution of 15000 (at m/z = 200). AGC target for MS and MS2 scans were set to 3E6 and 1E5, respectively, within a maximum injection time of 100 and 60 ms for MS and MS2 scans, respectively. Dynamic exclusion was set to 30 ms.

LC-MS/MS analysis for in-solution digestion

Peptides (injection volume of 3 μL) were separated at a flow rate of 250 nL/min with the Thermo Easy-nLC 1200 (Thermo Fisher Scientific) using a home-packed 30 cm-column (inner diameter: 75 microns; packed in-house with ReproSil-Pur C18-AQ 1.9-micron beads, Dr. Maisch GmbH). The column temperature was held at 60°C and peptides were separated using a gradient of buffer A (0.1% formic acid) with increasing buffer B (0.1% formic acid, 80% acetonitrile) content. The percentage of buffer B was ramped from 2 to 30% over 120 min, followed by a ramp to 60% over 10 min, then to 95% over the next 5 min and finally, percentage of buffer B was maintained at 95% for another 5 min. Eluting peptides were directly sprayed onto the benchtop Orbitrap mass spectrometer Q Exactive HF (Thermo Fisher Scientific). The mass spectrometer was operated in a data dependent mode with survey scans from 300 to 1750 m/z (resolution of 60000 at m/z = 200), and up to 15 of the top precursors were selected and fragmented using higher energy collisional dissociation (HCD with a normalized collision energy value of 28). The MS2 spectra were recorded at a resolution of 15000 (at m/z = 200). AGC target for MS1 and MS2 scans were set to 3E6 and 1E5, respectively, within a maximum injection time of 100 ms for MS1 and 25 ms for MS2 scans. Dynamic exclusion was set to 30 ms.

MS data analysis

Raw data were processed using the MaxQuant computational platform (MaxQuant version 1.6.5.0, RRID: SCR_014485) with standard settings applied. Briefly, the peak list was searched against the UniProt database of *S. cerevisiae* with an allowed precursor mass deviation of 4.5 ppm and an allowed fragment mass deviation of 20 ppm. MaxQuant, by default, enables individual peptide mass tolerances, which was used in the search. Cysteine carbamidomethylation, methionine oxidation and N-terminal acetylation were set as variable modifications. The match between the run option was enabled, and proteins were quantified across samples using the label free quantification algorithm in MaxQuant (MaxQuant version 1.6.5.0, RRID: SCR_014485) as label free quantification (LFQ) intensities.

Analysis of urmylation site structuredness

AlphaFold2 structures were retrieved using the Protti package[96] with modifications. Amino acids that were part of structural elements were assigned with a value of 1, whereas residues of unstructured regions were set to 0. The mean and bootstrapped 95% confidence intervals of the structuredness were calculated at each position and compared to the same number of randomly sampled positions from the same substrates. Curves were smoothened with a 21 amino acid moving average and centered around urmylation modification sites identified by mass spectrometry.

Modeling of the Urm1-Uba4 core complex from *S. cerevisiae*

A local installation of AlphaFold-multimer (version 2.3.0; RRID: SCR_023662) was run with the sequences of Urm1 and residues 1–326 of Uba4 from *S. cerevisiae* assuming a 2:2 stoichiometry as input and using full_db as a database preset. Predicted models were relaxed using the Amber relaxation procedure. The five output models essentially only differed in the regions preceding and following the adenylation domain of Uba4.

Sequence alignment using ConSurf

Conservation of the Urm1 and Uba4 sequences was analyzed using the ConSurf alignment server (ConSurf, RRID: SCR_015753).[97] Searches conducted were sourced from the UNIref. 90 database, a clustered version derived from the UniProt database. 1534 homologues in total were extracted from the UniProt database using HMMER. Of these, 1411 homologues passed thresholds (min/max similarity, coverage) and 1150 of them are CD-HIT distinctive. The calculations were made on the basis of 300 hits, sampled from pooled distinctive hits. The search algorithm used is HMMER with an E-value of 0.0001 and an iteration of 1.

Analysis of *sc*Urm1 and *sc*Ub electrostatic surface potential

Electrostatic potential maps for the crystal structure of *sc*Urm1 (PDB: 2PKO) and *sc*Ub (PDB: 1UBQ) were calculated with the APBS server (Adaptive Poisson-Boltzmann Solver, RRID: SCR_008387) at different pH values and visualized with PyMol (PyMol, RRID: SCR_000305) using the APBS Electrostatics plugin.

QUANTIFICATION AND STATISTICAL ANALYSIS

Assembly of graphs and statistical analyses were conducted using Prism 9.3.1 (GraphPad, RRID: SCR_002798) and Perseus (Perseus version 1.6.15, RRID: SCR_015753). All statistical tests utilized are indicated within the respective figure legends. For multiple comparisons, one- and two-way ANOVA were used with Dunnett and Holm-Sidak corrections applied. For comparison of two groups, statistical significance was derived using Student's t-tests and Mann-Whitney tests.

Supplemental figures
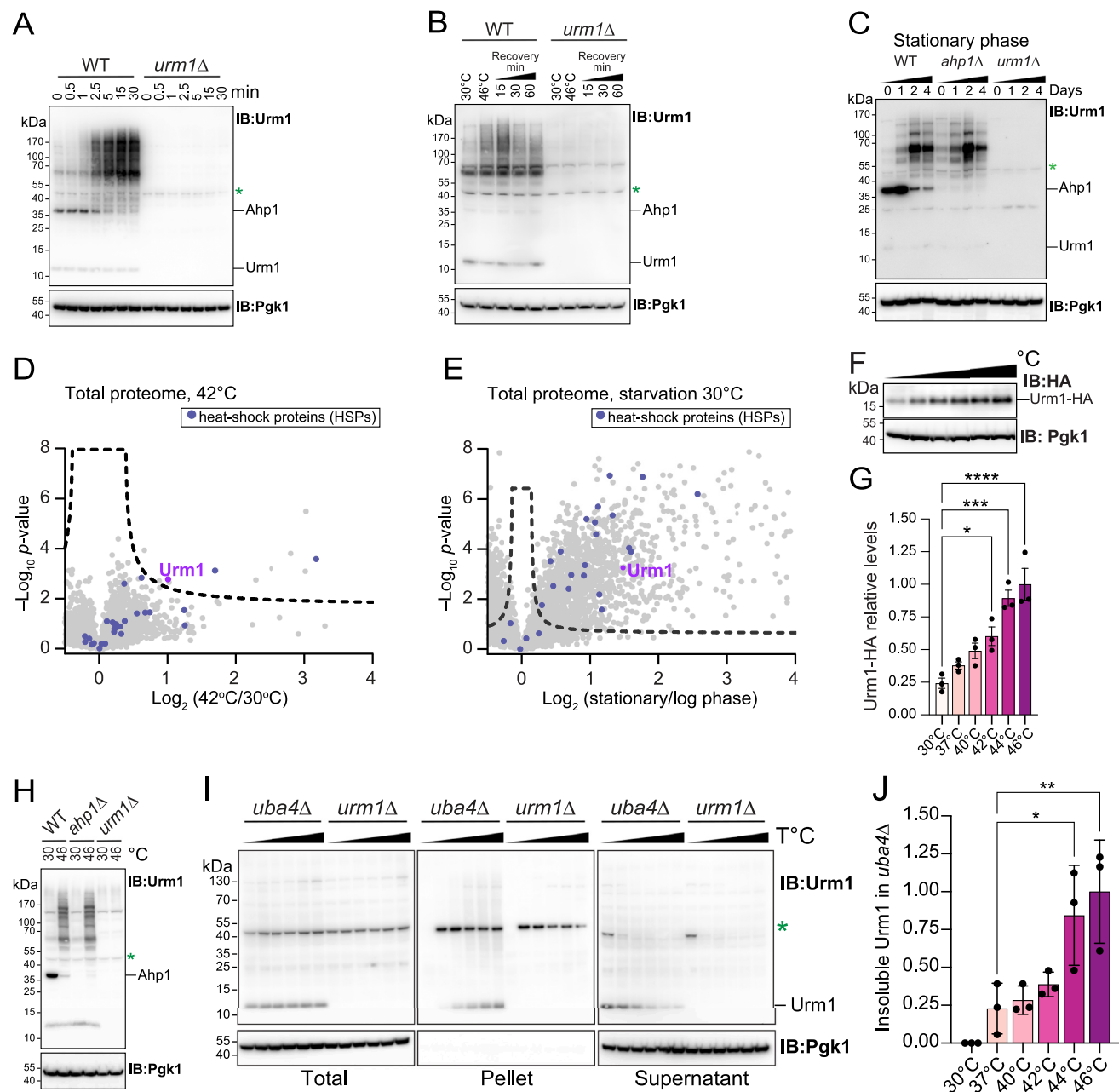
Figure S1. Urmylation upon heat stress and starvation, related to Figure 1

(A) Kinetics of protein urmylation upon HS. WT and *urm1Δ* cells, grown to mid-log phase at 30°C, were shifted to 46°C. Cells were collected at the indicated time points and total protein extracts (see STAR Methods) analyzed using SDS-PAGE and immunoblotting with Urm1 antibody as in Figure 1A. An asterisk indicates cross-reactivity (*n* = 3).

(B) Reversibility of urmylation. Total protein extracts from WT and *urm1Δ* cells exposed to HS (46°C, 30 min) and recovery at 30°C as indicated were analyzed by immunoblotting with Urm1 antibody. An asterisk shows cross-reactivity (*n* = 3).

(C) Protein urmylation under conditions of starvation. WT, *ahp1Δ*, and *urm1Δ* cells were grown to stationary phase for the indicated number of days. Total cell extracts were analyzed using SDS-PAGE and immunoblotting with Urm1 antibody. An asterisk indicates cross-reactivity (*n* = 2).

(D and E) Total proteome analysis after thermal and starvation induced stress. (D) Total protein extracts from WT cells grown at 30°C and following incubation at 42°C for 15 min were analyzed using label free proteomics (see STAR Methods). A black dashed line indicates an FDR cutoff of 0.05 (*n* = 3). A volcano plot displays

(legend continued on next page)

heat shock proteins (HSPs; blue) and Urm1 (purple). See also Table S1A. (E) A similar analysis as conducted in (E) shows the upregulation of Urm1 following growth of WT cells to stationary phase for 3 days (*n* = 4). See also Table S1B.

(F and G) Levels of Urm1-HA (non-conjugatable Urm1) as a function of temperature. (F) Cells producing Urm1-HA, driven from the endogenous *URM1* promoter, were propagated to mid-log phase, then shifted to the indicated temperatures for 15 min. Urm1-HA levels were assessed by immunoblotting using an anti-HA antibody. An antibody against Pgk1 was utilized as a control (*n* = 3). (G) Quantification of Urm1-HA levels using densitometry and normalized to Pgk1 levels. Error bars display mean ± SEM (*n* = 3). *p*-Values were assessed by one way ANOVA with Dunnett's correction. *, $p < 0.05$; ***, $p < 0.001$; ****, $p < 0.0001$.

(H) Ahp1 represents a predominant Urm1 modified target. Total protein extracts from WT, *ahp1Δ*, and *urm1Δ* cells were incubated at the indicated temperatures for 15 min. Total cell extracts were analyzed by immunoblotting with Urm1 antibody. An asterisk shows cross-reactivity (*n* = 2).

(I) Urm1 solubility in the absence of conjugation. Detergent solubilized cellular extracts isolated from *uba4Δ* and *urm1Δ* cells exposed to HS at different temperatures for 15 min as in Figure 1A. Lysates were separated into pellet and soluble fractions by centrifugation (see STAR Methods). Fractions were analyzed by anti-Urm1 and anti-Pgk1 immunoblotting. 25% of total and supernatant fractions and 100% of pellet fractions were analyzed. Asterisk indicates cross-reactivity (*n* = 3).

(J) Quantification of HS-induced accumulation of free Urm1 in the insoluble pellet fraction as in (I) by densitometry and normalized to total free Urm1. Error bars display mean ± SEM (*n* = 3). *p*-Values were assessed by one way ANOVA with Dunnett's correction. *, $p < 0.05$; **, $p < 0.01$.
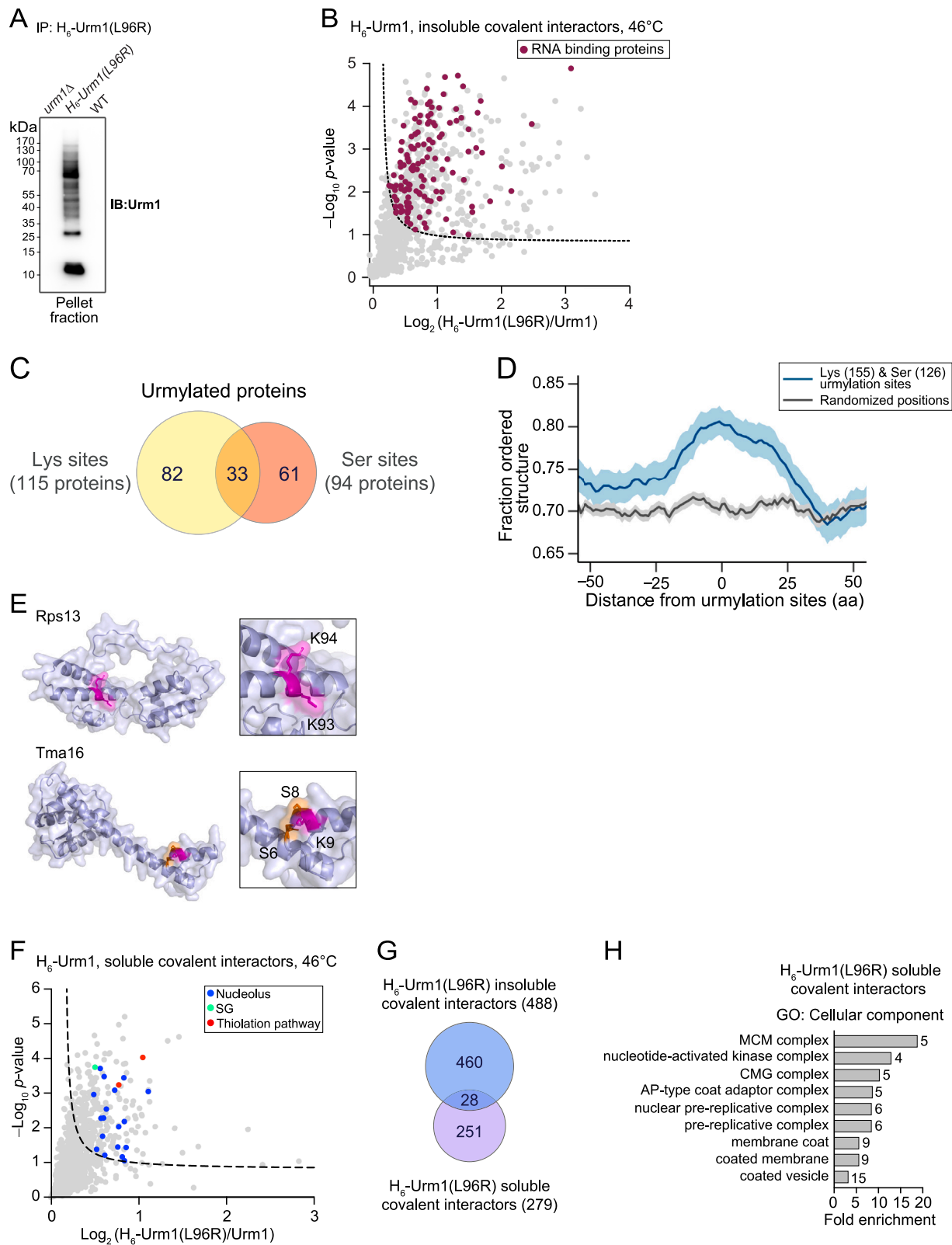
Figure S2. Identification of Urm1 Target Proteins, related to Figure 1

(A) Affinity purification of Urm1 modified proteins from the pellet fraction of cells expressing the H_6-tagged variant of Urm1, Urm1(L96R). Insoluble H_6-Urm1(L96R) modified proteins were affinity purified as described in Figure 1C (see STAR Methods). WT and *urm1*Δ lysates were utilized as controls for immunoblotting with anti-Urm1 antibody (*n* = 2).

(B) Distribution of RNA binding proteins (RBPs) among covalent Urm1 interactors from the insoluble pellet fraction. A volcano plot displays H_6-Urm1(L96R) covalent interactors belonging to the categories RNA binding (data re-displayed from Figure 1C). A black dashed line indicates an FDR cutoff of 0.05 (*n* = 4). See Table S1C.

(C) Venn diagram showing numbers of proteins with identified urmylation sites (branched trypsin peptides derived from Urm1(L96R)) on lysines and serines, or both, of proteins covalently modified with Urm1. See also Table S1H.

(D) Preferred location of urmylation sites in structured protein regions based on AlphaFold2 (RRID: SCR_023662) predictions. The graph displays the general structuredness of the positioning of urmylation sites detected within Urm1 modified proteins. The blue line indicates the mean positioning of lysine and serine residues modified by Urm1 and gray lines indicates the structuredness for random positions in Urm1 modified proteins. Shaded areas indicate a 95% confidence interval. See also Table S1G.

(E) Topological positioning of urmylation sites in Urm1 covalent interactors, small ribosomal protein Rps13 and translation machinery-associated protein Tma16. Displayed is a 3-dimensional representation of Rps13 and Tma16, derived from AlphaFold2 (RRID: SCR_023662), and the positioning of K and S modifications within these proteins, highlighted in magenta and orange, respectively. Zoomed images indicate the precise locations of modified K and S residues, respectively. See Tables S1E–S1H.

(F) Characterization of soluble Urm1 covalent interactors following HS (46°C, 15 min). Cells expressing H_6-Urm1(L96R)*,* as in Figure 1C, were harvested and subjected to fractionation, as in Figure 1A. Soluble H_6-Urm1(L96R) interactors were affinity purified and subjected to label free proteomics for identification (see STAR Methods). A volcano plot displays the enrichment of soluble urmylated proteins in H_6-Urm1(L96R) cells relative to WT. Urm1 modified thiolation components, nucleolar, and SG proteins are highlighted. A black dashed line indicates an FDR cutoff of 0.05 (*n* = 4). See also Table S1I.

(G) A Venn diagram showing limited overlap between soluble and insoluble covalent Urm1 interactomes. Numbers of proteins are indicated. See also Table S1I.

(H) GO term analysis (cellular component) representing the categories of soluble Urm1 modified proteins. Numbers listed indicate the number of proteins belonging to each GO category. See also Table S1J.
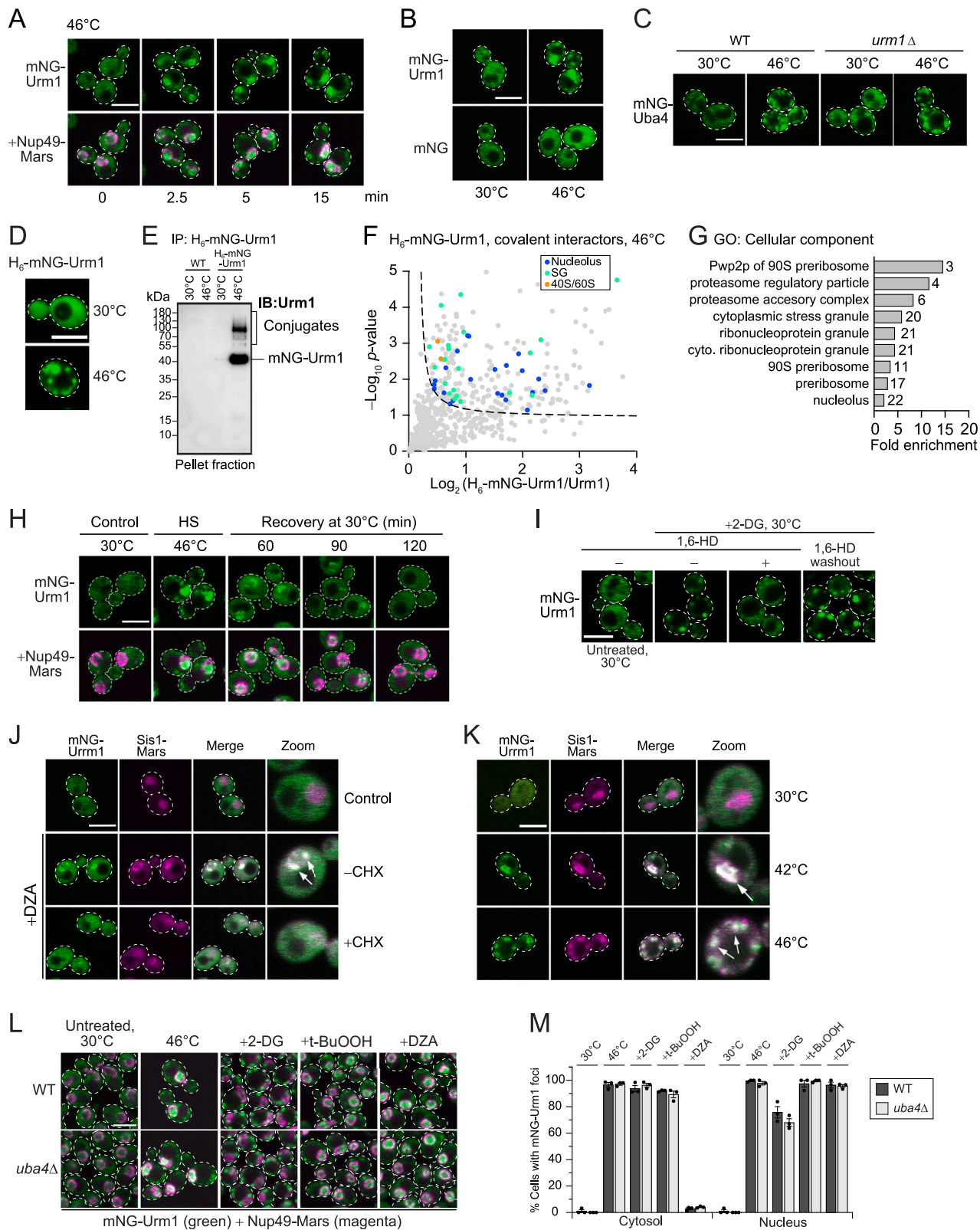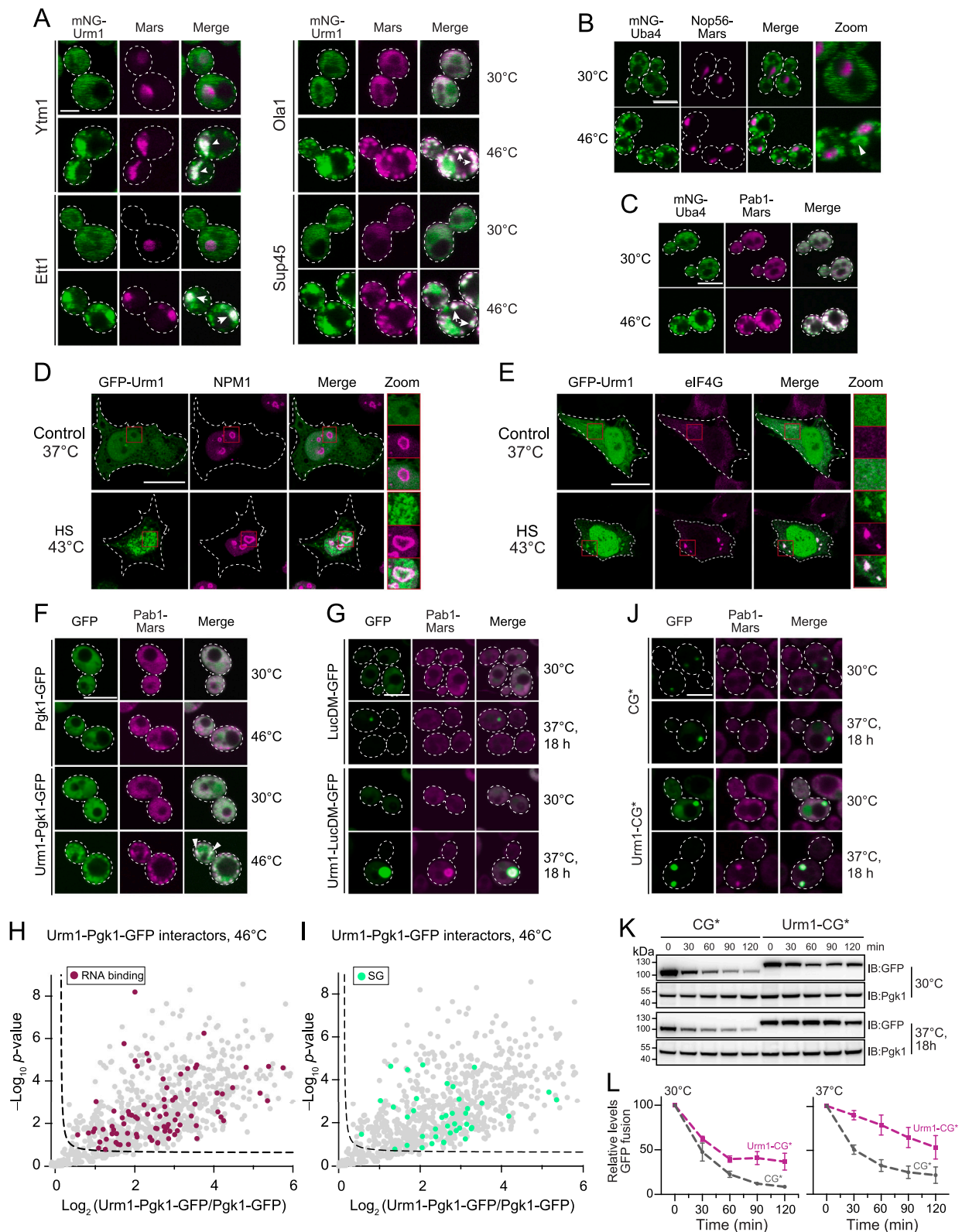
(legend on next page)

Figure S3. Urm1 and Uba4 form condensates upon HS, related to Figure 2

(A) Cellular distribution of mNG-Urm1 following HS at 46°C for the times indicated. Cells co-expressing mNG-Urm1 and Nup49-Mars (endogenous promoters) were grown to mid-log phase at 30°C then shifted to 46°C. Live cell images were acquired using a confocal microscope ($n = 2$). Scale bar, 5 μm.

(B) Distribution of mNG-Urm1, and mNG alone, following HS. Cells expressing either mNG-Urm1 or mNG, both driven from the endogenous *URM1* promoter, were propagated overnight at 30°C then shifted to 46°C for 15 min. Live cell imaging was conducted using a confocal microscope ($n = 2$). Scale bar, 5 μm.

(C) Subcellular distribution of mNG-Uba4 following HS. WT and *urm1Δ* cells expressing mNG-Uba4 (endogenous promoter) were grown to mid-log phase, then shifted to 46°C (15 min). mNG-Uba4 was observed using live cell confocal microscopy ($n = 3$). Scale bar, 5 μm.

(D) Subcellular distribution of H₆-mNG-Urm1 with and without HS. Cells expressing H$_6$-mNG-Urm1 (*ADH1* promoter) were propagated to mid-log phase at 30°C, then shifted to 46°C for 15 min. Live cell imaging was conducted using a confocal microscope ($n = 2$). Scale bar, 5 μm.

(E) Affinity purification of H$_6$-mNG-Urm1 modified proteins from the insoluble pellet fraction following HS. Insoluble H$_6$-mNG-Urm1 modified proteins were affinity purified from cells propagated at 30°C or following HS (46°C, 15 min) as described in Figure 1C (see STAR Methods). Lysates from WT cells were utilized as controls for immunoblotting with an anti-mNeonGreen antibody. The positions of free and covalently attached H$_6$-mNG-Urm1 are indicated ($n = 2$).

(F) Identification of insoluble proteins modified by H$_6$-mNG-Urm1 upon HS (46°C, 15 min). H$_6$-mNG-Urm1 was enriched from the insoluble pellet fraction and analyzed using label free proteomics as in Figure 1C (see STAR Methods). A Volcano plot showing the enrichment of urmylated proteins in H$_6$-mNG-Urm1 cells relative to WT. Modified nucleolar, ribosomal, and SG proteins are highlighted. A black dashed line indicates an FDR cutoff of 0.05 ($n = 4$). See also Table S2A.

(G) GO term analysis (cellular component) representing the categories of mNG-Urm1 modified proteins enriched from the insoluble pellet fraction. Values listed indicate the number of proteins belonging to each GO category. See also Table S2B.

(H) Cellular distribution of mNG-Urm1 upon recovery from HS. Cells expressing mNG-Urm1 and Nup49-Mars as in (C) were grown to mid-log phase at 30°C, then shifted to 46°C for 15 min. Cells were then returned to 30°C for recovery for 60-, 90-, and 120-min. Live cell images were acquired both pre- and post-recovery using confocal microscopy ($n = 4$). Scale bar, 5 μm.

(I) The behavior of mNG-Urm1 foci as condensates following treatment of cells with 1,6-hexanediol (1,6-HD). Mid-log phase WT cells, producing mNG-Urm1 (endogenous promoter), were treated with 2-DG for 2 h to induce starvation (see STAR Methods). Subsequently, cells were treated with 5% 1,6-HD for 5 min or, were washed twice, then shifted back into media containing 2-DG for 30 min. Live cell imaging was conducted using a confocal microscope ($n = 3$). Scale bar, 5 μm.

(J) Cellular distribution of mNG-Urm1 and Sis1-Mars following DZA treatment of cells as in Figure 2E. Confocal microscopy was employed to follow the localization of mNG-Urm1 relative to Sis1-Mars (expressed from endogenous promoters). Arrows indicate foci containing both proteins ($n = 3$). Scale bar, 5 μm.

(K) Localization of Urm1 relative to Sis1 upon HS. The cellular distribution of mNG-Urm1 relative to Sis1-Mars (endogenous promoter) was analyzed using a confocal microscope for live cell imaging following mid-log phase growth at 30°C and upon shift of cells to 42°C and 46°C for 15 min ($n = 3$). Arrows point to nuclear (42°C) and cytoplasmic foci (46°C) where mNG-Urm1 and Sis1-Mars colocalize. Scale bar, 5 μm.

(L) Cellular distribution of mNG-Urm1 in *uba4Δ* cells under diverse stress conditions. Live cell confocal microscopy was employed to follow the subcellular distribution of mNG-Urm1 (endogenous promoter) relative to Nup49-Mars (endogenous promoters) in WT and *uba4Δ* cells at 30°C, following shift to 46°C for 15 min as in Figure 2A and 2-DG treatment as in Figure 2C, t-BuOOH treatment as in Figure 2C, and DZA treatment as in Figure 2E ($n = 3$). Scale bar, 5 μm.

(M) Quantification of cytosolic and nuclear mNG-Urm1 foci under the conditions as in (L) in WT and *uba4Δ* cells. Bar graphs display the percentage of foci-containing cells. A minimum of 50 cells per category were included in the analysis. Error bars display mean ± SEM ($n = 3$).

Figure S4. Urm1 and Uba4 form condensates in cytoplasm and nucleus, related to Figure 3

(A) Localization of mNG-Urm1 relative to proteins covalently modified with Urm1. The subcellular distribution of mNG-Urm1 was followed relative to two covalently modified substrates residing in the nucleolus (Ytm1-Mars and Ett1-Mars), as well as two substrates residing in SGs (Ola1-Mars and Sup45-Mars), all driven from their endogenous promoters. Cells were propagated to mid-log phase at 30°C, then shifted to 46°C for 15 min. Images were acquired using a confocal microscope (n = 3). Arrow heads point to nuclear and cytoplasmic foci in which mNG-Urm1 co-localizes with the Mars-tagged Urm1 target proteins. Scale bar, 5 μm.

(B) Cellular localization of mNG-Uba4 relative to the nucleolus. Confocal microscopy was used to analyze mNG-Uba4 relative to Nop56-Mars (endogenous promoters) in cells as in Figure 3A grown under basal conditions at 30°C and following acute HS (46°C, 15 min) (n = 3). Scale bar, 5 μm. An arrow head points to a large mNG-Uba4 aggregate adjacent to the nucleolus.

(C) Cellular localization of mNG-Uba4 relative to SGs. The distribution of mNG-Uba4 and Pab1-Mars (endogenous promoters) was analyzed as described in Figure 3B. Live cell imaging was performed using a confocal microscope (n = 4). Scale bar, 5 μm.

(D) Subcellular distribution of GFP-Urm1 relative to nucleoli in mammalian cells. HeLa cells, transiently transfected with a plasmid producing GFP-Urm1were propagated under basal growth conditions at 37°C, then subjected to HS (2 h at 43°C). Following fixation, images of cells were acquired using a confocal microscope. Immunostaining with an antibody against NPM1 was used to label nucleoli (n = 3). Scale bar, 20 μm. Zoomed areas are marked with red squares.

(E) Distribution of GFP-Urm1 relative to SGs in mammalian cells. The localization of SGs was followed in HeLa cells by immunostaining against the SG component eIF4G. GFP-Urm1 was expressed by transient transfection and images of fixed cells were acquired before and after HS as in (D) (n = 3). Scale bar, 20 μm. Zoomed areas are marked with red squares.

(F) Distribution of Urm1-Pgk1 relative to SGs in yeast cells. Confocal microscopy was employed to follow the localization of plasmid borne Urm1-Pgk1-GFP (GAL1 promoter) in cells producing the SG marker Pab1-Mars (endogenous promoter). Log phase cells, grown at 30°C, were exposed to HS (46°C, 15 min) and were analyzed using live cell confocal microscopy (n = 2). Scale bar, 5 μm. Arrow heads point to SGs containing Urm1-Pgk1.

(G) Analysis of Urm1-LucDM-GFP under conditions of mild HS. Cells expressing either LucDM-GFP or Urm1-LucDM-GFP (GAL1 promoter) and Pab1-Mars (endogenous promoter) were analyzed using live cell confocal microscopy under basal growth conditions (30°C) and following growth at 37°C for 18 h (n = 2). Brightness/contrast adjustments were used to improve weak fluorescence intensities. Scale bar, 5 μm.

(H) Interactome analysis of Urm1-Pgk1-GFP upon HS. Lysates isolated from cells exposed to HS (46°C, 15 min) were subjected to immunoprecipitation with anti-GFP nanobody (see STAR Methods). Pgk1-GFP served as background control. Precipitated material was analyzed by LC-MS/MS and label free proteomics. A volcano plot displays the Urm1-Pgk1-GFP interactome upon HS. RNA binding proteins (RBPs) are highlighted. A black dashed line indicates an FDR cutoff of 0.05 (n = 4). See also Table S3B.

(I) Distribution of SG proteins among covalent Urm1-Pgk1-GFP non-covalent interactors. A volcano plot displays Urm1-Pgk1-GFP interactors. Proteins belonging to the category SG are highlighted (data re-displayed from Figure S3H). A black dashed line indicates an FDR cut-off of 0.05 (n = 4). See also Table S3B.

(J) Analysis of Urm1-CG* under conditions of mild HS. Cells producing either CG* or Urm1-CG* (GAL1 promoter) and Pab1-Mars (endogenous promoter) were analyzed using live cell confocal microscopy following growth at 30°C and after mild HS at 37°C for 18 h (n = 3). Brightness/contrast adjustments were used to improve weak fluorescence intensities. Scale bar, 5 μm.

(K) Analysis of the turnover rates of both CG* and Urm1-CG*. The turnover rates of CG* and Urm1-CG* were analyzed under the growth conditions in (J) using a metabolic shutoff analysis (see STAR methods). Samples were collected at the indicated times post-shutoff (following glucose addition) and protein levels evaluated using immunoblotting with an anti-GFP antibody. An anti-Pgk1 antibody was used to evaluate protein loading (n = 3).

(L) Quantification of CG* and Urm1-CG* turnover as in (K) using densitometry and normalized to Pgk1 levels. Error bars display mean ± SEM (n = 3).
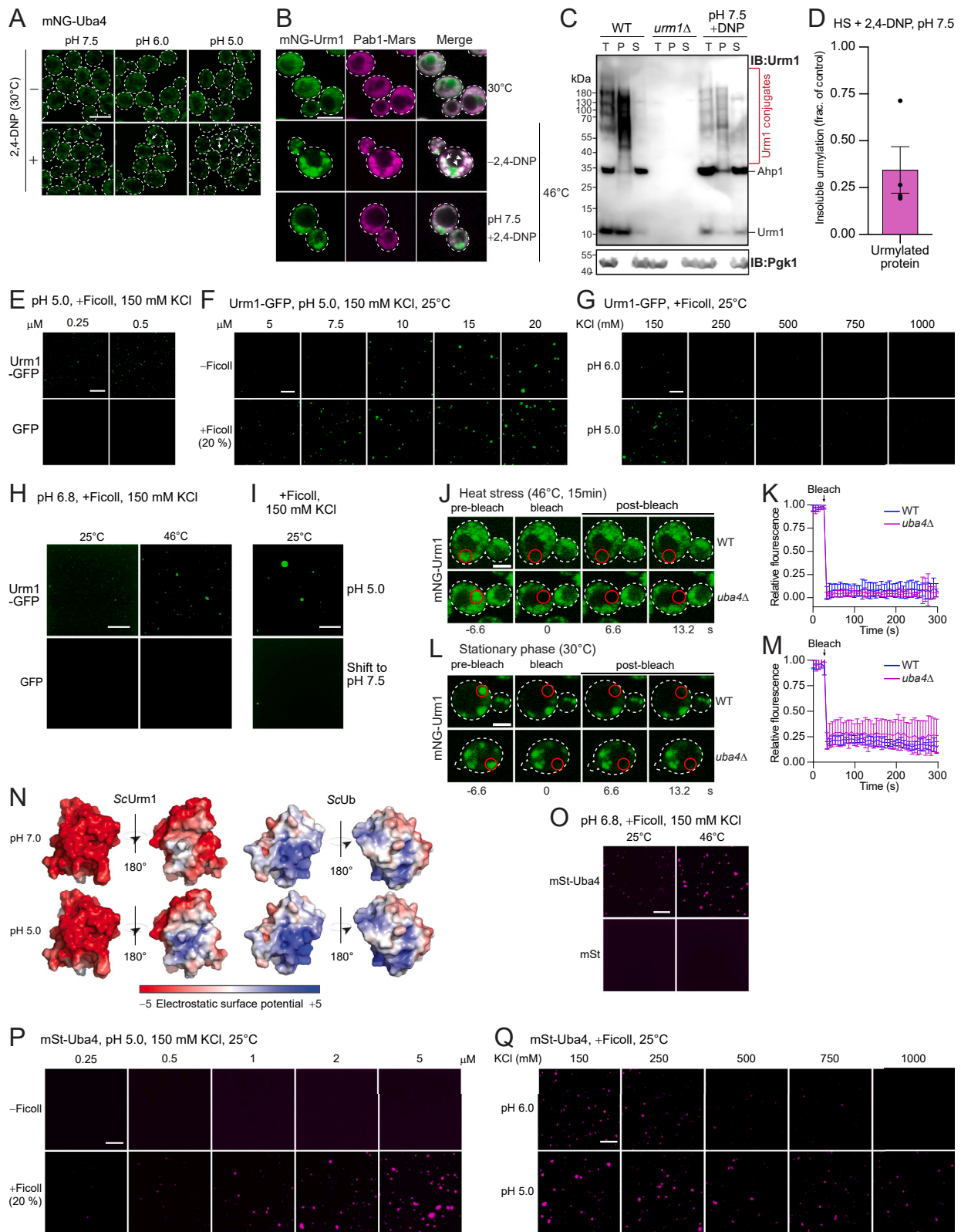
Figure S5. Purified Urm1 and Uba4 phase separate in response to acidic pH, related to Figure 4

(A) Behavior of mNG-Uba4 in live cells following intracellular acidification. Cells expressing mNG-Uba4 (endogenous promoter) were incubated in buffer of the indicated pH, either in the presence or absence of 2 mM 2,4-DNP, as described in Figure 4A. Live cell imaging was performed using a confocal microscope (*n* = 2). Arrows point to mNG-Uba4 foci formed at acidic pH in the presence of 2,4-DNP. Scale bar, 5 μm.

(B) Localization of mNG-Urm1 and Pab1-Mars following acute HS while maintaining cellular pH at 7.5. Cells synthesizing mNG-Urm1 and Pab1-Mars (expressed from the *URM1* and *PAB1* promoter, respectively) were propagated to mid-log phase, then shifted to 46°C in pH 7.5 media, in the presence or absence of 2,4-DNP, to inhibit intracellular acidification normally occurring with HS (see STAR Methods). Live cell imaging was conducted using a confocal microscope (*n* = 2). Arrows point to cytoplasmic foci where mNG-Urm1 and Pab1-Mars co-localize under HS in the absence of 2,4-DNP (control conditions). Scale bar, 5 μm.

(C) Solubility of urmylated proteins upon HS at pH 7.5. WT and *urm1Δ* cells were propagated to mid-log phase and exposed to HS under conditions where intracellular acidification was inhibited as in (A). Fractionation analysis to separate total, soluble, and pellet fractions was conducted as in Figure 1A. Immuno-blotting was conducted using antibodies against Urm1 and Pgk1 (loading control). The positions of free Urm1 and Ahp1, as well as Urm1 conjugates quantified (C) are indicated (*n* = 4).

(D) Quantification of insoluble urmylation under conditions of maintained neutral pH (7.5) following HS as in (B) by densitometry. Insoluble urmylation in DNP treated samples is normalized to untreated WT cells exposed to HS (*n* = 4). Error bars display mean ± SEM.

(E) Urm1-GFP condensate formation in the nanomolar range. Recombinant Urm1-GFP and, GFP alone, at 250 and 500 nM, were incubated in pH 5 buffer/150 mM KCl at 25°C containing 20% Ficoll. Images of fluorescent proteins were acquired using a confocal microscope (*n* = 3). The sensitivity of the photomultipliers was increased to visualize protein droplets at this concentration range. Contrast adjustments were applied to reduce background. Scale bar, 7.5 μm.

(F) Urm1-GFP condensate formation as a function of protein concentration. Purified Urm1-GFP, at the indicated concentrations, was incubated in pH 5 buffer/ 150 mM KCl at 25°C, either in the presence or absence of 20% Ficoll. Images of Urm1-GFP assemblies were acquired using a confocal microscope (*n* = 2). Contrast adjustments were applied to reduce background. Scale bar, 7.5 μm.

(G) Salt sensitivity of Urm1-GFP condensate formation. Purified Urm1-GFP (10 μM) was imaged using confocal microscopy following incubation in buffer of the indicated pH, salt concentrations (25°C, 20% Ficoll) (*n* = 2). Contrast adjustments were applied to reduce background. Scale bars, 7.5 μm.

(H) Urm1-GFP condensate formation following incubation at an elevated temperature. Urm1-GFP and GFP (5 μM each) were incubated in pH 6.8 buffer containing 20% Ficoll/150 mM KCl at 25°C or 46°C (15 min). Images were acquired using confocal microscopy (*n* = 2). Contrast adjustments were applied to reduce background. Scale bar, 7.5 μm.

(I) Partial reversibility of Urm1-GFP condensates at pH 7.5. Purified Urm1-GFP (5 μM) was incubated in pH 5 buffer/150 mM KCl at 25°C containing 20% Ficoll. Condensates were sedimented by centrifugation and resuspended in either buffer of pH 7.5 or 5.0 containing 150 mM KCl with 20% Ficoll at 25°C, followed by incubation of 30 min and analysis. (*n* = 3). Scale bar, 7.5 μm.

(J and K) FRAP analysis of mNG-Urm1 condensates in the absence of Uba4 following HS. (J) FRAP was utilized to analyze the dynamicity of mNG-Urm1 foci in cells following HS at 46°C, 15 min in WT and *uba4Δ* cells. Red circles represent the bleached region of interest (*n* = 2). Scale bar, 2.5 μm. (K) A graph display of the normalized and corrected FRAP values with error bars of 8 independent bleaching experiments per biological replicate of panel (J).

(L and M) FRAP analysis of mNG-Urm1 condensates in the absence of Uba4 following starvation. (L) FRAP analysis, as conducted in (J), was used to analyze the dynamics of starvation induced mNG-Urm1 foci in WT and *uba4Δ* cells. Red circles represent the bleached region of interest (*n* = 3). Scale bar, 2.5 μm. (M) A graph display of the normalized and corrected FRAP values with error bars of 8 independent bleaching experiments per biological replicate of panel (L).

(N) Surface electrostatic potential of *Sc*Urm1 and *Sc*Ub with changing pH. The surface properties of *Sc*Urm1 (PDB: 2PKO) and *Sc*Ub (PDB: 1UBQ) are displayed according to their electrostatic potential as predicted at both pH 7 and pH 5 using the Adaptive Poisson-Boltzmann Solver (APBS) algorithm. Red and blue represent negative and positive electrostatic potential, respectively.

(O) Condensate formation of purified mSt-Uba4 at elevated temperature. mSt-Uba4 and mSt alone (2 μM each) was analyzed by confocal microscopy following incubation in the presence of 20% Ficoll/150 mM KCl/pH 6.8 at 25°C or 46°C (15 min) (*n* = 3). Scale bar, 7.5 μm.

(P) Dependence of mSt-Uba4 assembly on concentration and the presence of crowding agent. Purified mSt-Uba4 was incubated in pH 5 buffer/150 mM KCl with or without 20% Ficoll at 25°C. Condensate formation was evaluated using a confocal microscope (*n* = 3). Scale bar, 7.5 μm.

(Q) Salt sensitivity of mSt-Uba4 condensate formation. Purified mSt-Uba4 (2 μM) was imaged using confocal microscopy following incubation in buffer of the indicated pH and KCl concentrations at 25°C with 20% Ficoll (*n* = 2). Scale bar, 7.5 μm.

A +Ficoll, 150 mM KCl, 25°C


B +Ficoll, 25°C

C 5 µM Urm1 + 2 µM Uba4 + ATP
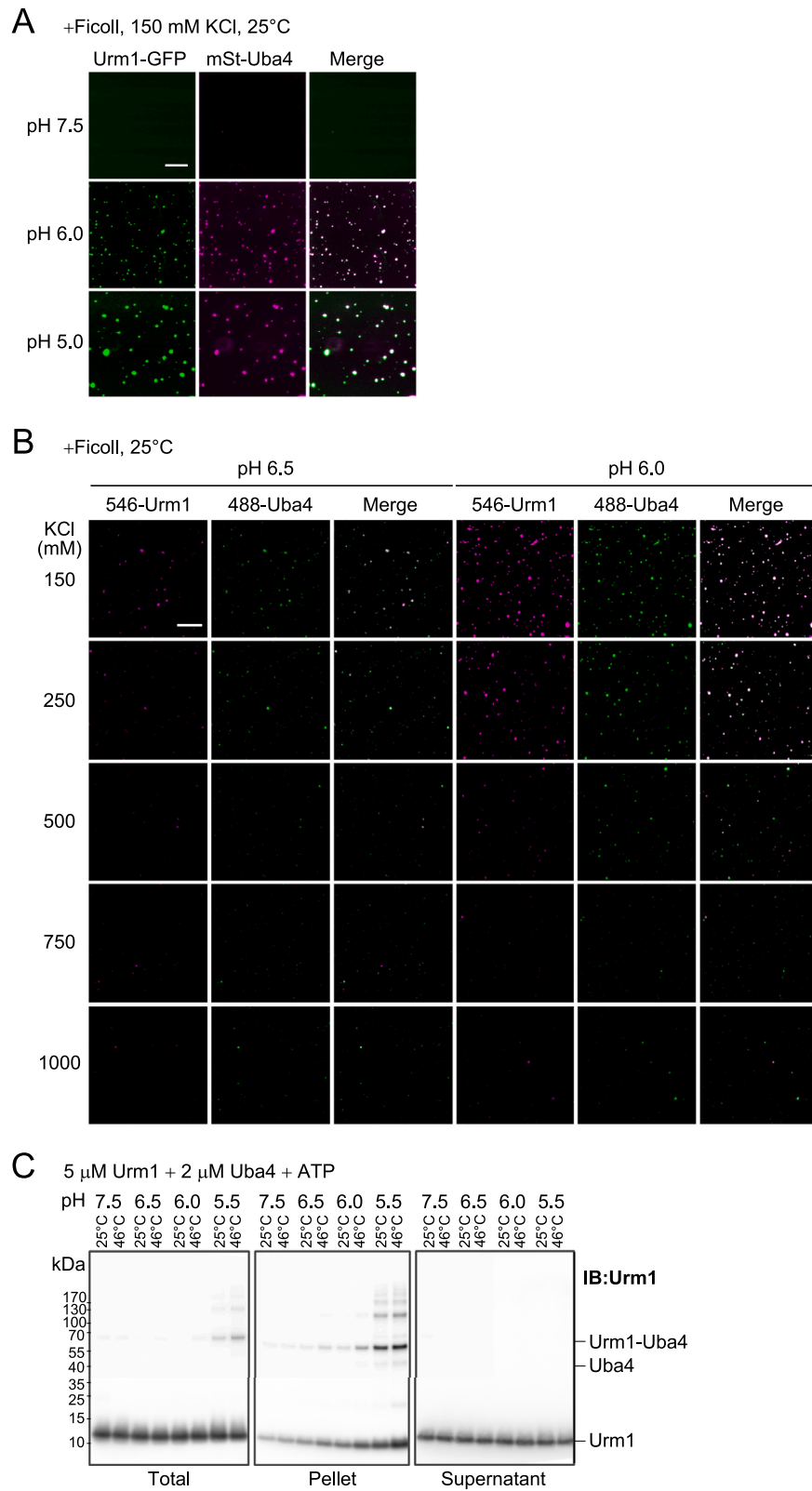
Figure S6. Purified Urm1 and Uba4 form a co-condensate, related to Figure 5

(A) Co-demixing of Urm1-GFP and mSt-Uba4. Purified Urm1-GFP (5 μM) and mSt-Uba4 (2 μM) were incubated in buffer of the indicated pH containing 150 mM KCl/20% Ficoll at 25°C. Images were acquired using confocal microscopy (*n* = 2). Contrast adjustments were applied to reduce background. Scale bar, 7.5 μm.

(B) Urm1 and Uba4 co-condensate formation is salt sensitive. Purified Urm1 (5 μM) and Uba4 (2 μM) (fluorescent labeled as in Figure 5A and mixed with unlabeled protein) were incubated at 25°C for 15 min in buffer of the indicated pH containing 20% Ficoll at the KCl concentrations indicated. Images of assembled protein were acquired using a confocal microscope (*n* = 3). Contrast adjustments were applied to reduce background. Scale bar, 7.5 μm.

(C) pH-dependent Urm1-Uba4 co-condensation results in urmylation of Uba4. Purified unlabeled Urm1 (5 μM) and Uba4 (2 μM) were incubated for 15 min at 25°C or 46°C in buffer at the indicated pH containing 20% Ficoll/150 mM KCl. Total fractions were separated into pellet and supernatant by centrifugation (15 min, 20,000 x *g*) (see STAR Methods), followed by analysis using SDS-PAGE and immunoblotting with an anti-Urm1 antibody (*n* = 2).
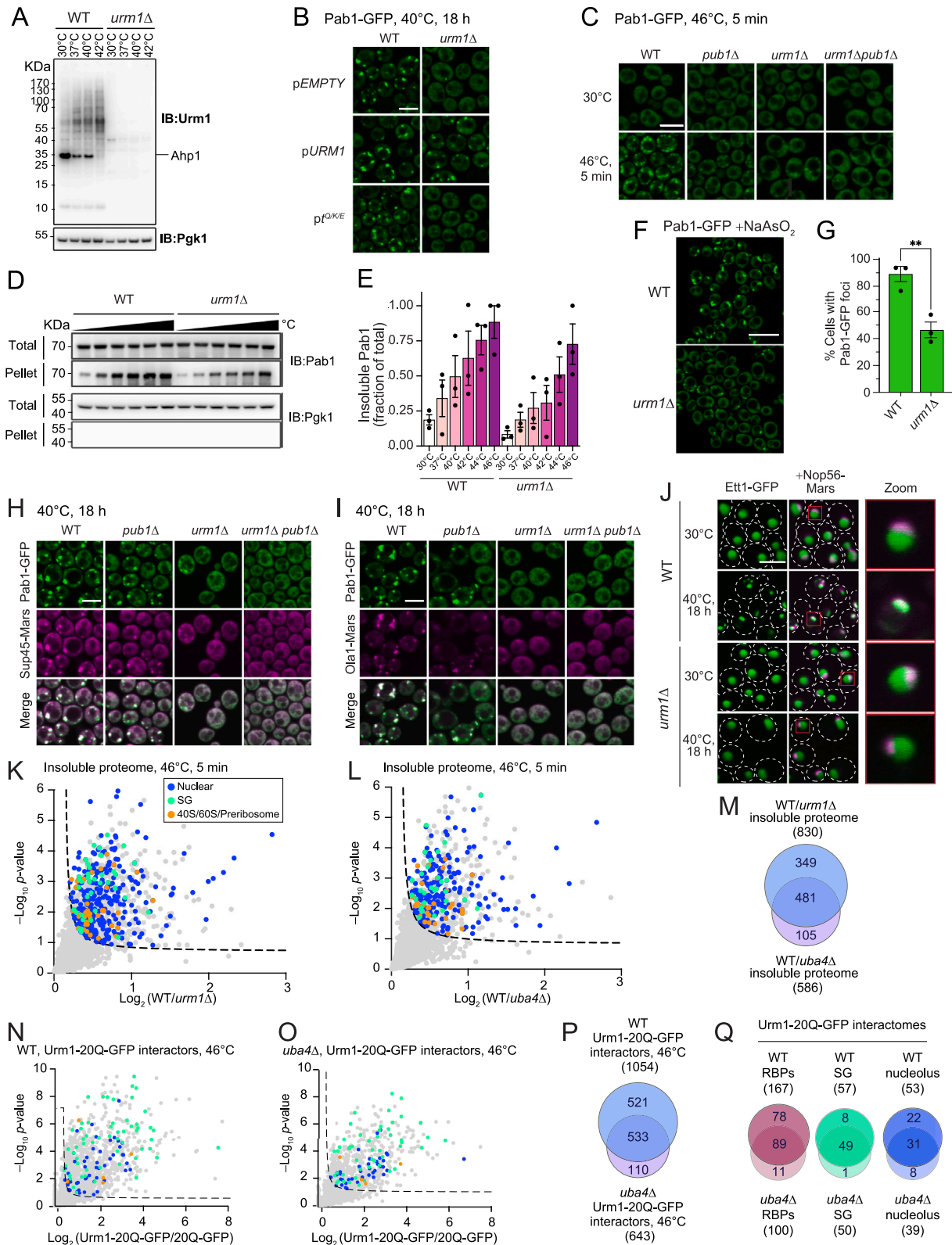
Figure S7. Condensate assembly defects resultant from loss of Urm1 function, related to Figure 6

(A) Protein urmylation following prolonged HS. WT and *urm1*Δ cells, grown to mid-log phase at 30°C, were shifted to the indicated temperatures for 18 h. Total cell extracts were analyzed by SDS-PAGE and immunoblotting using Urm1 antibody as in Figure 1A. Pgk1 was analyzed as loading control (*n* = 4).

(B) Expression of Urm1 but not of tRNAs targeted by thiolation rescues Pab1-GFP assembly in *urm1*Δ cells. WT and *urm1*Δ cells, producing Pab1-GFP (endogenous promoter), also harboring a plasmid expressing either WT *URM1* (*ADH1* promoter), or three tRNAs modified by thiolation (*ADH1* promoter; t$^{Q/K/E}$), were propagated at 40°C for 18 h, then imaged using live cell confocal microscopy (*n* = 3). Scale bar, 5 μm.

(C) SG assembly defect upon acute HS. Cells of the indicated genotypes, expressing Pab1-GFP (endogenous promoter), were imaged under basal growth conditions (30°C) and following shift to 46°C for 5 min using a confocal microscope (*n* = 3). Scale bar, 5 μm.

(D and E) Solubility of Pab1 following HS in WT and *urm1*Δ cells. (E) WT and *urm1*Δ cells, propagated to mid-log phase at 30°C, were incubated at 30°C–46°C for 15 min, as in Figure 1A. Cells were subsequently lysed in buffer containing 0.5% Triton X-100 and total extracts were separated into total and pellet fractions (also described in Figure 1A; see STAR Methods). Immunoblotting was performed using an anti-Pab1 antibody. Pgk1 was analyzed as loading control (*n* = 3). (E) Quantification of insoluble Pab1 as a function of temperature as in (D) by densitometry and normalized to total Pab1 levels (*n* = 3). Error bars display mean ± SEM.

(F) Pab1-GFP condensate formation following sodium arsenite treatment in WT and *urm1*Δ cells. WT and *urm1*Δ cells producing Pab1-GFP (endogenous promoter) were propagated to mid-log phase then treated with 1 mM sodium arsenite for 1 h. Live cell images were acquired using a confocal microscope (*n* = 3). Scale bars, 5 μm.

(G) Quantification of Pab1-GFP foci following sodium arsenite treatment in WT and *urm1*Δ as in (F). A bar graph display the percentage of foci-containing cells (140 cells counted per replicate). Error bars display mean ± SEM (*n* = 3). *p*-Values were assessed using unpaired t-test. ** *p* < 0.01.

(H and I) Cellular distribution of the SG proteins Sup45 and Ola1 relative to Pab1 following prolonged HS. Cells of the indicated genotypes producing Pab1-GFP in combination with either Sup45-Mars (H) or Ola1-Mars (I) (all proteins examined expressed from the endogenous promoters), were propagated at 40°C for 18 h, then subjected to live cell imaging using a confocal microscope (*n* = 3). Scale bar, 5 μm.

(J) Localization of Ett1 relative to the nucleolus following HS in *urm1*Δ cells. WT and *urm1*Δ cells, expressing Ett1-GFP and Nop56-Mars (endogenous promoters), were imaged following growth under basal conditions at 30°C and following prolonged HS at 40°C for 18 h using live cell confocal microscopy (*n* = 4). Brightness/contrast adjustments were made to enhance the Nop56-Mars signal. Scale bars, 5 μm.

(K) Distribution of aggregation prone nuclear proteins in WT and *urm1*Δ insoluble proteomes following acute HS. Detergent solubilized extracts, isolated from WT and *urm1*Δ cells, following acute HS (46°C, 5 min), were fractionated as described in Figure 1A. Insoluble protein was analyzed using LC-MS/MS and label free proteomics (see STAR Methods). A volcano plot represents the distribution of proteins with categories of interest highlighted. A black dashed line indicates an FDR cutoff of 0.05 (*n* = 4). See also Table S4C.

(L) Distribution of aggregation prone nuclear proteins in WT and *uba4*Δ insoluble proteomes following acute HS as in (K). A volcano plot represents the distribution of proteins with categories of interest highlighted. A black dashed line indicates an FDR cutoff of 0.05 (*n* = 4). See also Table S4D.

(M) Venn diagram showing the total number of significantly enriched proteins (above 0.05 FDR cutoff) in the insoluble fraction of WT compared to cells lacking either Urm1 or Uba4. See also Table S4D.

(N) Interactome analysis of Urm1-20Q-GFP following HS as in Figure 3E. Cell extracts isolated from cells exposed to HS (46°C, 15 min) were subjected to immunoprecipitation with anti-GFP nanobody (see STAR Methods). 20Q-GFP served as background control. Immunoprecipitates were analyzed by LC-MS/MS and label free proteomics (*n* = 4). A volcano plot displays the Urm1-20Q-GFP interactome upon HS. Proteins of interest are highlighted. A black dashed line indicates an FDR cutoff of 0.05 (*n* = 4). See also Table S4E.

(O) Interactome analysis of Urm1-20Q-GFP in cells lacking Uba4 following HS as in (N). Immunoprecipitates were analyzed by LC-MS/MS and label free proteomics. A volcano plot displays the Urm1-20Q-GFP interactome upon HS. Proteins of interest are highlighted. A black dashed line indicates an FDR cutoff of 0.05 (*n* = 4). See also Table S4F.

(P) Venn diagram displaying overlap between the Urm1-20Q-GFP interactomes in WT and *uba4*Δ cells. Numbers of proteins for each category are listed. See also Table S4F.

(Q) Venn diagrams displaying as in (P) proteins belonging to the categories RBP, SG and nucleolus. Numbers of proteins for each category are listed. See also Table S4F.